PROBABILISTIC DECLINE CURVE ANALYSIS IN UNCONVENTIONAL RESERVOIRS USING BAYESIAN AND APPROXIMATE BAYESIAN INFERENCE

By

Anand A. Korde, B.E.

A Thesis Submitted in Partial Fulfillment of the Requirements

for the Degree of

Master of Science

in

Petroleum Engineering

University of Alaska Fairbanks

August 2019

APPROVED:

Dr. Obadare Awoleke, Committee Chair
Dr. Scott Goddard, Committee Co-Chair
Dr. Abhijit Dandekar, Committee Member
Dr. Abhijit Dandekar, Chair
Department of Petroleum Engineering
Dr. William Schnabel, Dean
College of Engineering and Mines
Dr. Michael Castellini, *Dean of the Graduate School*

ABSTRACT

In this work, a probabilistic methodology for Decline Curve Analysis (DCA) in unconventional reservoirs is presented using a combination of Bayesian statistical methods and deterministic models. Accurate reserve estimation and uncertainty quantification are the primary objectives of this study.

The Bayesian inferencing techniques described in this work utilizes three sampling mechanisms, namely the Gibbs Sampling (implemented in OpenBUGS), the Metropolis Algorithm, and Approximate Bayesian Computation (ABC) to sample parameter values from their posterior distributions. These different sampling mechanisms are applied in conjunction with DCA models like Arps, Power Law Exponential (PLE), Stretched Exponential Production Decline (SEPD), Duong and Logistic Growth Analysis (LGA) to estimate prediction intervals. Production is forecasted, and uncertainty bounds are established using these prediction intervals. A complete workflow and the summary steps for each of the sampling techniques are provided to permit readers to replicate results.

To examine the reliability, the methodology was tested over 74 oil and gas wells located in the three main sub plays of the Permian Basin, namely, the Delaware play, the Central Basin Platform, and the Midland play. Results show that the examined DCA-Bayesian models are successful in providing a high coverage rate, low production prediction errors and narrow uncertainty bounds for the production history data sets. The methodology was also successfully applied to unconventional reservoirs with as low as 6 months of available production history. Depending on the amount of production history available, the combined deterministic-stochastic model that provides the best fit can vary. It is therefore recommended that all possible combinations of the deterministic and stochastic models be applied to the available production history data. This is in order to obtain more confidence in the conclusions related to the reserve estimates and uncertainty bounds.

The novelty of this methodology relies in using multiple combinations of DCA-Bayesian models to achieve accurate reserve estimates and narrow uncertainty bounds. The paper can help assess shale plays as most of the shale plays are in the early stages of production when the reserve estimations are carried out.

DEDICATION

This thesis is dedicated to beloved mother Jyoti Korde and my dearest friend Priyal Dalvi for their undying love and support.

Table of Contents

LIST OF FIGURES

Page

LIST OF TABLES

Page

ACKNOWLEDGEMENTS

I would like to extend my gratitude to my principal advisor, Dr. Obadare Awoleke, for his recommendations during the entire duration of this thesis. I would also like to thank my committee co-chair, Dr. Scott Goddard for his time and invaluable guidance towards the statistical and modeling part of this research. His suggestions have been instrumental in steering me in the right direction when needed.

It gives me great pleasure to show my appreciation towards the chair of the Petroleum Engineering Department, Dr. Abhijit Dandekar, for his confidence in me throughout my time at the University of Alaska, Fairbanks.

I am forever indebted to my parents, Mr. Avinash Korde and Mrs. Jyoti Korde for their unconditional love and faith in me. This accomplishment would not have been possible without their continued motivation and financial assistance. I am also thankful to my friends especially, Ankit, Parth, and Priyal for talking me through the difficult times.

Chapter 1

INTRODUCTION AND LITERATURE REVIEW

1.1 Need for accurate reserve forecasting and uncertainty analysis in shale plays

In recent years, there has been a shift in the development of reserves from conventional reservoirs to unconventional reservoirs. Some valid reasons behind this industry-wide transition can be the depletion of the mature conventional reserves, ever-increasing demand for oil and gas, and recent technological advancements. The unconventional oil and gas boom has dramatically impacted the U.S. as it has created a technological renaissance and helped the local petroleum-based economies. According to the U.S. Energy Information Administration (EIA) estimates, about 7 million barrels per day (MMB/D) of crude oil was produced directly from unconventional resources in 2018, which accounts to about 60% of total U.S. crude oil production. In comparison, only 12% of the total crude oil production in 2008 were from unconventional sources. Similarly, the U.S. shale gas production has been on the rise. The production of shale gas has increased from 16% of the total natural gas production in 2008 to 70% of the total natural gas production in 2018. According to EIA estimates, the total shale gas production as of December 2018 was about 65 billion cubic feet per day (BCF/D). These numbers indicate that the shale resources have been successful in overturning the age-old thought that domestic oil and gas production was at its peak in 2005. One may argue that as of today, there are only four countries producing shale gas commercially (U.S., China, Canada, and Argentina), but the rapid technological improvements are unquestionably expected to encourage the development of shale oil and gas resources in other countries in the coming years.

Fig. 1.1 below shows a comparison of the amount of hydrocarbons produced from the conventional and unconventional sources in the U.S. It also provides a forecast of future distribution of oil and gas based on these sources.

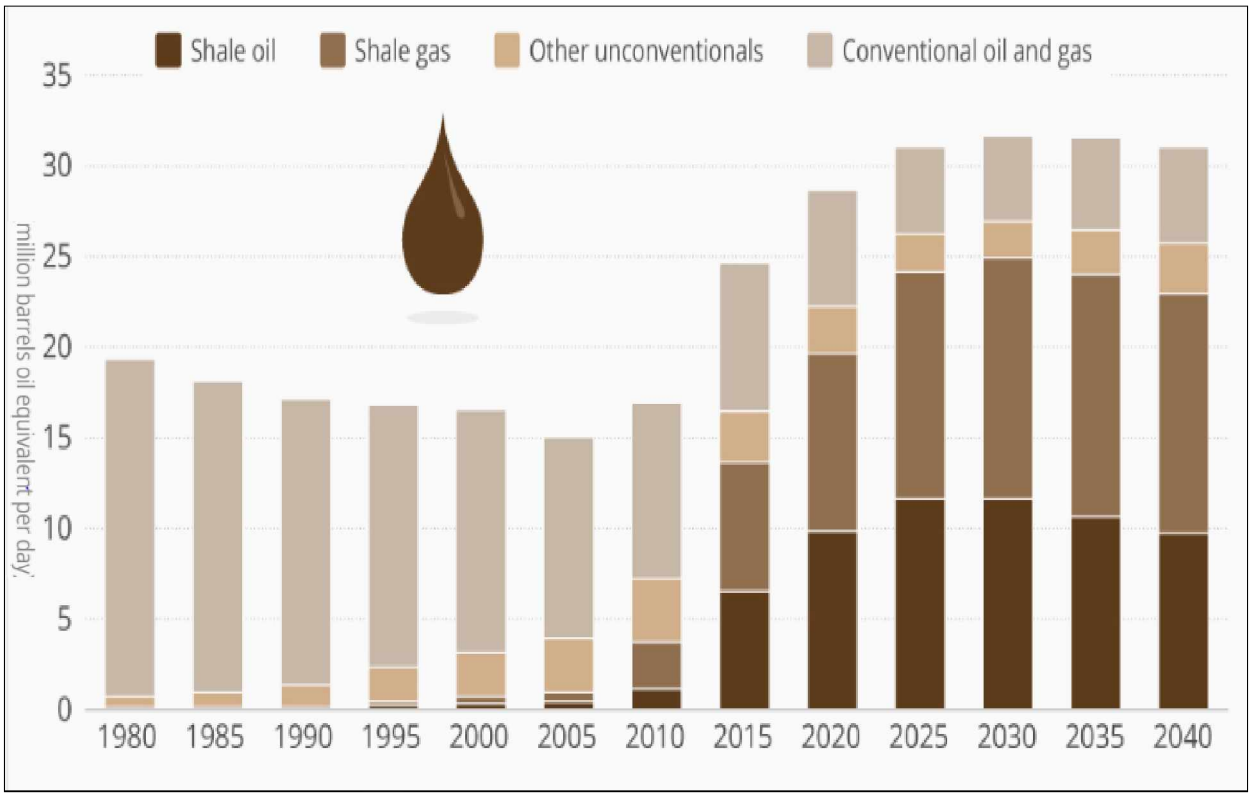

Fig. 1.1: Historical and projected U.S. oil and gas production (McCarthy, 2017)

Fig. 1.2 and **Fig. 1.3** below show the distribution of shale oil and gas production in the U.S. for major plays.

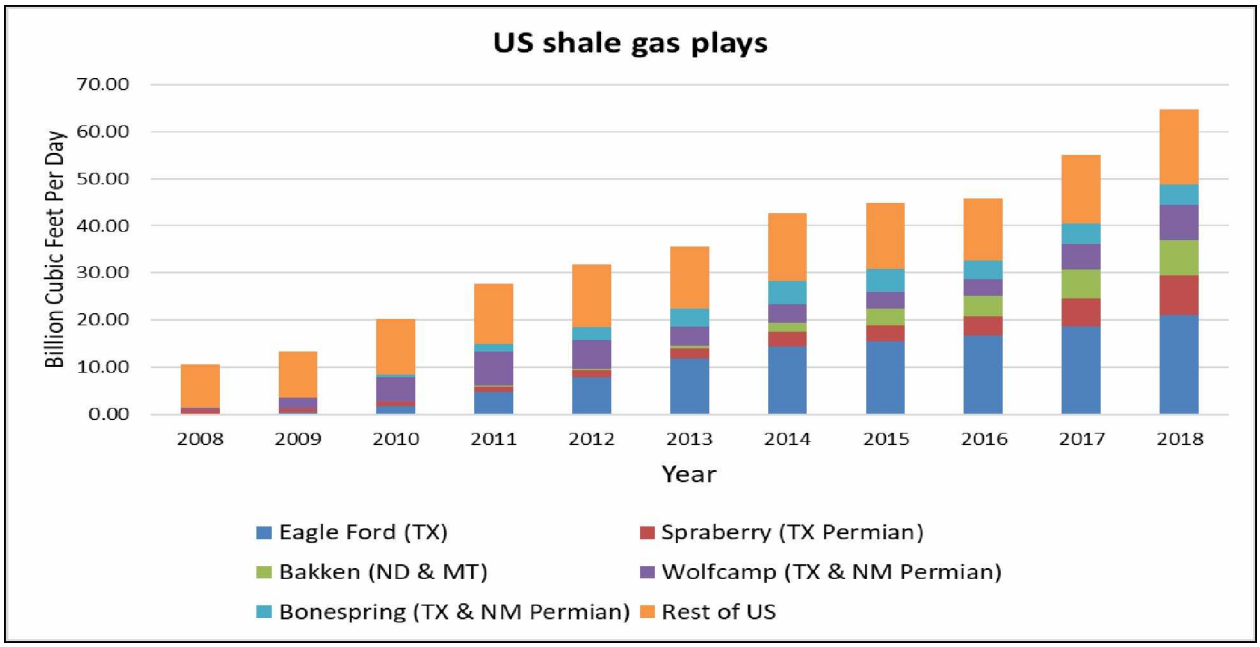

Fig. 1.2: U.S. Shale gas production by major plays (EIA, 2018a)

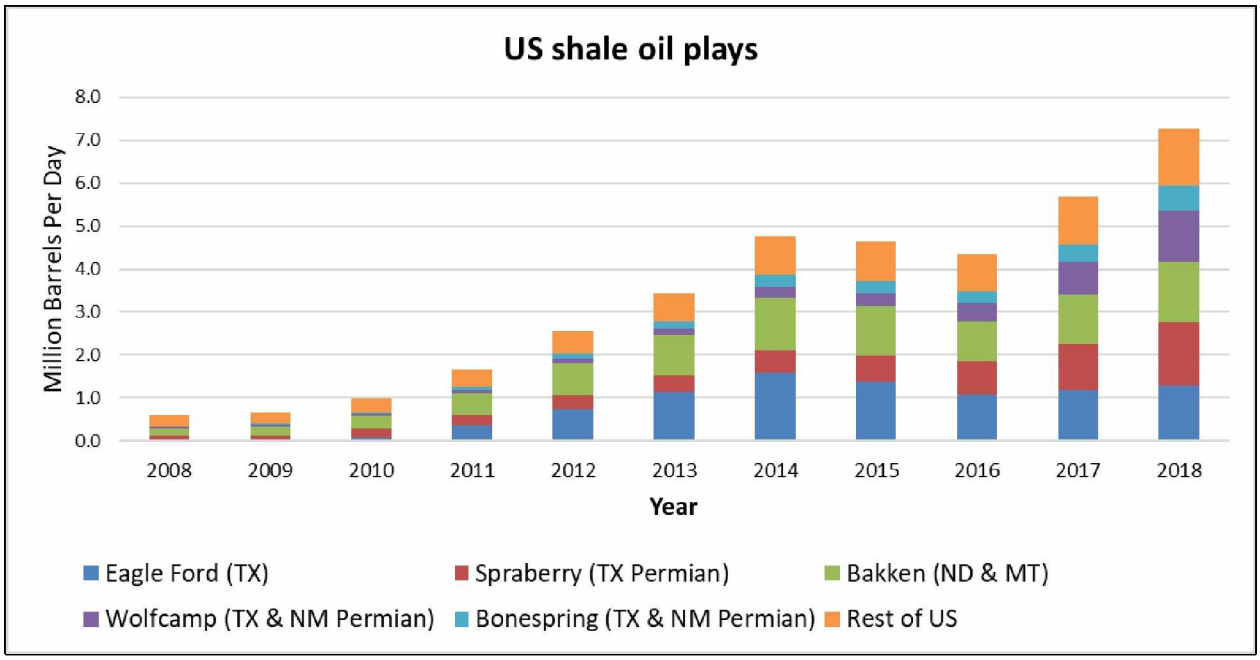

Fig. 1.3: U.S. Shale oil production by major plays (EIA, 2018a)

The Petroleum Resource Management System (PRMS) defines unconventional resources as follows:

Unconventional resources are present in hydrocarbon buildups that are pervasive throughout a large area and that are not significantly affected by hydrodynamic influences (also called "continuous-type deposits") in general. Such accumulations require specialized extraction technology, and raw production may require significant processing before the sale (SPE et al, 2011). As of today, horizontal well drilling with multistage fracturing has become a routine practice for developing unconventional reserves. These methods although more efficacious, are more expensive and therefore, it is of the utmost importance that the drilling project meets a suitable Estimated Ultimate Recovery (EUR) threshold for a project to be considered feasible and profitable.

The Arps DCA forecasting technique has been successfully applied to the conventional reservoirs. Theoretical justification for using Arps' equations in conventional reservoirs was provided by Fetkovich (1980) in his papers. However, such theoretical justification does not exist for the application of Arps' DCA in unconventional systems. Decline curve analysis (DCA) has been the most common method for modeling the production profile of a reservoir and for forecasting remaining reserves or the estimated ultimate recovery (EUR) of a well. The method pioneered by J.J. Arps in 1912 is based on three basic equations, namely 1) the exponential decline, 2) the hyperbolic decline, and 3) the harmonic decline (Arps, 1945) as presented by Eq.1, Eq.2, and Eq.3 respectively.

$$q_t = q_i * \exp(-D_t) \quad \text{.....(1)}$$

$$q_t = \left[\frac{q_t}{(1+b*D_i*t)^{\frac{1}{b}}}\right] \quad \text{.....(2)}$$

$$q_t = \left[\frac{q_i}{(1+b*t)}\right] \quad \text{.....(3)}$$

Here, q_t represents production rate at time t, Million Cubic Feet per month (MMCF/month); q_i represents the stabilized rate at $t = 0$; MMCF/month; D_i represents decline rate at flow q_i and b is the Arps decline constant. When $b = 0$, the equation takes the exponential form (Eq.1), while when $b = 1$, the equation takes the harmonic form (Eq.3). For any value of b between 0 and 1, the equation stays in the hyperbolic form (Eq.2).

These equations have the following assumptions:

1. The reservoir is in BDF.
2. The reservoir fluid is slightly compressible, and the bottom-hole pressure is constant.
3. The skin factor does not change.
4. The b value remains constant throughout the well life.

Transient flow and boundary-dominated flow (BDF) are the two main types of flows in a reservoir. During a transient flow, the pressure response (or pressure pulse) from a well moves outwards, towards the boundary, and the reservoir acts as an infinite reservoir as it has no apparent outer boundary. When the pressure response reaches the boundary, the flow type changes from the transient flow to the BDF. The rate at which the pressure response moves outwards is inversely proportional to the permeability of the reservoir. Since the permeability in conventional reservoirs is higher (relative to unconventional reservoirs), the pressure response moves faster, and BDF is achieved within a few days of production. Thus, the well spends most of its time in a BDF. However, in an unconventional system, the permeability of the reservoir is extremely low (less than 0.1 millidarcys), and the well spends most of its time in the transient flow rather than BDF. Any analysis with Arps equations in an unconventional system will return a b value higher than one because of the low permeability and elongated transient flow period (Fetkovich, 1980). This limits the applicability of Arps DCA to forecast unconventional reserves. Valko and Lee (2010) show that the Arps model overestimates reserves significantly in the unconventional reservoir setting. Such optimism in the reserve estimation can lead to significant disappointments in

petroleum projects. Bearing in mind the increasing dependencies of oil and gas production on shale resources worldwide and considering the vital role reserve estimates play to identify and aid business plans, resolving the shortcomings of the Arps DCA methodology and establishing novel reliable techniques for estimating the unconventional reserves becomes an important objective.

Further, for optimal development, it is essential to carry out the reserve assessment at an early stage. This can lead to a considerable amount of uncertainty in the reserve estimates. Variable Simulated Reservoir Volume (SRV), complex flow geometry, short production history, and variability in completion properties are some reasons due to which uncertainty can exist in the unconventional reservoirs (Agarwal et al., 2012). According to McVay and Dossary (2014), even moderate overconfidence and optimism in reserve estimation can lead to portfolio disappointment of 30 to 35 percent. McVay and Dossary (2014) also explained that expected disappointments (realizing actual cumulative production is less than estimated cumulative production) and expected decision errors (selecting the wrong projects) could be avoided by reliably and accurately quantifying uncertainty. This can lead to the identification of superior projects and overall improvement of the industry performance. Thus, addressing the issue of accurate uncertainty quantification becomes necessary.

1.2 State of knowledge

1.2.1 Deterministic Models

To facilitate the prediction of expected productivity and ultimate recovery in shale plays, researchers have suggested numerous deterministic models in the past decade. These models developed to address the drawbacks of the traditional Arps equation include: 1) Power Law Exponential (PLE) model (Ilk et al., 2008), 2) Stretched Exponential Production Decline (SEPD) model (Valko, 2009), 3) Duong's model (Duong, 2011), and 4) Logistic Growth Analysis (LGA) model (Clark et al., 2011).

1) Power Law Exponential

Ilk et al. (2008) developed a model based on a power law loss ratio for reserve estimation in unconventional reservoirs. This model replaces b and D_i parameters from the Arps exponential model with new parameters $\hat{D}$, D_∞ and n and takes the following form:

Power law equation,

$$q_t = q_i * \exp\left(-\mathrm{D}_\infty * \mathrm{t} - \left(\frac{\hat{\mathrm{D}}}{\mathrm{n}}\right) * \mathrm{t}^{\mathrm{n}}\right). \quad \text{.....(4)}$$

PLE model has four parameters as compared to the three parameters in the original Arps model. In Eq. 4, q_t represents the production at time t, q_i is the initial production, $\hat{D}$ is the power law decline constant, 1/month, D_∞ is the power law decline at an infinite time constant, 1/month, and n is the dimensionless time exponent. The PLE model is advantageous as the extra parameter in the model allows the model to account for both BDF and transient flow. The model also has a similar form to the Arps model (exponential) which gives it a familiar feel. According to Paryani (2015), the PLE model originates from the exponential family of curves like Arps exponential equation and behaves similarly to the Arps exponential model. Paryani (2015) also stated that the PLE model produces a conservative production forecast when compared to the Arps model.

2) Stretched Exponential Production Decline

Valko (2009) introduced the SEPD model. The model can handle high initial rates followed by a rapid decline which is a common trend in shale plays. SEPD has a different approach compared to PLE and radically rearranges the PLE model by eliminating the D_∞ component.

SEPD equation:

$$q_t = q_i * \exp\{-\left(\frac{\mathrm{t}}{\tau}\right)^{\eta}\}. \quad \text{.....(5)}$$

In Eq. 5, q_t represents the production at time *t*, q_i is the initial production, τ is the characteristic time parameter, month, η is the dimensionless exponent parameter. In an exponential decay, the model acknowledges the heterogeneity of a reservoir and the actual production decline is determined by a significant number of contributing volumes individually, but with a specific distribution of characteristic time constants (Valko and Lee, 2010). It predicts a lower EUR that would be obtained from extrapolation of Transient flow regime without the transition to exponential decline as in the case of Arps (Shah, 2013).

3) Duong's method

Duong (2011) established the Duong's method or the rate-decline analysis for fracture dominated shale reservoir model. The model assumes that the matrix contribution to the EUR is negligible as compared to the fracture contribution. The model involves three parameters of which two are strongly correlated. Estimating one of these two strongly correlated parameters can make this model a two-parameter model.

Duong's equation:

$$q_t = q_i * \mathrm{t}^{-\mathrm{m}} * \exp\left[\left(\frac{\alpha}{1-\mathrm{m}}\right) * \mathrm{t}^{1-\mathrm{m}} - 1\right] \quad \text{.....(6)}$$

In Eq. 6, q_t represents the production at time *t*, q_i is the initial production, α is the intercept of Duong's model, 1/month, m is the dimensionless slope parameter. Duong's method provides more conservative estimates for cumulative production as compared to PLE and Arps method (Duong, 2011).

4) Logistic Growth Analysis

Clark et al. (2011), proposed the LGA model to estimate reserves for extremely low permeability reservoirs. It comprises of three parameters and is derived from the hyperbolic family of curves.

LGA equation:

$$q_t = \left[\frac{k * n * a * t^n}{(a+t^n)^2}\right] \qquad (7)$$

In Eq. 7, q_t represents the production at time t, q_i is the initial production, k is the carrying capacity (EUR), MMCF, n is the dimensionless slope parameter, and a is the time to the power n at which the half of the carrying capacity has been produced, months. Clark et al., (2011) indicate that the LGA model estimates for cumulative production are more modest than the Arps model.

1.2.2 Probabilistic Methods

Probabilistic Decline Curve Analysis (PDCA) methods were devised to quantify uncertainty in the production forecast and reserve estimates by generating probability distributions of the decline forecasts with prediction intervals (PIs) rather than generating single point production predictions. Most commonly, P10, P50, and P90 provide a measure of the PIs with P10-P90 being the apparent 80% prediction interval (PI). Here, “P” refers to percentile, thus, P10 is the point in the distribution where 10% of the estimates exceed the predicted P10 value. Similarly, P50 and P90 are the points in the distribution where 50% and 90% of the estimates exceed the predicted P50 and P90 values respectively. Some of these PDCA methods include, 1) Bootstrap method (Jochen and Spivey, 1996), and Modified Bootstrap method or MBM (Cheng et al., 2010), 2) Bayesian method using MCMC (Gong et al., 2011), 3) Approximate Bayesian Computation or ABC (Paryani 2015; Paryani et al., 2017), and 4) Time Series Analysis or TSA (Joshi et al., 2018).

1) Bootstrap and Modified Bootstrap Method

Jochen and Spivey (1996), introduced the Bootstrap method which is a statistical approach to DCA using Monte Carlo analysis and non-linear regression. The process involves generating a large number of synthetic data sets from the original data set by random sampling. Each synthetic data set determines a set of decline curve parameters. Every set of decline curve parameters determine the reserve estimates. A set of all such reserve estimates form a distribution of the reserve estimates and is used to quantify uncertainty.

The advantage of this method apart from providing a means to quantify uncertainty is that it does not require assumption of the prior distribution of the decline curve parameters. However, this method assumes that the original data is independent and identically distributed. This assumption is incorrect as the production history data is time dependent and cannot be treated as independent.

Cheng et al. (2010) addressed this issue by introducing a more rigorous model-based bootstrap technique called MBM. MBM involves generating the synthetic data sets using block resampling of the residuals obtained by application of decline models like the hyperbolic or exponential equation to the actual data set. There are three stages for the MBM method which involve DCA on the most recent 20%, 30% and 50% of the generated synthetic data. These three stages determine three distributions of the reserve estimates which give the P10, P50 and P90 levels. Actual P90 and actual P10 are considered to be the minimum and maximum of the P90 and P10 values generated by the three distributions, whereas the actual P50 is the mean of the P50 values generated by the three distributions.

The MBM technique was tested on 100 mature conventional oil and gas wells having sufficient production history data by Cheng et al. (2010). Their results show that MBM has better coverage rate (83%) as compared to the Bootstrap method (34%). Gong et al. (2011) further demonstrated that the MBM method was well-calibrated for the conventional reservoirs and unconventional reservoirs.

2) Bayesian PDCA by Gong et al.

Gong et al. (2011) applied Bayesian statistics to DCA for reserve estimation and uncertainty quantification in the unconventional reservoirs. The methodology involves a combination of the Arps DCA model and the Markov Chain Monte Carlo (MCMC) technique. A Metropolis algorithm is the sampling strategy used to sample from the target distribution. Three main constituents to this technique are the prior distribution, the likelihood function, and the posterior distribution (target distribution). They consider the Arps model parameters as random variables and define the prior distribution as a uniform distribution over the upper and the lower limits of the random variables. The likelihood function was defined as the conditional probability of the available historical production data given the DCA parameters. The posterior distribution was defined as the distribution of the DCA parameters after the available historical production data is considered. Posterior distributions of each of the random variables are used to determine the production forecast and the uncertainty estimates.

Gong et al. (2011) in their case study of 167 wells, showed that using their Bayesian inferencing technique requires far less computational time (25 minutes) compared to the MBM technique (6.5 hours). They also indicated that the Bayesian method had a low relative error, low absolute errors, and low error in true reserves compared to the MBM.

3) Approximate Bayesian Computation

Paryani (2015) used the ABC methodology to quantify the uncertainty associated with DCA models. The primary purpose of developing this methodology was to simplify the Bayesian inferencing procedure by approximating the complex likelihood function. The likelihood is approximated using summary statistics of the simulated and observed data sets. If the difference in the summary statistics (observed vs. simulated) is more than the set threshold, the sample is excluded using rejection sampling. ABC method is discussed in detail in the methodology section (chapter 3) of this study.

Paryani (2015) in their study of 121 wells (100 gas wells and 21 oil wells), concluded that the ABC methodology is computationally faster than the likelihood-based numerical approximation as the likelihood is not evaluated directly. They also indicated that the LGA model provides better coverage rate compared to other known deterministic models.

4) Time Series Analysis

Joshi et al. (2018) combined LGA and time series modeling techniques to quantify uncertainty in unconventional reservoirs. They first determined the trend in the production history data using the LGA model with two different non-linear regression schemes, namely ordinary least squares and weighted least squares. Thereafter, the stationary residual data sets are produced by subtracting the predicted production profiles from the actual production history data. Further, a statistical technique of TSA is carried out for model identification, model estimation, and production forecasting. Model identification stage determines the type and order of the Auto-regressive Moving Average model (ARMA). Model estimation stage estimates the coefficients of the identified ARMA model. The production forecasting stage generates the P10, P50, and P90 values.

A study of 100 wells indicates LGA method quantifies uncertainty reliably with as little as 20 months of production history data. The coverage rate for 80% PI was 84% for 40 months of known production data and 90% for 50 months of known production history data.

1.3 Limitations of the previous work

The MBM technique provides better a coverage rate for 80% PIs than the original Bootstrap technique, but as shown by Gong et al. (2011), requires a considerably longer computational time.

The Bayesian PDCA technique by Gong et al. (2011) could be preferable for reserve estimation and uncertainty quantification in comparison with other mentioned PDCA techniques, but it has

not been extensively tested with deterministic models other than the Arps model. Further, the Gong method utilizes a large amount of historic production data (5 to 10 years) for its analysis and thus, has not been applied to unconventional reservoirs with limited production history. Also, if additional valid models (other than DCA-Bayesian model) supporting the forecasts are available, the ability to rely on these estimation can certainly increase.

The TSA approach introduced by Joshi et al. (2018) depends on the identification of the dominant trend. If several prevailing trends appear in the early time production history data, the method may fail to quantify uncertainty. Also, the TSA technique has not been tested with deterministic models other than the LGA model or on conventional wells.

Since new shale plays have limited production history data available, it is important to study the application of the probabilistic methods on reserve estimation and uncertainty quantification of wells with limited available production history. Also, if one can establish statistical models and model-fitting techniques that can be applied to the known deterministic models within the Bayesian framework, numerous combinations of DCA-Bayesian models can be generated. This can help in increasing the ability to rely on the predicted forecasts. The engineers can also test these models over a portion of available production history data to compare their forecasts with the remaining production history data. This can lead to identification of combination models with 1) higher accuracy in terms of lower prediction errors, 2) higher Coverage Rate (CR) and 3) lower uncertainty in terms of narrow P10-P90 intervals.

1.4 Objectives

Thus the objectives of this research work are as follows:

1. To identify various MCMC-based sampling techniques that can be used to perform Bayesian data analysis in accordance with the above mentioned deterministic models.

2. To identify the potential hybrid models that can be applied to different sectors of the Permian Basin using our dataset to increase the ability to rely on the forecasts. The hybrid model in this context means a combined deterministic and probabilistic model.
3. To test the performance of these hybrid models on varying available production history data from the Permian Basin and identify hybrid models that perform better in terms of prediction error, Coverage Rate (CR) and interval width bounds and thereby, improving the accuracy of the forecasts

The applicability of the methodology, based on the analysis of 74 wells from the Permian Basin is discussed in the results section (chapter 3) of the thesis. The following section gives an overview of the Permian Basin.

1.5 Overview of the Permian Basin

The Permian Basin is an old and widely acknowledged hydrocarbon producing region in North America. It extends from the south-eastern part of New Mexico to the western part of Texas covering around 86,000 square miles over 52 counties. Mass deposition, continental collision, and sub-basin sediment filling are the three main attributes leading to the evolution of the Basin. The Basin is divided into three main sub-basins, namely, 1) Midland Basin, 2) Central Basin Platform and 3) Delaware Basin as shown in **Fig. 1.4** below. Other regions of the Permian include Marfa Basin, Val Verde Basin, Ozona Arch, Northwest Shelf, Hovey Channel, and the Eastern Shelf.

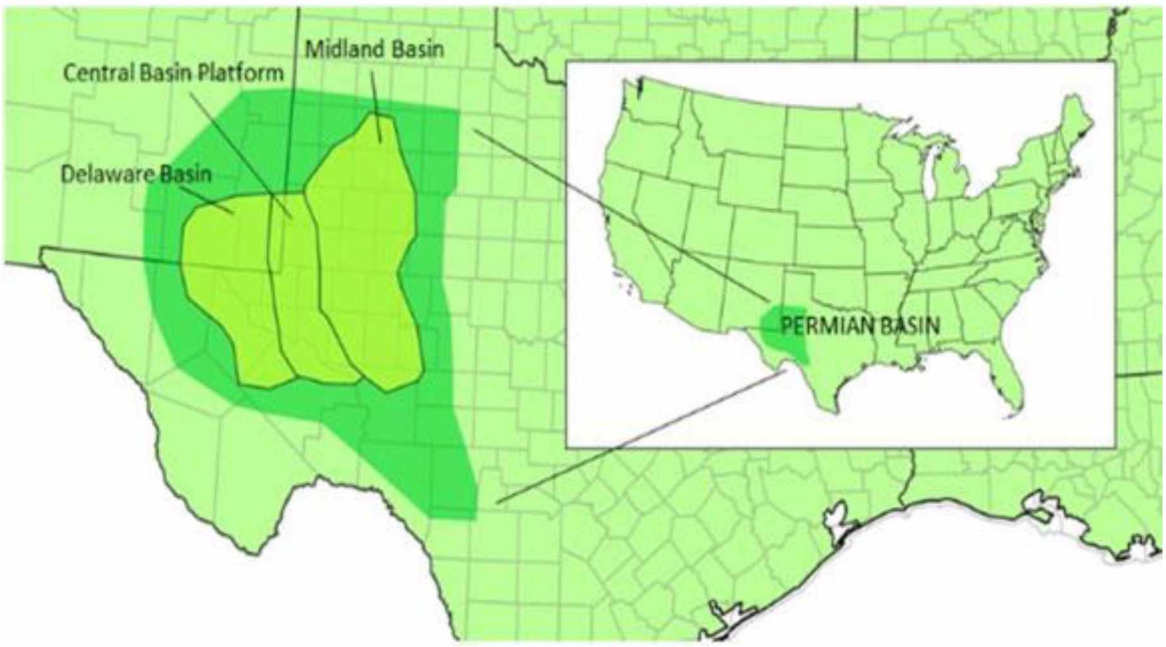

Fig. 1.4: Location map of the Permian Basin (Tarka Resources, 2019)

1.5.1 Midland sub play

As shown in the above figure (**Fig. 1.4**), the Midland sub play is located towards the eastern region of the Permian Basin. The region is known to accumulate large quantities of clastic sediments from the Ouachita orogenic belt during the Pennsylvanian period (EIA, 2018b). The deposition of these sediments led to the formation of a dense subaqueous deltaic system. The two stratigraphic sections that make up the Leonardian and Wolfcampian are the Spraberry (along with the Dean) and the Wolfcamp formations (see **Fig. 1.5**). The Basin has a multilayer stratigraphy with diverse geologic zones as shown in **Fig. 1.6** below.

Drilling companies initially focused on drilling vertical wells through the Spraberry formation, extending into the Wolfcamp formation. However, after the 1980s, multi-stage hydraulic fracturing techniques have facilitated exploration of deeper intervals of the Wolfcamp and Spraberry shales. Wolfcamp and Spraberry plays are together known as "Wolfberry" play.

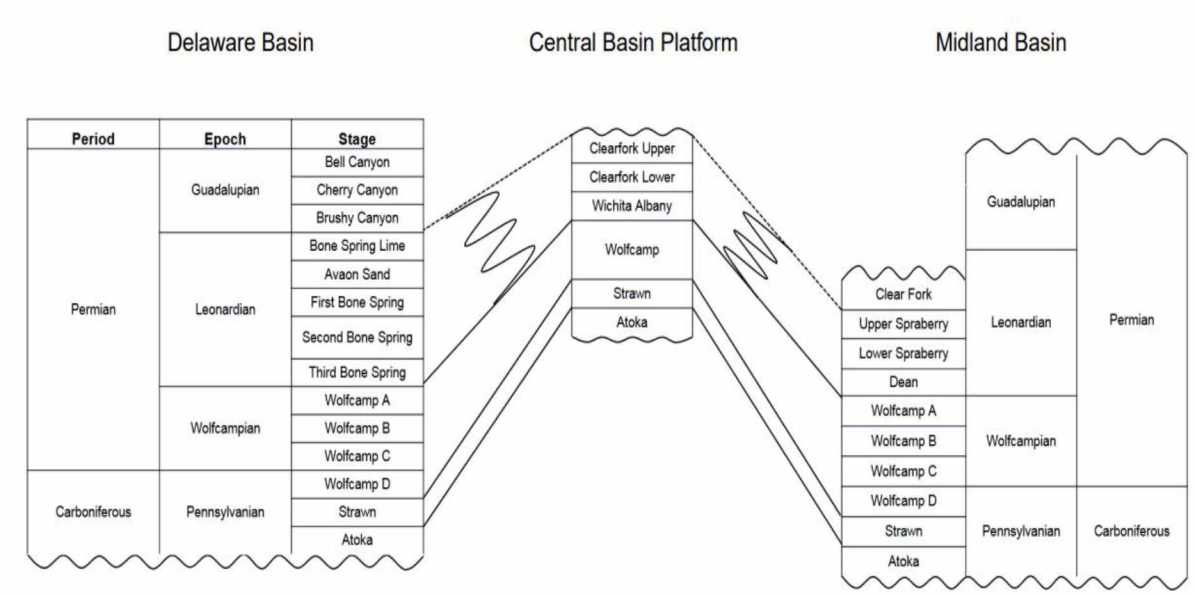

Fig. 1.5: General stratigraphic schema of Upper Carboniferous to Upper Permian intervals for the Permian region (EIA, 2018b)

1.5.2 Central Basin Platform

Central Basin platform lies in the central part of the Permian Basin (see **Fig. 1.4**) and has a higher elevation as compared to the other two basins (Midland and Delaware), resulting in a dissimilar depositional environment. Permian Basin's stratigraphic interval rapidly thins to the Central Basin Platform, in comparison to the gradual thickness decline towards western Delaware and eastern Midland Basin. Central Basin is divided into several formations like Wolfcamp, Abo, San Andreas, Seven Rivers, and Yates. The sequence mainly comprises of carbonate reef deposits and shallow marine clastic sediments (Ward et al., 1986).

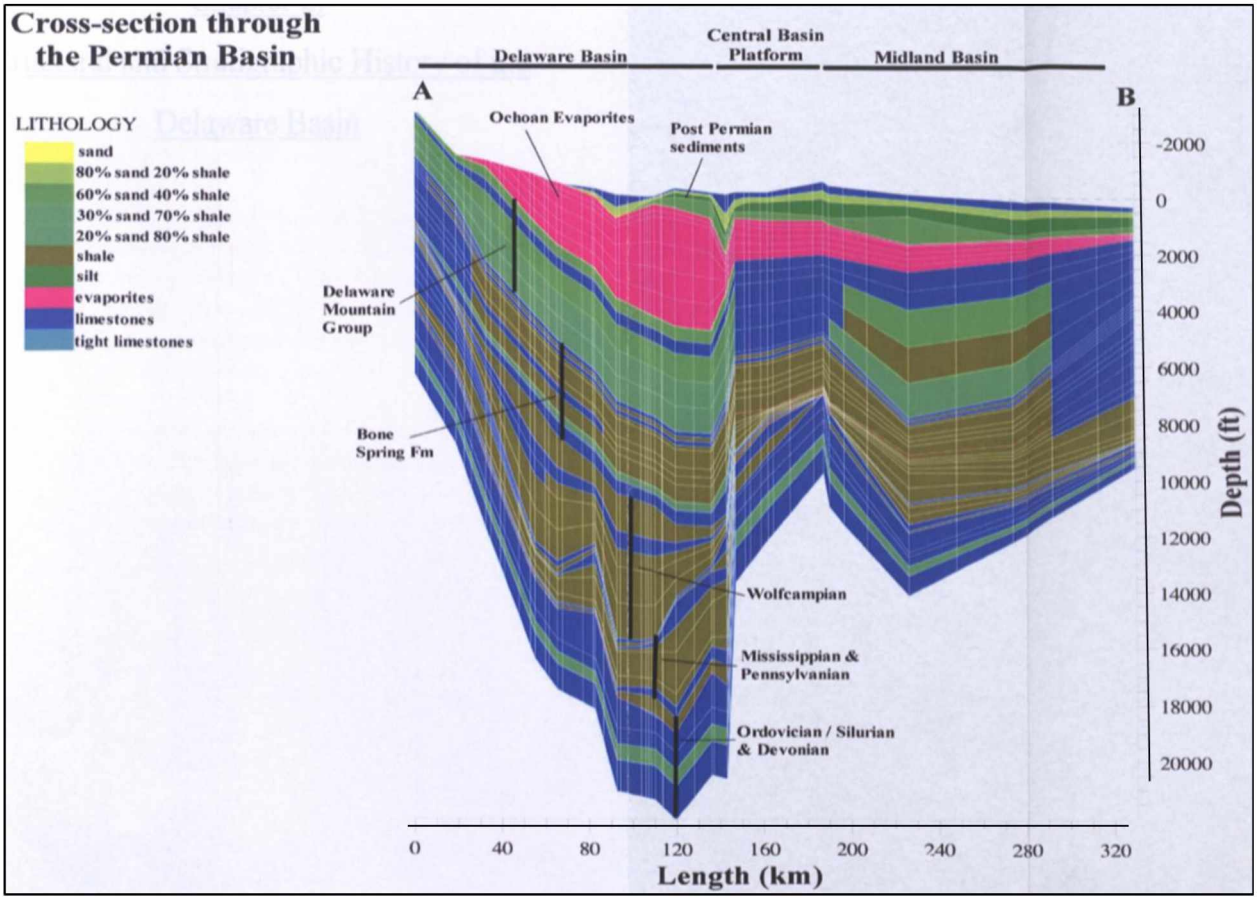

Fig. 1.6: Lithology cross section of Permian Basin (Sinclair, 2007)

1.5.3 Delaware sub play

As shown in the above figure (**Fig. 1.4**), Delaware sub-basin is located towards the western region of the Permian Basin. Delaware Basin is around 2000 feet deeper than the Midland Basin, and thus, sediments experience significantly high pressure during burial. Delaware Basin has different stratigraphy compared to the Midland Basin in the Leonardian strata (see **Fig. 1.5**). However, both Basins share an analogous Wolfcamp formation, which is also an ideal heterogenetic resource of hydrocarbons. Bone Spring and Avalon are other main formations in the Delaware Basin. Wolfcamp and Bone Spring formations are together known as the "Wolfbone" formation. The deeper part of the Delaware Basin is multi-stacked like the Midland Basin (see **Fig. 1.6**).

According to EIA, as of today, most of the activity in the Delaware Basin has been in the Bone Spring formation. The formation boasts 5-7 potentially commercial zones with a median 3,000 - 3,500' vertical section. Although the hydrocarbon mix differs along the intervals, most of it is significantly oil weighted.

1.5.4 Production in the Permian

Overall, the Permian region has produced hydrocarbons for about 100 years and provided more than 33.4 billion barrels of oil and about 118 trillion cubic feet of natural gas as of September 2018 (EIA, 2018b). **Fig. 1.7** below, shows the constant increase in the production of both, oil and natural gas from the Permian region.

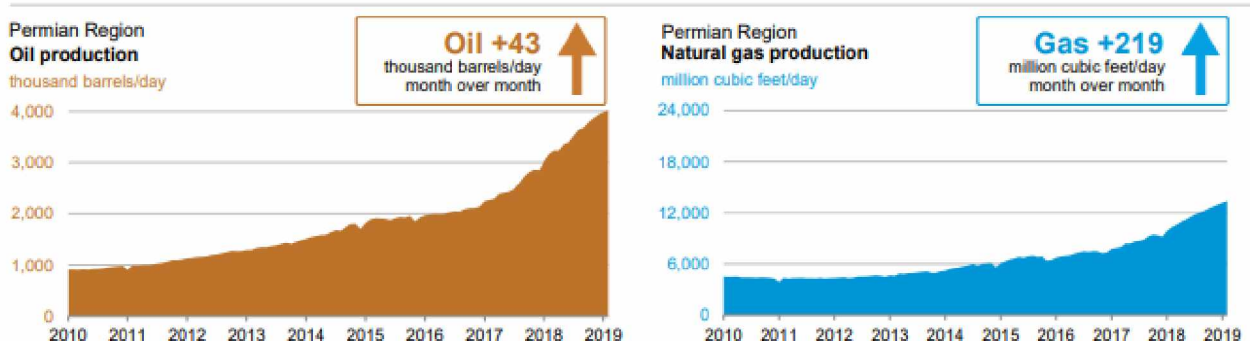

Fig. 1.7: Oil and natural gas production in the Permian region (EIA, 2019)

Permian Basin is also considered to be one of the most prolific U.S. shale plays. In this study, we focus on reserve estimation and uncertainty quantification of hydrocarbons produced from the Midland (Terry and Upton Counties), Central Platform (Ward County) and Delaware (Ward County) sub plays. The methodology adopted for the analysis is discussed extensively in chapter 2 of the thesis.

Chapter 2

METHODOLOGY

The methodology devised in this research requires combining deterministic DCA models and Bayesian inferencing leading to the development of what we call hybrid models. Bayesian inferencing is a statistical data prediction technique that utilizes parameter estimation not only to forecast future data but also to provide a credible interval of the uncertainty in the forecast. To recognize and benefit from the methodology developed in this research work, it is imperative to understand the basic building blocks such as Bayes' theorem, MCMC methodology, and the sampling mechanisms, that contribute to the final product of this study.

2.1 Frequentist vs. Bayesian

Generalizations that aim at finding a pattern that does not just hold true for a particular sample but the population as a whole are dealt with a branch of statistics known as inferential statistics. In other words, it is the process of deducing properties of a population or probability distribution from the data. Researchers around the globe appreciate the importance of statistical inferencing in addressing critical issues but quite frequently, are not aware of the underlying theories that assist model estimation. In statistical inferencing, there are two broad approaches: 1) the frequentist and 2) the Bayesian paradigms.

Frequentist methods define probability as the limit of an event's relative frequency, computing the probability of an event in the long run of the experiment (i.e., the experiment is repeated under identical circumstances). The normal goal of this mechanism is to determine the parameter values that maximize the likelihood function evaluated at the observed data. It is essential to ensure that the sample is representative of the population.

The Bayesian methodology, in contrast, offers a tool to update individual beliefs in the presence of new data. The representation of the uncertainty is achieved by defining a prior probability distribution over the possible values of the parameters and by using sampled values to update this distribution. This updating process is done by applying Bayes' theorem. **Table 1** below, summarizes the similarities and differences between the Frequentist and Bayesian statistics.

	Frequentist statistics	Bayesian statistics
Definition of the p value	The probability of observing the same or more extreme data assuming that the null hypothesis is true in the population	The probability of the (null) hypothesis
Large samples needed?	Usually, when normal theory-based methods are used	Not necessarily
Inclusion of prior knowledge possible?	No	Yes
Nature of the parameters in the model	Unknown but fixed	Unknown and therefore random
Population parameter	One true value	A distribution of values reflecting uncertainty
Uncertainty is defined by	The sampling distribution based on the idea of infinite repeated sampling	Probability distribution for the population parameter
Estimated intervals	Confidence interval: Over an infinity of samples taken from the population, 95% of these contain the true population value	Credibility interval: A 95% probability that the population value is within the limits of the interval

Table 1: Overview of the similarities and differences between Frequentist and Bayesian statistics (Schoot et al., 2013)

Bayesian inferencing being an uncertainty-based approach, can provide a structured approach to reserve estimation. In order to understand Bayesian inferencing, we first need to understand the underlying Bayes' theorem.

2.2 Bayes theorem and its constituents

Although the application of the Bayesian statistics to the petroleum industry is relatively new, these are the same concepts applied in the 1740s when the statistician, Thomas Bayes first laid the foundation of the technique. The following equation represents one form of Bayes' theorem:

$$P(A|B) = \frac{P(B|A)*P(A)}{P(B)} \quad \text{.....(8)}$$

Here, *A* and *B* are events. *P(A|B) is* the conditional probability in which, event *A* occurs after event *B* has occurred; *P(B|A) is* the conditional probability in which, event *B* occurs after the event *A* has occurred; *P(A)* and *P(B)* are the marginal probabilities of event *A* and event *B* taking place respectively.

We restate Eq. 8 as:

$$P(\theta|Y) = \frac{P(Y|\theta)*P(\theta)}{P(Y)} \quad \text{.....(9a)}$$

Here *Y* refers to the observations or the data and θ is a set of parameters in the model.

Simply put,

$$P(Parameter\ Set|Data) = \left[\frac{P(Data|parameter\ set)*\ P\ (Parameter\ Set)}{P(Data)}\right] \quad \text{.....(9b)}$$

There are four constituents of the Bayes theorem: 1) the prior distribution, 2) the likelihood function, 3) the posterior distribution, and 4) the marginal likelihood. The following sections discuss these in detail.

2.2.1 Prior distribution

In Eq. 9a, $P(\theta)$ represents the prior distribution. It is the probability distribution of the background knowledge of all the key parameters of a DCA model in question. Here, the background knowledge can be obtained based on expert opinion, a formerly conducted logical analysis, or other such dependable sources. Based on the background knowledge, there are three main types of priors; 1) non-informative priors; possessing no information about the data before the data is observed, 2) partially informative priors; possessing very little information about the data before the data is observed and 3) informative priors; incorporating significant cumulative understanding of the data before observing the data. We use partially informative priors in our study to avoid the common tendency of underestimating uncertainty. These priors take the form of uniform distributions and are constrained with a lower limit and an upper limit for each parameter in question. For example, in the case of the Arps model, which has qi, b, and Di as the key parameters, the prior for parameter b is a uniform distribution between 0 and 2. **Table 2** below provides a list of key parameters for the different DCA models and the prior distributions applied to these parameters in this study. The distribution boundaries are set large enough to include all plausible values of the parameters in the analysis.

DCA Model	Parameter	Units	Lower limit	Upper limit
Arps	qi	Mcf/D	1	100000
	b	-	0	2
	Di	1/year	0.1	50
PLE	qi	Mcf/D	1	100000
	D(hat)	-	0.001	10
	D∞	-	0.0001	1
	n	-	0.001	2
SEPD	qi	Mcf/D	1	100000
	η	-	0.01	5
	τ	-	0.15	10
Duong	qi	Mcf/D	0.01	100000
	a	-	0.5	5
	m	-	0.5	2
LGA	k	Mcf	1000	5000000
	n	-	0.01	1.2
	a	days	1	900

Table 2: Parameter constraints used in the study

2.2.2 Likelihood function

The second essential constituent of the Bayes theorem is given by $P(Y|\theta)$ in Eq. 9a and is known as the likelihood function. It is the joint probability density function of the data assuming the parameter set θ is known. The likelihood function epitomizes the information that is obtained from the data itself and is the way through which the data affects the posterior distribution. A Bayesian model can be defined entirely only when both the prior distribution and the likelihood function are fully specified or approximated. For our study, we use the same likelihood function as described by Gong et al. (2011), shown by Eq. 10.

$$f(Y|\theta) = \frac{1}{\sqrt{2\pi}\sigma}\exp\left(\frac{r(Y,\theta)^2}{\sigma^2}\right) \quad \text{.....(10)}$$

Here, Y is the observed data, θ is the set of DCA parameters, σ is the standard deviation of the statistical errors (and is one of the parameters in the set θ), and $r(Y,\theta)$ is the sample standard deviation of the residuals between the observed data and the decline curve defined by θ.

2.2.3 Posterior distribution

In Eq. 9a, the probability distribution given by $P(\theta|Y)$ is the joint posterior distribution of model parameters given observed data. The posterior distribution is a compromise of the prior knowledge and the observed data. It reflects the updated knowledge about the system and involves balancing prior knowledge with observed evidence. It is used to express uncertainty about the set of parameters in question, conditional on observed data.

2.2.4 Marginal Likelihood

Another constituent of the Bayes theorem is the marginal likelihood function or the prior predictive distribution of the data. $P(Y)$ represents the marginal likelihood in Eq. 9a. We express marginal likelihood in its true form in Eq.11.

$$P(Y) = \int P(Y|\theta)P(\theta)d\theta \quad \text{.....(11)}$$

The marginal likelihood of the data (Y) normalizes the joint posterior distribution, causing it to integrate to one. When $P(Y)$ is replaced by a constant, the joint posterior distribution becomes proportional to the product of the likelihood and the prior (Eq.12) and is termed as the unnormalized joint posterior.

$$P(\theta|Y) \propto P(Y|\theta)P(\theta) \quad \text{.....(12)}$$

Often the goal in Bayesian inference is to estimate the joint posterior distribution of parameters. This could entail the computation of the marginal posterior distribution. However, this computation involves solving intricate integrals. A more tractable solution to these computational difficulties is to use algorithms that can sample from the joint posterior distribution. Out of the different numerical approximations used to sample from the posterior, likelihood-based MCMC techniques such as the Metropolis and Gibbs sampler algorithms, and the non-likelihood based ABC algorithm form the underlying strategies used in this work.

2.3 MCMC

MCMC is merely a union of Monte Carlo integration and Markov Chains. Bayesian methods discovered more than a half-century ago, are being used to their full potential today because of the availability of the improved computing techniques and MCMC algorithms. Using MCMC, it is possible to draw samples from a distribution of interest, even if it is not possible to calculate it directly. The following topics describe the MCMC technique in detail.

2.3.1 Monte Carlo Integration

Let us consider the following equation,

$$\mathrm{J} = \int f(\theta)P(\theta)d\theta \quad \text{..(13)}$$

Here, $f(\theta)$ is a function of θ and $P(\theta)$ is a probability distribution. The integral given by Eq. 13, if derived analytically, provides us with the mean of $f(\theta)$. We can approximate the integral with the help of Monte Carlo Integration by simulating N values from the distribution $P(\theta)$ for some large number N. The simulated values can be used to calculate Eq.14.

$$\hat{J}_N = \frac{1}{N} * \sum_{i=1}^{N} f(\theta^{(i)}) \quad \ldots\ldots (14)$$

Here, Monte Carlo approximation $\hat{J}_N$ is a consistent estimator of the true value of J such that, as $N \rightarrow \infty$, $\hat{J}_N \rightarrow J$ in probability.

This works due to the weak law of large numbers for independent and identically distributed (iid) data. However, if the draws generated are not independent, as in our case, we can still sample draws that are dependent in a specific way from the posterior distribution $P(\theta|Y)$ using a Markov chain.

2.3.2 Markov Chain

A Markov chain is as a stochastic process in which given the present state, future states are independent of past states. A stochastic process is a consecutive set of random (not deterministic) quantities defined based on some known state space.

If we consider a draw of $\theta^{(t)}$ to be a state at iteration t, where t is a time component, the next draw $\theta^{(t+1)}$ in a Markov chain is dependent only on the draw $\theta^{(t)}$ and not on any past draws. This satiates the Markov property (or is Markovian in nature). A Markov chain will produce a large number of draws of θ that are each at least slightly dependent on the previous draw. Thus, θ jumps randomly around the parameter space and each new location depends on the previous location through the most recent location only. The basic principle on which the jumping takes place is governed by a mechanism known as the transition kernel. This mechanism is chosen in a particular way to ensure that the sequence has the joint posterior density as its stationary distribution. In our study, the Metropolis algorithm and the Gibbs sampler algorithm are two techniques that define different transition kernels.

2.4 Metropolis Algorithm

The Metropolis algorithm is a special case of the Metropolis-Hastings technique. It generates a Markov chain of values drawn from a target distribution. This is done via a proposal distribution which proposes draws that are either accepted or rejected. The proposal distribution is given by $\theta_{proposal} \sim N(\theta^{(t-1)}, \sigma_i)$. Here, the initial standard deviation, σ_i, for different DCA models is chosen to acquire good mixing for the MCMC simulations as given by Gonzalez et al., 2012. These standard deviation values are shown in **Table 3** below.

Method	Parameter	σi
Arps	Ln(qi)	0.2
	b	0.2
	Ln(Di)	0.4
PLE	Ln(qi)	0.2
	Ln(Dhat)	0.4
	ln(D∞)	0.2
	n	0.4
SEPD	Ln(qi)	0.2
	Ln(η)	0.4
	Ln(τ)	0.2
Duong	Ln(qi)	0.2
	a	0.2
	m	0.2
LGA	Ln(k)	0.4
	n	0.2
	a	0.4

Table 3: Starting values for standard deviation for proposal distribution in DCA models

We start with presetting an initial parameter value $\theta^{(0)}$ from the prior distribution. The proposal distribution proposes a new candidate $\theta_{proposal}$ value from its distributions which is centered on the previously sampled value. $\theta_{proposal}$ replaces the current candidate value $\theta^{(t-1)}$ if accepted. Acceptance or rejection of $\theta_{proposal}$ depends on an acceptance ratio. This acceptance ratio is the

ratio of the posterior probabilities of $\theta_{proposal}$ and $\theta^{(t-1)}$. If $\theta_{proposal}$ has better posterior probability than $\theta^{(t-1)}$, it is definitely accepted. Otherwise, a random uniform number U between 0 and 1 is drawn and $\theta_{proposal}$ is accepted if U is smaller than the acceptance ratio. However, if U is greater than the acceptance ratio, then $\theta_{proposal}$ is rejected and the current value $\theta^{(t-1)}$, is reused in the next iteration. Therefore, if the proposed value is accepted, we move to a new position, else, we stay in the same position until a new proposed value is accepted.

If the Markov chain formed is long enough and certain mild regularity conditions hold, the Metropolis algorithm is known to converge to the desired posterior distribution (Gong et al., 2011). The distribution of all such sampled values approximates the target distribution for a large number of iterations. Comparing **Fig. 2.1** and **Fig. 2.2** below, it can be seen that a distribution formed by a higher number of iterations represents the target distribution more accurately.

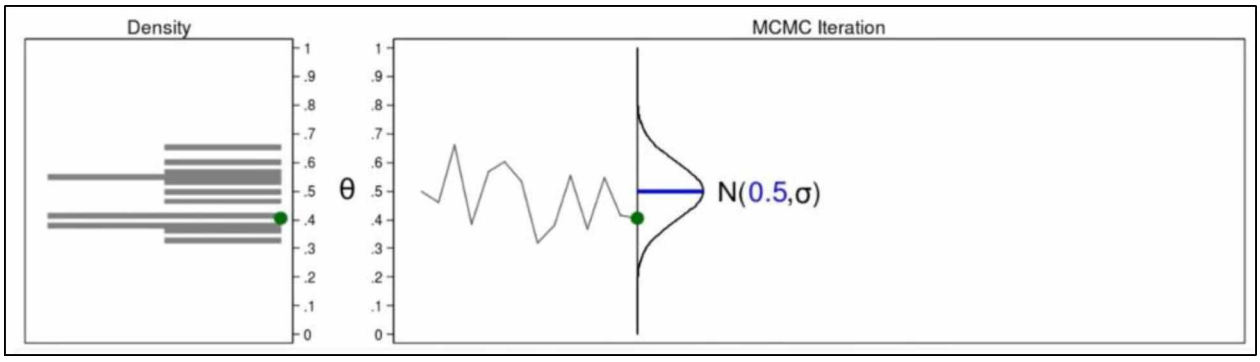

Fig. 2.1: Distribution formed by less number of samples drawn from proposal *N(0.5,σ)*

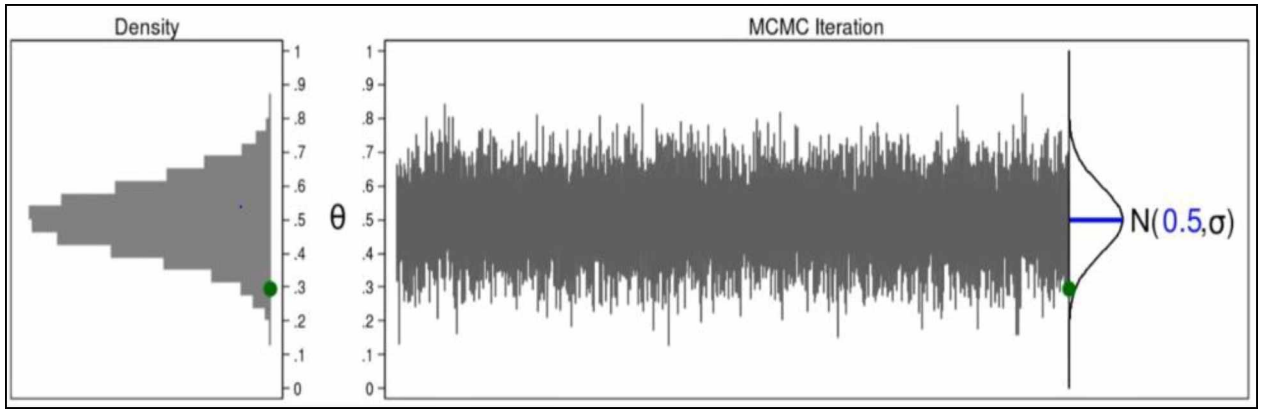

Fig. 2.2: Distribution formed by large number of samples drawn from the proposal N(0.5 ,σ)

Summary steps for the Metropolis algorithm:

1. Initialize:

   Select a starting parameter $\theta^{(0)}$ from the prior distribution at t=0.
2. At each iteration t=1,2,3…., draw a sample $\theta_{proposal}$ from a chosen symmetric distribution.
3. Calculate the acceptance ratio (R), such that; R is equal to the ratio of $P(\theta_{new}|Y)$ over $P(\theta^{(t-1)}|Y)$.
4. Accept or Reject:
   a. Produce a uniform random number U on (0, 1).
   b. If U < R($\theta_{new}, \theta^{(t-1)}$), $\theta proposed = \theta_{new}$

      Else, $\theta proposed = \theta^{(t-1)}$
5. Repeat step 2 and 3 until the threshold number of simulation runs are attained.

2.4.1 Application of Metropolis algorithm

We apply Bayesian inferencing with a MCMC Metropolis algorithm to the available DCA models like Arps (hyperbolic), SEPD, Duong, PLE and LGA. The underlying principle is the same as discussed in the Metropolis algorithm section. The process starts by selecting the monthly historical production data for a given well. We then divide the historical production data into two parts depending on the quantity of data available. The first part is used for forecasting with the DCA-Bayesian models and is known as the hindcast. The second part is used for validating the forecast predictions. We define the prior distribution and the initial proposal distribution based on the type of the DCA model as per Tables 1 and 2 respectively. The likelihood function is the same as given in Eq. 2. As we draw samples continuously during each iteration, a distribution of the parameters is estimated. We set 10%, 50%, and 90% quantiles to the sampled distribution to determine the P10, P50, and P90 prediction intervals. Comparing the estimates to the actual data (2nd part of the production history data), we measure the accuracy of the prediction in terms of percentage error between actual and predicted values. We also measure the P10-P90 interval width.

The aim for each well forecast is; 1) to have the actual production bounded within the predicted P10-P90 range, 2) to have a minimal prediction error, 3) to have a narrow P10-P90 interval width.

Although the number of iterations required for the convergence of each well data can vary, we set a burn-in period comprising of the first 2,000 iterations. We discard these 2,000 iterations. Samples are then collected after the burn-in period with the expectation that the Markov chain formed has converged during the burn-in period. As a standard, 20,000 iterations are simulated for each well forecast after the burn-in period. Computation for this methodology is carried out with the help of the R programming language (R project for Statistical Computing).

2.5 Gibbs Sampling using OpenBUGS

The Gibbs Sampler is a widely used MCMC technique. It is also the fundamental method underlying packages like BUGS (Bayesian inference Using Gibbs Sampler) and JAGS (Just Another Gibbs Sampler) which can be used with computational software like R. Similar to the Metropolis algorithm, the Gibbs sampler can be used to sample from a posterior distribution in two or more dimensions. Given all of the other parameters present in the model, this method repeatedly samples from the full conditional distribution of one parameter. In this method, all of the proposals ($\theta_{proposal}$ values) are accepted, and the Markov chain formed after a large number of iterations is guaranteed to converge asymptotically. The proposal distribution used in this method is the full conditional distribution of the true distribution.

Summary steps for Gibbs Sampling using OpenBUGS (Considering 3 random variables θ_1, θ_2, θ_3 of any DCA models):

1. Initialize:

   Select a random starting parameter $\theta^{(0)}$ from the prior distribution bracket (Table 2) at t=0.
2. At each iteration t=1,2,3,…, draw samples in the order:

a. Sample from full conditional distribution of $\theta_1^{(t)} \sim P(\theta_1 | Y, \theta_2^{(t-1)}, \theta_3^{(t-1)})$
b. Sample from full conditional distribution of $\theta_2^{(t)} \sim P(\theta_2 | Y, \theta_1^{(t)}, \theta_3^{(t-1)})$
c. Sample from full conditional distribution of $\theta_3^{(t)} \sim P(\theta_3 | Y, \theta_1^{(t)}, \theta_2^{(t)})$

in general we follow: $\theta_j^{(t)} \sim P(\theta_j | Y, \theta_1^{(t)}, \theta_2^{(t)}, \ldots, \theta_{j-1}^{(t)}, \theta_{j+1}^{(t-1)}, \ldots, \theta_{jn}^{(t-1)})$.

3. Record the updated values of θ_1, θ_2 and θ_3 and repeat the above steps until a threshold number of simulation runs are attained.

2.5.1 Application of Gibbs Sampling using OpenBUGS

For our study, we apply the MCMC Gibbs Sampler method to the same set of DCA models as in the Metropolis method. We defined the prior distribution and the likelihood function in the same manner as in the case of the Metropolis algorithm and used the open-source software OpenBUGS to carry out the sampling process mentioned above. We utilized the R programming language to integrate the results from the OpenBUGS software. The number of iterations and burn-in value limits are kept the same as in Metropolis, so that the two methods can be used to compute the uncertainty in an identical manner.

2.6 Summary of key differences between the Metropolis algorithm and the Gibbs sampler

a. A direct comparison between the Metropolis algorithm and the Gibbs sampler is only possible provided same priors are used for each algorithm and convergence is obtained from a large number of samples drawn from the posteriors.
b. In theory, both Metropolis and Gibbs sampler algorithm should converge to the same posterior, however, one algorithm may converge faster than other.
c. Gibbs sampler accepts all the proposal values as it draws samples from the conditional distribution of one variable over all other variables at a time. Metropolis algorithm accepts or rejects proposed values depending on the acceptance ratio.
d. Using Gibbs sampling we can achieve a faster convergence of the sampled chain if the conditional distribution of each random variable with respect to other variables is known

or derived easily. If conditional distributions are difficult to derive, the Gibbs sampler method may not prove to be a convenient sampling technique.

e. The Metropolis algorithm permits the proposed candidate to take big jumps within the set priors, this can help provide more flexibility to tune the jumps and ease up parameter mixing as compared to the Gibbs sampling.

Fig. 2.3 below, provides a general flowchart to the likelihood-based Metropolis algorithm and the Gibbs sampler method.

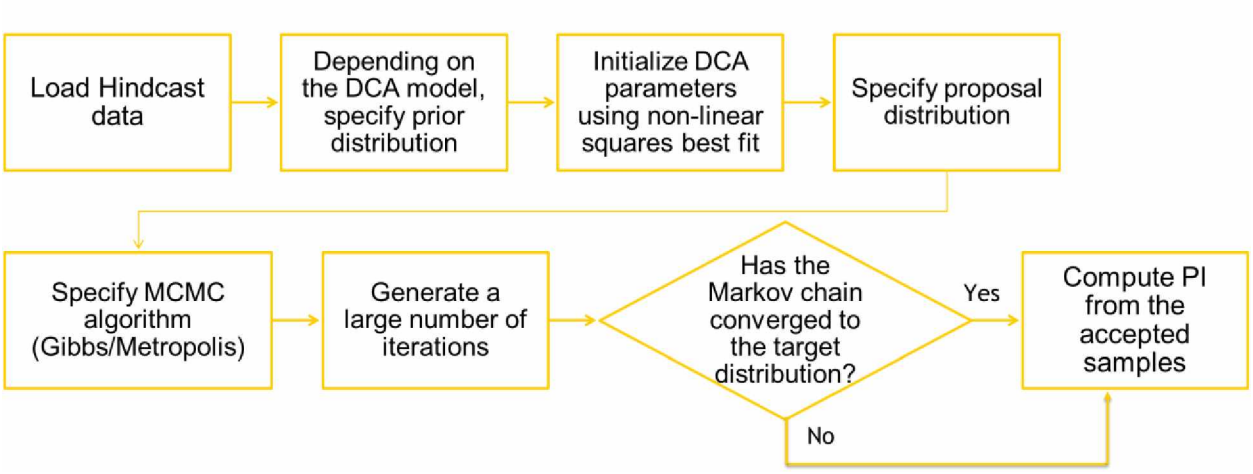

Fig. 2.3: Flowchart for the Bayesian MCMC method using Metropolis algorithm or Gibbs sampler

2.7 Approximate Bayesian Computation (ABC)

Another method used to predict the posterior distribution of model parameters rooted in Bayesian statistics is the ABC technique. Although the MCMC technique is theoretically well-established, its significance is centered on the implementation of the likelihood function. This is because the likelihood function is used to portray the probability of the observed data and helps to quantify the support lent to particular values of parameters. The formulation of the likelihood function for

simple models can be relatively simple, but for many complex models, it can be a complicated process making the statistical technique computationally expensive.

The ABC technique is used to bypass the requirement of a likelihood function while approximating the posterior. It is considered to be quicker than the MCMC techniques since the likelihood is not evaluated directly but replaced with an approximation that is usually easier to calculate (Paryani, 2015).

The method involves three essential elements: 1) the prior distribution, 2) the summary statistics, and 3) the DCA model. This method as applied in this work depends on the principle of rejection sampling. During each iteration, a set of parameters is drawn from the prior distribution. Based on the DCA model in use, production rate at the given time step is estimated. Then the predicted production is compared to the actual production. If the distance measured between the actual and the predicted data is beyond a set threshold, the rejection sampling mechanism rejects the sampled set of parameters. A collection of all the accepted samples form a chain as in the case of likelihood-based methods and is used to determine uncertainty intervals P10, P50, and P90. A critical difference between the likelihood-free ABC method and the likelihood-based MCMC method is that the samples drawn in the ABC method at every iteration are not dependent on each other.

Summary steps for ABC:

1. Sample a set of parameter values (θ_i) from the prior distribution at t=0.
2. Using the sampled parameter values θ_i, simulate a data set D_{hat} based on the DCA model.
3. Compare the summary statistics of the simulated D_{hat} to the summary statistics of the observed data D.
4. If the summary statistics of the generated D_{hat} are too dissimilar to the summary statistics of the observed data D, the sampled parameter value is discarded. (Acceptance tolerance $\varepsilon > 0$ is used for this step).
5. Repeat the above steps until a threshold number of simulation runs are attained.

2.7.1 Application of ABC

The application of the ABC method is also similar to the likelihood-based methods, where the data is divided to set the hindcast number of months for the ABC analysis and the remaining data is used to validate the forecast. The ABC method is applied in combination with the known DCA models like Arps hyperbolic, SEPD, Duong and LGA. We define the prior distribution in the same manner as the likelihood-based methods (given by Table 1). A set of parameter values (samples), randomly drawn from the prior distributions form the simulated production history data set. For our study, we sample 100,000 simulated data sets. Summary statistics used for comparing the simulated data to the actual data are the mean, median absolute deviation and standard deviation. Simulated data sets that are not within the set threshold limits are rejected. The maximum threshold value used is 0.01, which means only 1% difference in the summary statistics is considered acceptable. All the accepted simulated parameters then form a distribution and are used for uncertainty analysis and reserve forecasting.

Note that in this study, the ABC method is not applied to the PLE model as the results obtained were not satisfactory. The main reason for this inadequacy might be related to the higher number of parameters (4) that are varied in the PLE model as compared to the other DCA models (3).

We use R statistical software with the 'abc' package (Csillery et al., 2012) to perform this computation. **Fig. 2.4** below, provides a general flowchart to the likelihood-free ABC method.

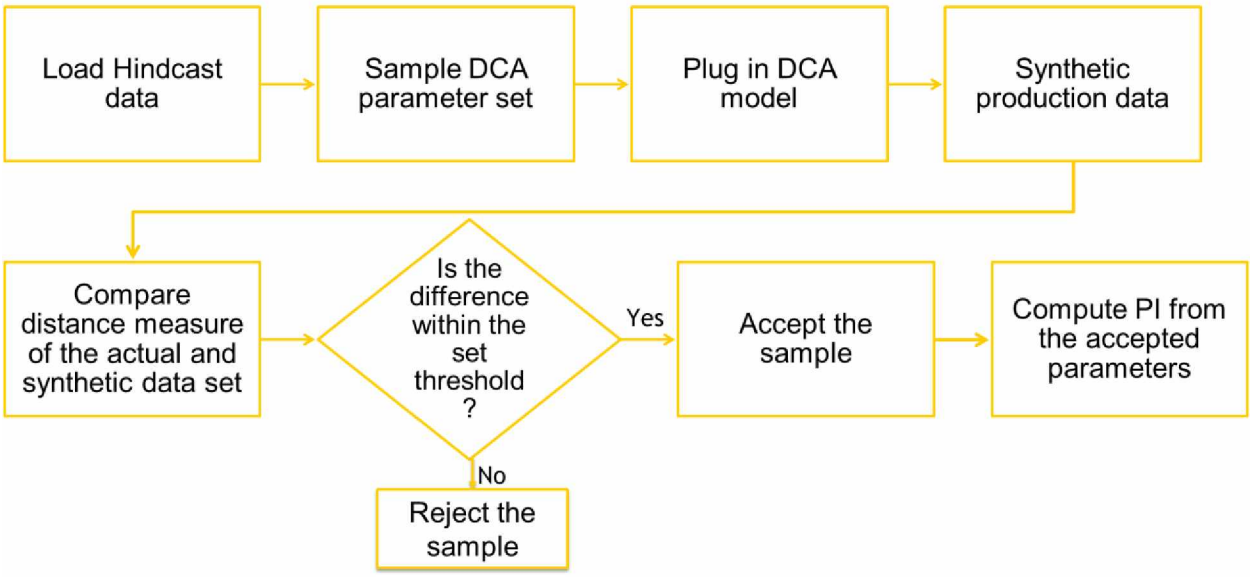

Fig. 2.4: Flowchart for Bayesian ABC technique

2.8 Validation of the methodology

In order to validate the techniques used in this study, we compare our reserve forecast and uncertainty estimation results to the reserve forecast and uncertainty estimation results generated in the Gong et al. (2014) paper (see **Fig. 2.5**). Uncertainty was quantified using the same data set by applying the Arps model to the Bayesian PDCA technique for the likelihood-based Metropolis algorithm (see **Fig**. **2.6**) and Gibbs sampler method (see **Fig. 2.7**), and the likelihood-free ABC method (see **Fig**. **2.8**). The number of months used as hindcast in all the following methods was 45. The burn-in period was 2,000 iterations and the sample distribution was produced using 20,000 iterations.

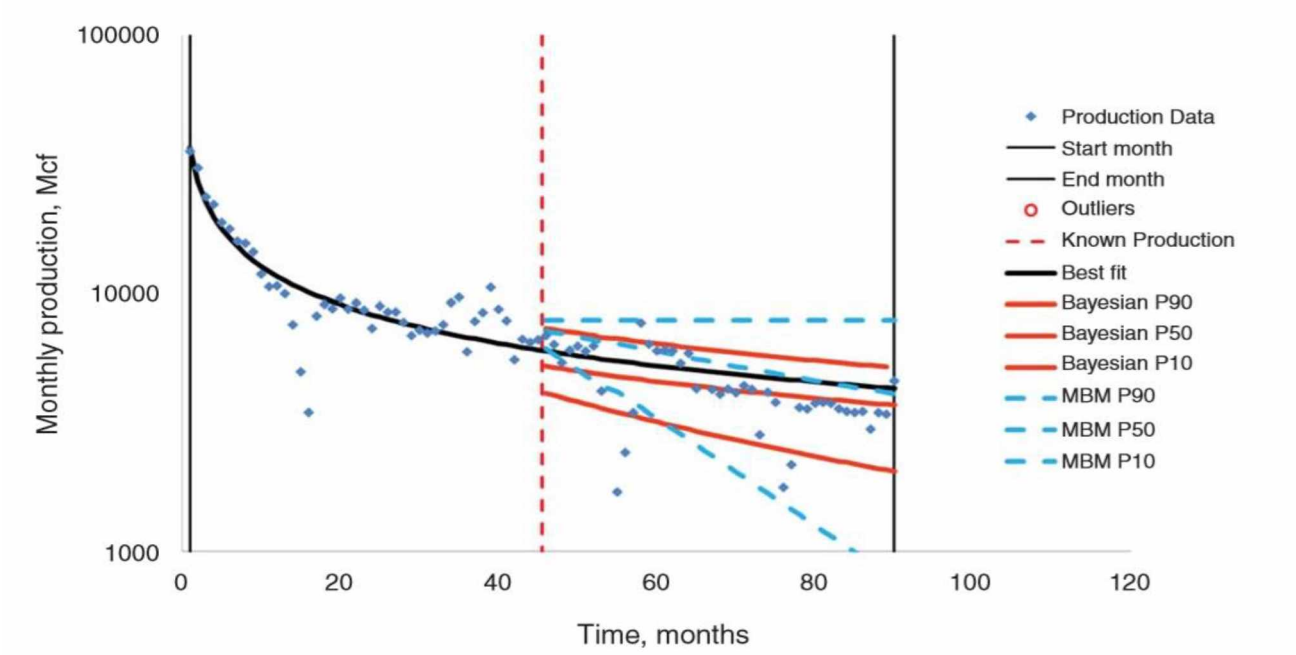

Fig. 2.5: Probabilistic forecast (Gong et al., 2014)

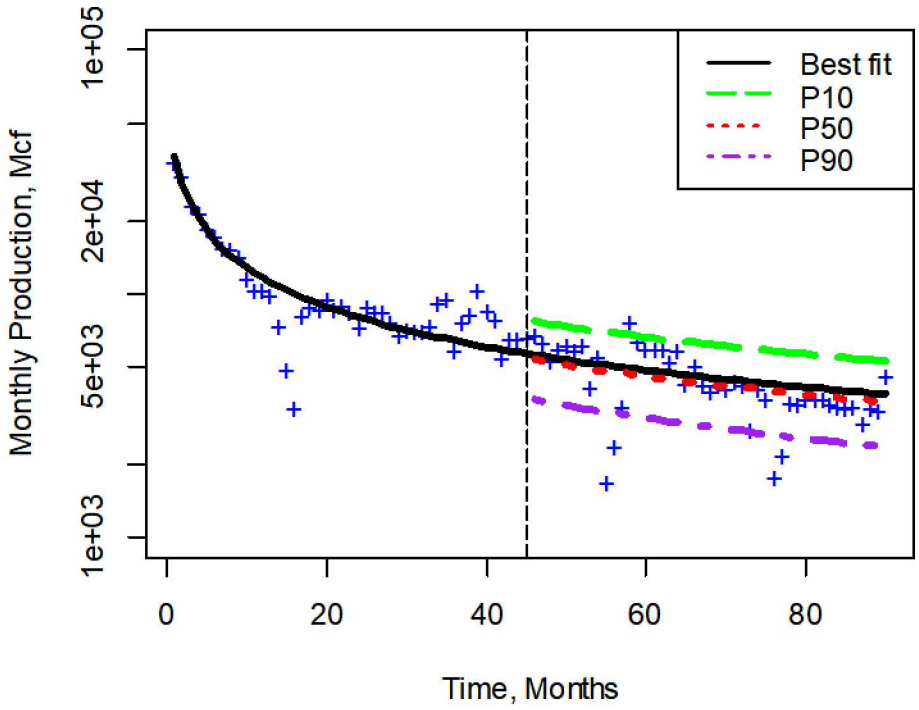

Fig. 2.6: Probabilistic forecast using Metropolis algorithm

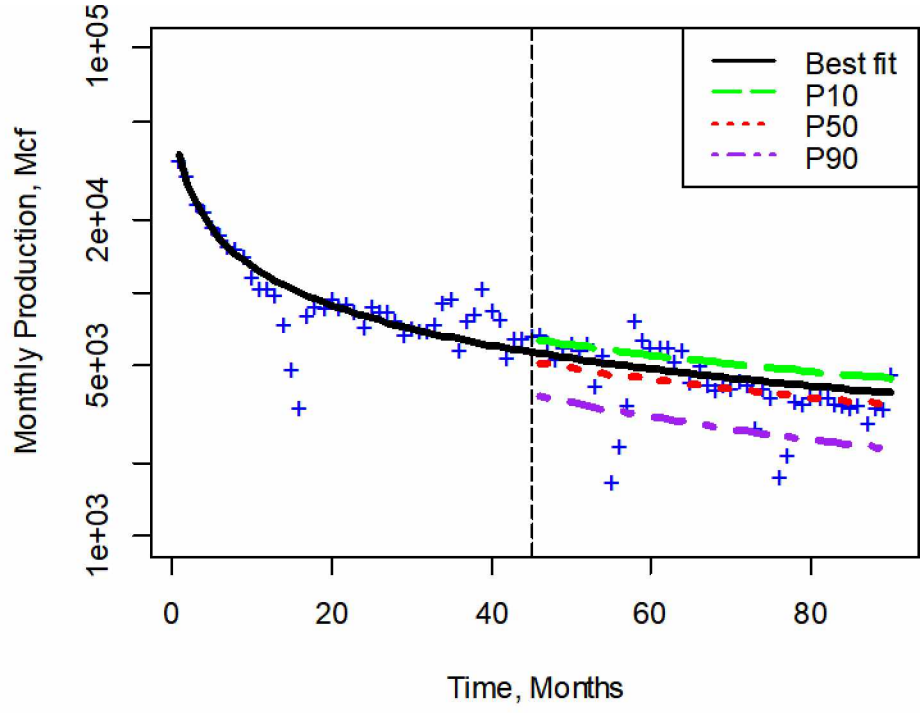

Fig. 2.5: Probabilistic forecast using Gibbs sampler

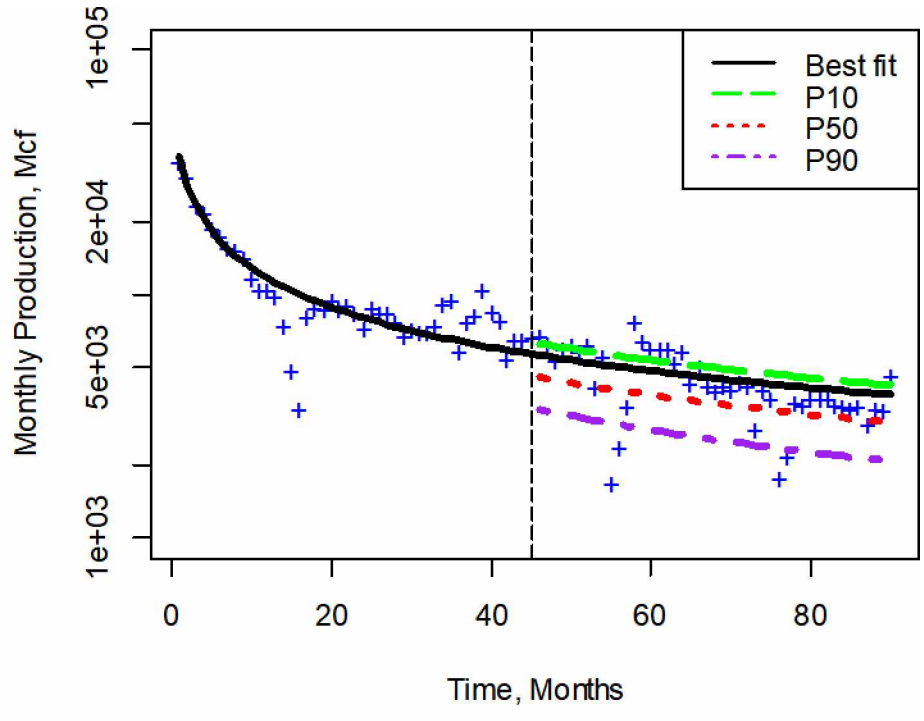

Fig. 2.6: Probabilistic forecast using the ABC method

2.9 Convergence Diagnostics:

In the case of Bayesian inferencing, the convergence is said to occur when the Markov chain produced with the help of the sampling process converges to the posterior distribution of interest. It is challenging to investigate convergence as it is in the form of distribution and not individual point estimates. As of now, there exists no single method which can technically guarantee the convergence of a Markov chain. Thus, the best bet is to use methods that can provide evidence against the non-convergence of the Markov chain. There are diagnostic methods and plots mentioned below which can help to assess the convergence.

2.9.1 Trace plot

One of the simplest tools to visualize convergence is a trace plot. A trace plot is a time series plot of the parameter values generated from the Markov chain at every single iteration. A separate trace plot for each parameter of the given model can be generated to assess its convergence separately. If the plot is centered on a constant mean, it indicates convergence. Likewise, if the plot forms a clear pattern or trend (for example, a constant increase/decline), it may be indicative of the non-convergent nature of the MCMC chain. Parameter values not traversing the sample space also indicate non-convergence.

Similarly, multiple chains of the underlying parameter values of a given model can be constructed and overlaid on the same graph to assess the quality of mixing. Poor quality of mixing is evidence of the chains being non-convergent.

As an example, a trace plot containing two posterior chains for the parameter 'q' from the Arps model is shown in **Fig. 2.9** below.

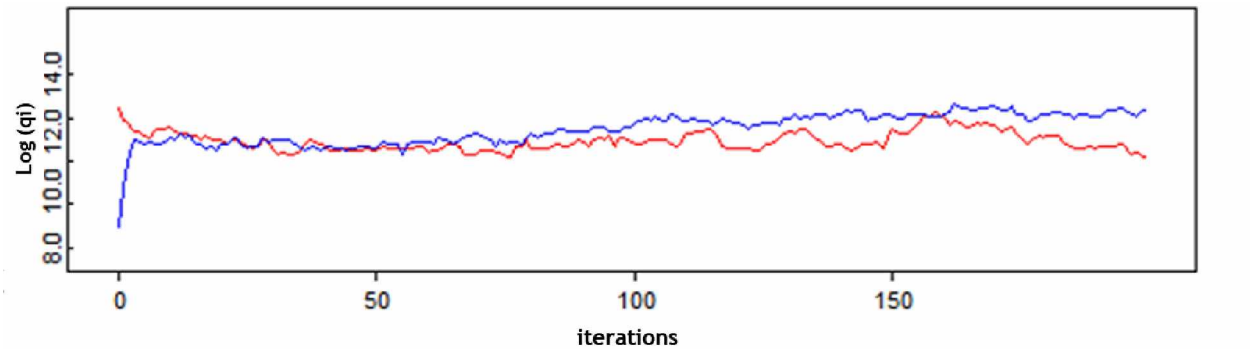

Fig. 2.7: Trace plot of parameter qi with 200 iterations

It can be seen that although the two chains show no apparent pattern, and traverse the sample space reasonably well, they are represented distinctly and do not show good mixing. This can be indicative of non-convergence.

If we compare the same plot (**Fig. 2.9**) to **Fig. 2.10** below, it can be seen that the chains traverse the sample space better and do not show an obvious distinction, demonstrating good mixing. Though both the trace plots (**Fig. 2.9** and **Fig.2.10**) are generated from the same set of hindcast data, convergence can only be validated in **Fig 2.10** because the chains are longer and exclude first few iterations while sampling the posterior.

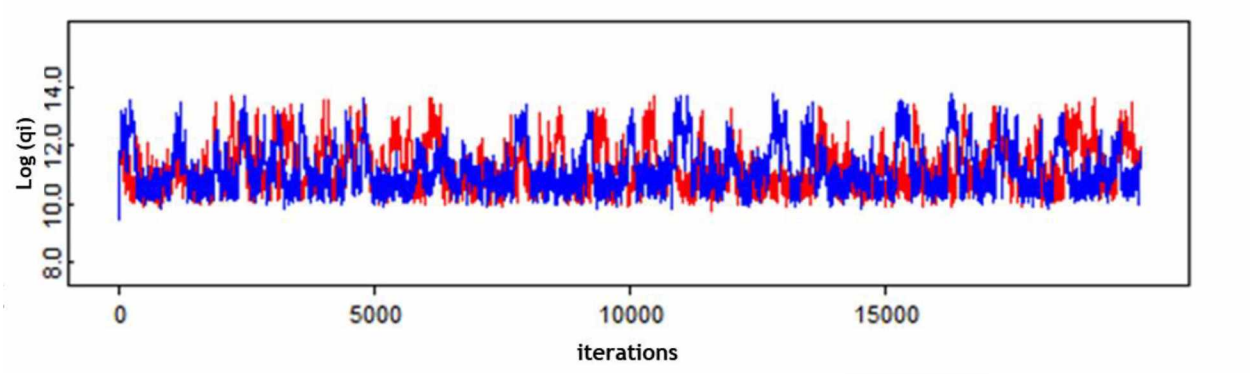

Fig. 2.8: Trace plot of parameter qi with 20,000 iterations

Trace plots and histogram plots for the validation techniques used in **Fig. 2.6**, **Fig 2.7** and **Fig. 2.8** are shown below in **Fig. 2.11**, **Fig. 2.12**, and **Fig 2.13** respectively. Additionally, sample trace plots for each of the sampling technique used in the study are included in the Appendix.

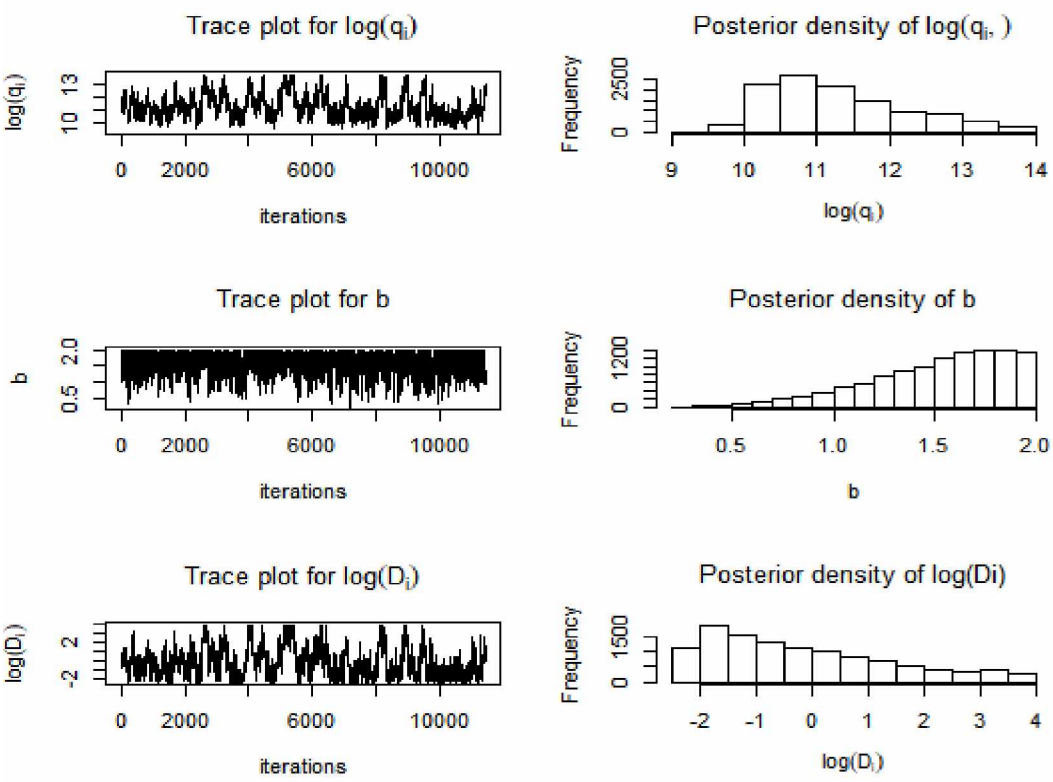

Fig. 2.11: Trace plots and Histograms of posterior distribution (Metropolis algorithm)

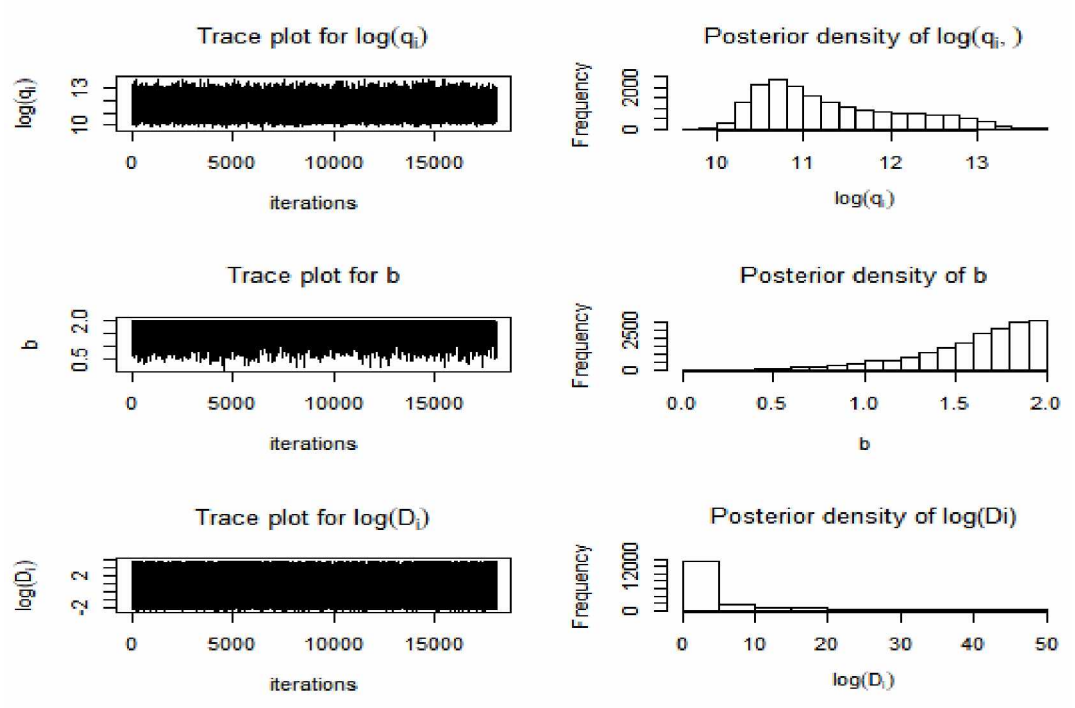

Fig. 2.12: Trace plots and Histograms of posterior distribution (Gibbs sampling)

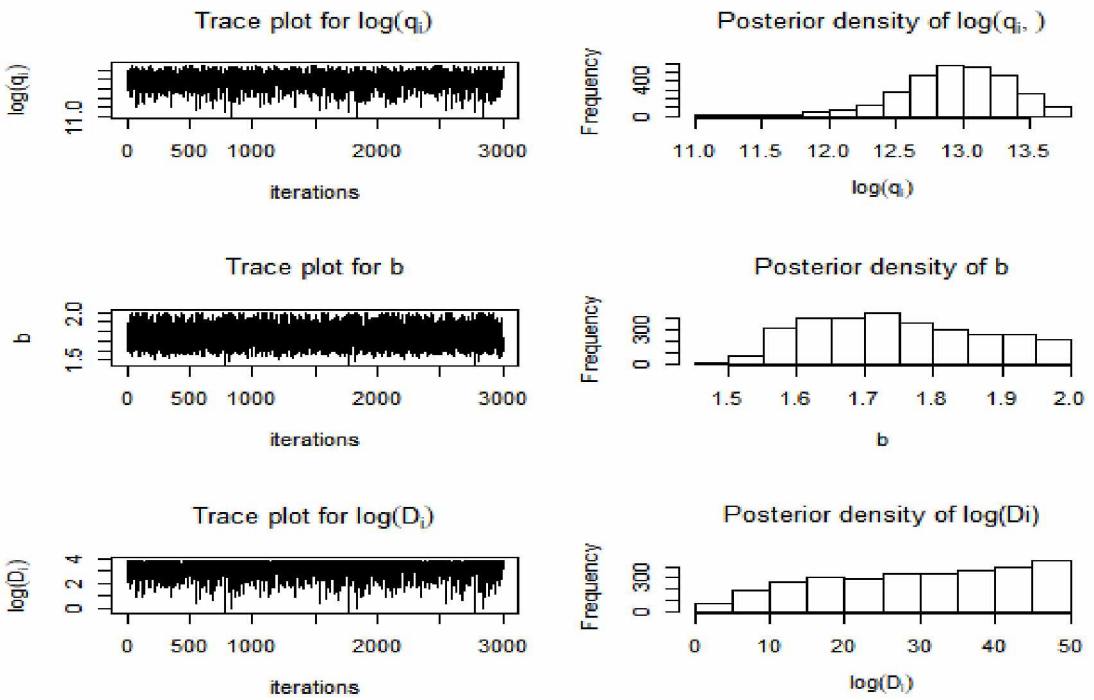

Fig. 2.13: Trace plots and Histograms of posterior distribution (ABC algorithm)

2.9.2: Gelman and Rubin convergence test

The Gelman and Rubin convergence test (Gelman and Rubin, 1992) is another method which can be used to provide evidence against non-convergence of an MCMC chain. The method requires the construction of two or more chains of sampled values of the parameters and uses only the second half of the total iterations. For example, if we construct two chains of 20,000 iterations each, the method will only use the last 10,000 from both the chains for its analysis.

We first calculate, the potential scale reduction factor (*PSRF*), based on Eq. 15.

$$PSRF = \sqrt{\frac{n-1}{n} + \frac{(m+1)B/n}{mW}} \quad \ldots\ldots(15)$$

In Eq. 15, B/n is the variance between the chains, n is the number of iterations used, m is the number of chains and W is the mean of variance within the chains. The variance between the chains (B/n) should continue to grow smaller relative to mean-variance within the chains, as the chains converge to a common target distribution. Thus, *PSRF* calculated should be closer to 1 (a large *PSRF* would indicate that the variance in between the chains is greater than variance within the chains).

To assess the convergence of a set of parameters simultaneously, a multivariate potential scale reduction factor (*MPSRF*) is used based on Eq. 16.

$$MPSRF \geq \max\{PSRF_i\} \quad \ldots\ldots(16)$$

Here i indexes the parameter in use. A 97.5% quantile of the MPSRF is computed for each parameter. According to the Gelman and Rubin convergence test, if the computed quantile has a value greater than 1.2, it represents non-convergence.

The Gelman and Rubin test results can be easily computed using the 'gelman.diag' function from package 'coda' (Plummer et al., 2006) in the R computational software. The function provides us with the median *PSRF* and its 97.5% quantile for each parameter. It also provides us with *MPSRF* value.

Fig. 2.14 below, shows changes in the median *PSRF* through the iterations for a posterior distribution of parameters qi, b, and D of the Arps model. The distribution constructed using two chains per parameter and 20,000 iterations generate a 97.5% quantile value 1 for parameters b and D. 97.5% quantile value generated for parameter q is 1.01. *MPSRF* is calculated to be 1. As the 97.5% quantile values of each parameter are less than 1.2 and as the *MPSRF* is 1, we can confirm that the Gelman and Rubin test fails to provide evidence against non-convergence.

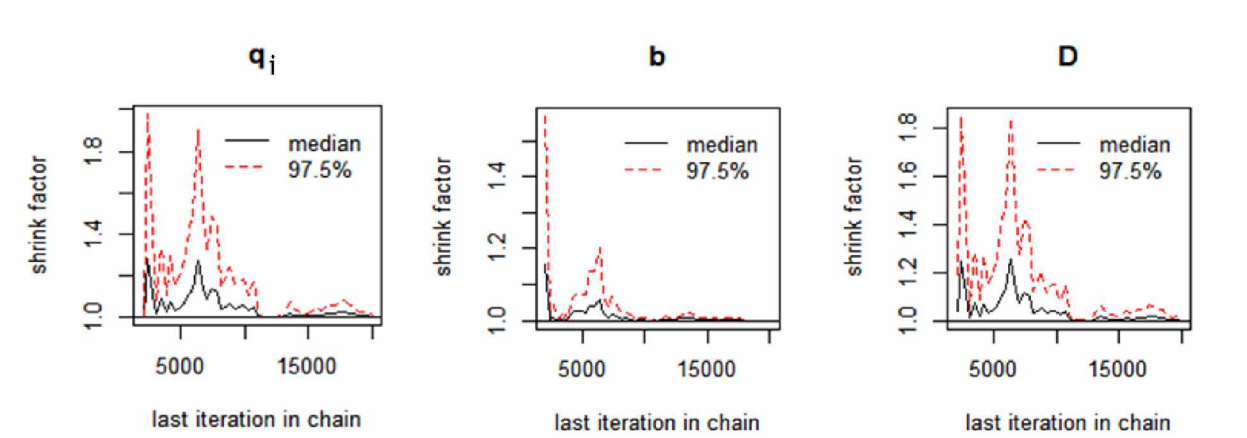

Fig. 2.14: Gelman and Rubin diagnostic plots for Arps model parameters

Chapter 3

RESULTS AND DISCUSSION

The Bayesian PDCA inferencing methodology using distinct sampling techniques is described in the previous chapter. It could successfully estimate the reserves and provide adequate uncertainty quantification. However, it is essential to test the reliability of these techniques. It is also crucial to test the performance of these techniques in circumstances where the available historical production data is limited; because, in literature, there have not been many methods shown to perform well in limited production history scenarios.

3.1 Permian Basin Study

In this chapter, we apply the reserve estimation and uncertainty quantification techniques discussed in the previous chapter to 74 oil and gas wells in the Permian Basin. Bayesian inferencing is applied using three sampling techniques with five deterministic models. The sampling techniques involve 1) the Gibbs sampler, 2) the Metropolis algorithm and 3) ABC sampling. Deterministic models involve 1) Arps model, 2) Duong's model, 3) SEPD model, 4) PLE model, and 5) LGA model. The production history data used for the oil and gas wells in this study were obtained from the Drillinginfo website (Drillinginfo, 1998). Various operators producing oil and gas report the monthly production history data to the state agencies in the subsequent months. This data is then checked for gross abnormalities and corrections are made if needed before it is available to the Drillinginfo users. The criteria for the Permian basin wells included a selection of wells drilled horizontally with a single stage or multi-stage fracturing. Minimum required production for each well was set to six and a half years or 78 months. Wells were chosen after the year 2003 and until the year 2018. Among the selected wells, some of the wells had been re-stimulated. For such wells, the portion of the production history after the re-stimulation was considered for the analysis, provided it satisfied the minimum production time criteria (at least 78 months of production).

Table 4 below, shows the number of wells from different regions of the Permian Basin used in the study.

Primary Basin	Sub Basin	County	No. wells	Production type
Permian	Delaware	Ward	22	Gas
	Midland	Midland	19	Gas
		Terry	14	Oil
		Upton	9	Oil
	Central Platform	Ward	10	Gas

Table 4: Well Statistics

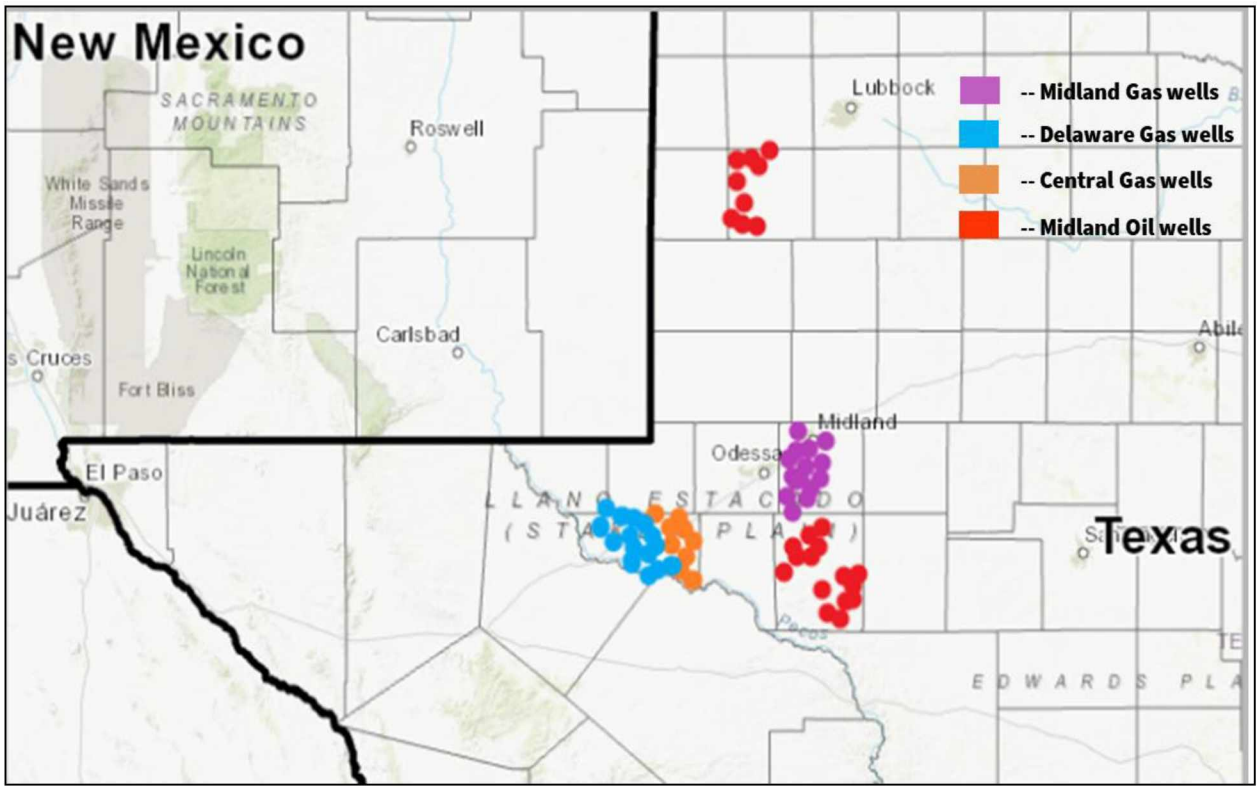

Fig. 3.1: Location of wells in the Permian Basin

The location of these wells in the Permian Basin is shown above in **Fig. 3.1**. Delaware gas wells are shown in blue, Midland oil and gas wells are shown in red and purple respectively and the Central Platform gas wells are shown in orange.

The objective here is to: 1) Calculate the Coverage Rate (CR) of the well production history data set for each hybrid model. CR is the percentage number of wells (out of the total wells) whose actual cumulative production falls within the predicted cumulative P10-P90 range. 2) Determine the hybrid model that generate the least prediction error. Prediction error for each well data set is calculated with the help of Eq. 16 below. 3) Determine the hybrid model that can generate the narrowest prediction interval bounds. Difference between the interval bounds for each well is calculated using Eq. 17 below. Once the interval bound width for each well is calculated, an average interval width is generated and used for further assessment for the given region. Note that in Eq. 16 and Eq. 17, the quantity 'Actual' refers to the actual/true cumulative production of the respective well.

$$error = \frac{|P50 - Actual|}{Actual} \quad \ldots\ldots(16)$$

$$Bound\ interval = \log(|P10 - Actual| + |P90 - Actual|) \quad \ldots(17)$$

Results for varying production history (6, 9, 12, 15, 30, 45, 60 months) for Delaware Basin, Midland Basin, and Central Basin Platform are represented in **Fig. 3.2 through Fig. 3.46**. Based on the observed model performances, these results are classified as satisfactory and excellent for 12 and 45 months respectively.

3.1.1 Delaware Basin Gas Wells

We applied Bayesian inferencing technique using hybrid models on 22 gas wells of the Delaware region. **Figs. 3.2 to 3.10.** represent the results for 1) the prediction error comparison **(Figs. 3.2, 3.3 and 3.4**), 2) CR comparison (**Figs. 3.5, 3.6 and 3.7**) and 3) interval width comparison (**Figs. 3.8, 3.9 and 3.10**) for Gibbs, Metropolis and ABC sampling respectively.

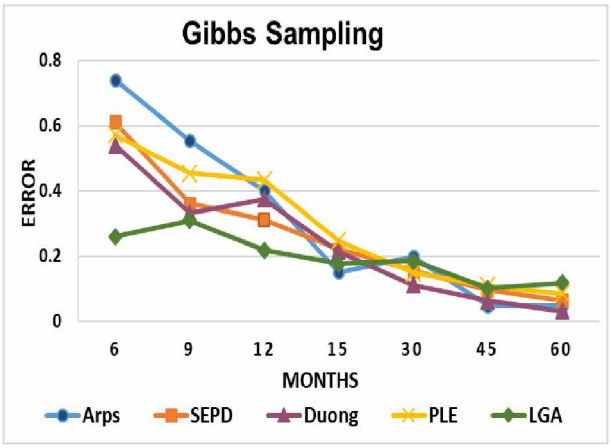

Fig. 3.2: Error plot for varying production history using Gibbs sampling in Delaware Basin

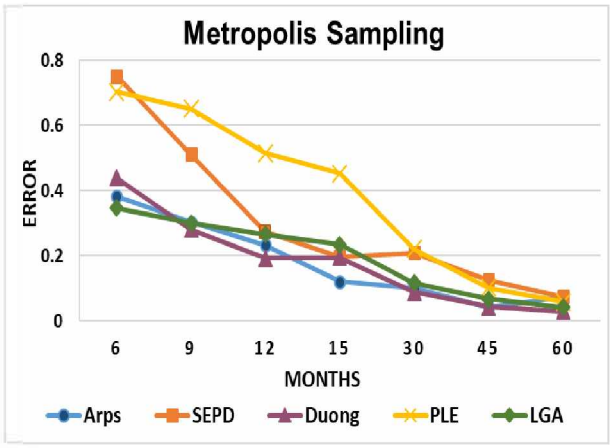

Fig. 3.3: Error plot for varying production history using Metropolis sampling in Delaware Basin

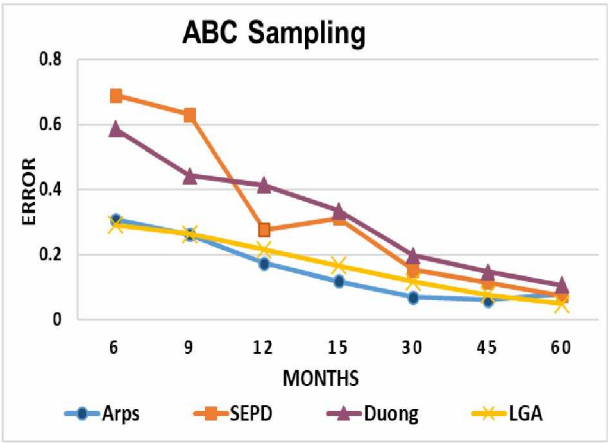

Fig. 3.4: Error plot for varying production history using ABC sampling in Delaware Basin

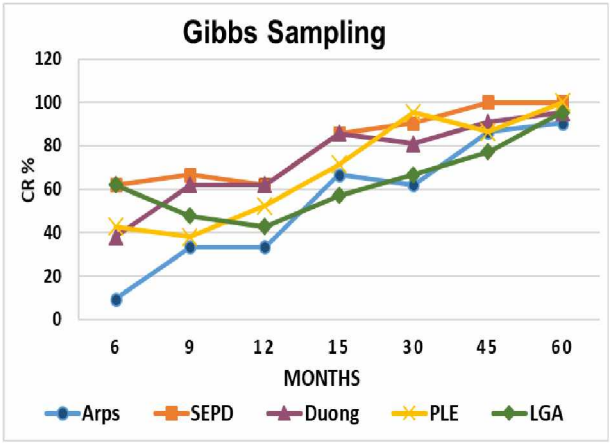

Fig. 3.5: CR plot for varying production history using Gibbs sampling in Delaware Basin

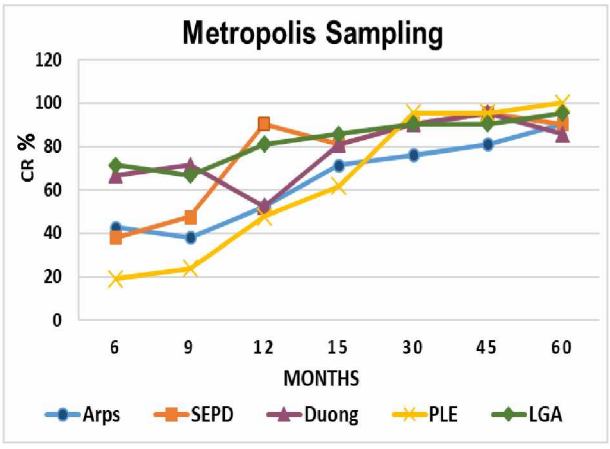

Fig. 3.6: CR plot for varying production history using Metropolis sampling in Delaware Basin

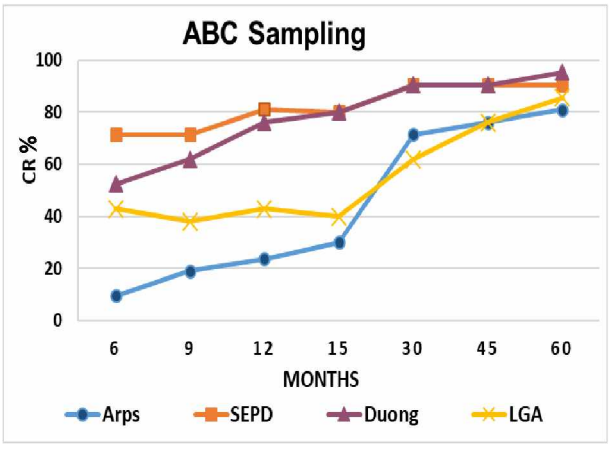

Fig. 3.7: CR plot for varying production history using ABC sampling in Delaware Basin

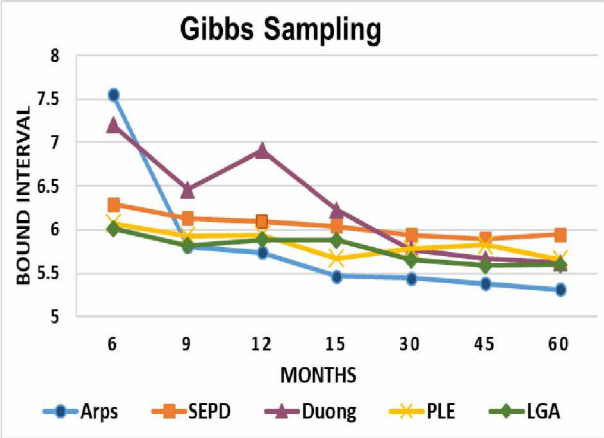

Fig. 3.8: Bound interval plot for varying production history using Gibbs sampling in Delaware Basin

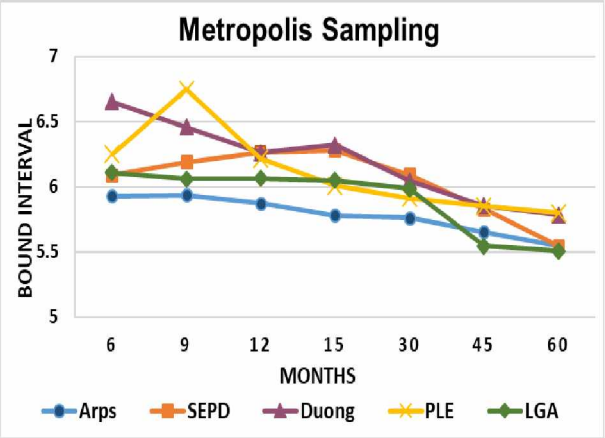

Fig. 3.9: Bound interval plot for varying production history using Metropolis sampling in Delaware Basin

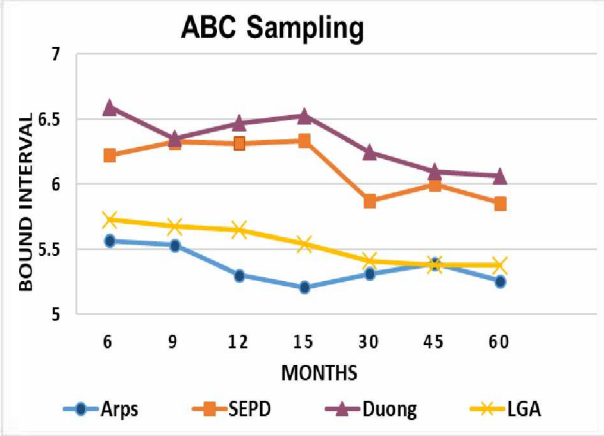

Fig. 3.10: Bound interval plot for varying production history using ABC sampling in Delaware Basin

For 12 months of available production history data, prediction error as low as 17.4% can be achieved using Arps-ABC hybrid model, CR as high as 90.47% can be achieved using SEPD-Metropolis hybrid model and interval width as low as 5.65 can be achieved using LGA-ABC hybrid model.

For 45 months of available production history data, prediction error as low as 4.2% can be achieved using Arps-Metropolis hybrid model, CR as high as 100% can be achieved using SEPD-Gibbs hybrid model and interval width as low as 5.38 can be achieved using Arps-Gibbs hybrid model.

3.1.2 Midland Basin Gas Wells

Further, we applied Bayesian inferencing technique using hybrid models on 24 oil and 19 gas wells of the Midland region. **Figs. 3.11 to 3.19** represent the results for the prediction error comparison (**Figs. 3.11, 3.12 and 3.13**), CR comparison (**Figs. 3.14, 3.15 and 3.16**) and interval width comparison (**Fig 3.17, 3.18 and 3.19**) for Gibbs, Metropolis and ABC sampling respectively.

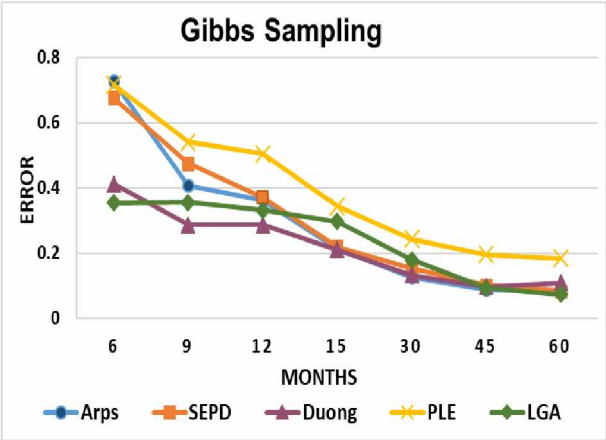

Fig. 3.11: Error plot for varying production history using Gibbs sampling in Midland Basin (Gas wells)

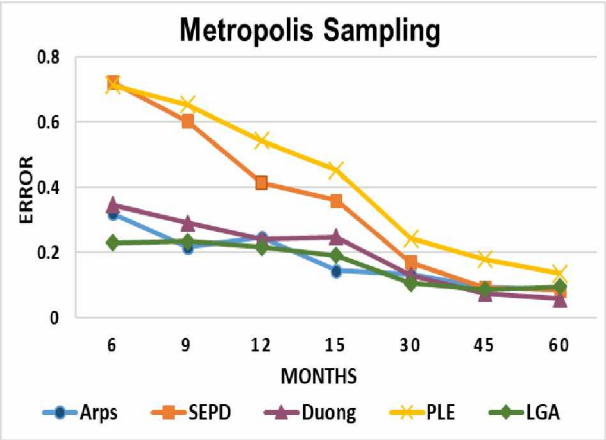

Fig. 3.12: Error plot for varying production history using Metropolis sampling in Midland Basin (Gas wells)

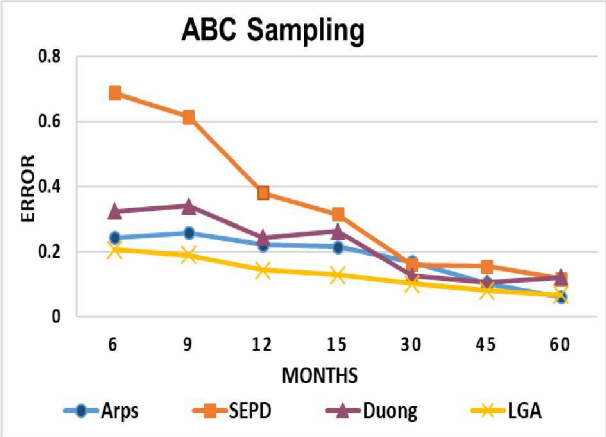

Fig. 3.13: Error plot for varying production history using ABC sampling in Midland Basin (Gas wells)

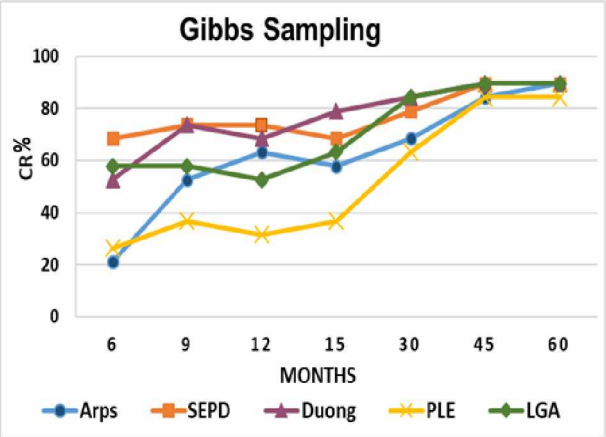

Fig. 3.14: CR plot for varying production history using Gibbs sampling in Midland Basin (Gas wells)

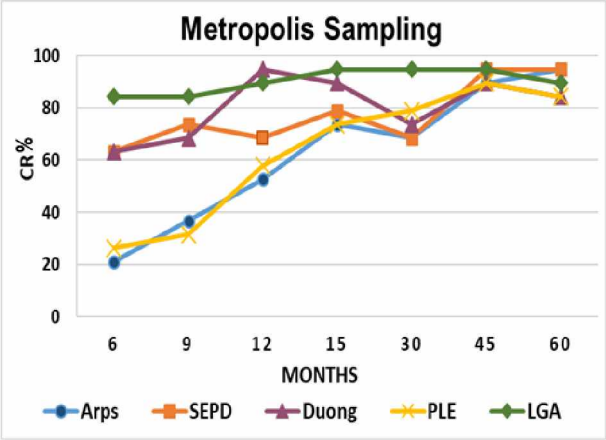

Fig. 3.15: CR plot for varying production history using Metropolis sampling in Midland Basin (Gas wells)

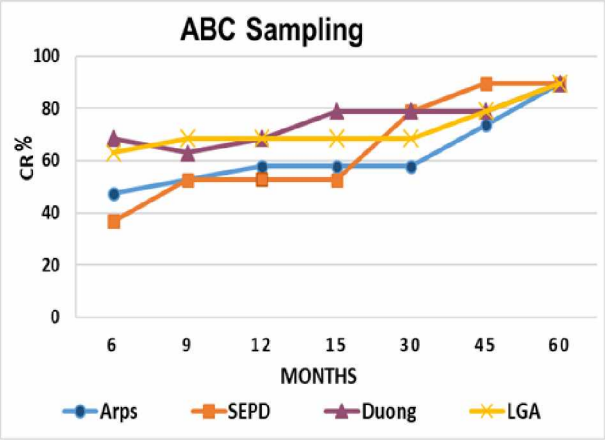

Fig. 3.16: CR plot for varying production history using ABC sampling in Midland Basin (Gas wells)

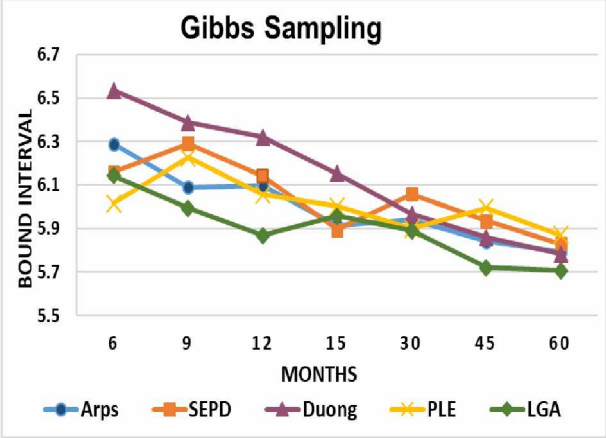

Fig. 3.17: Bound interval plot for varying production history using Gibbs sampling in Midland Basin (Gas wells)

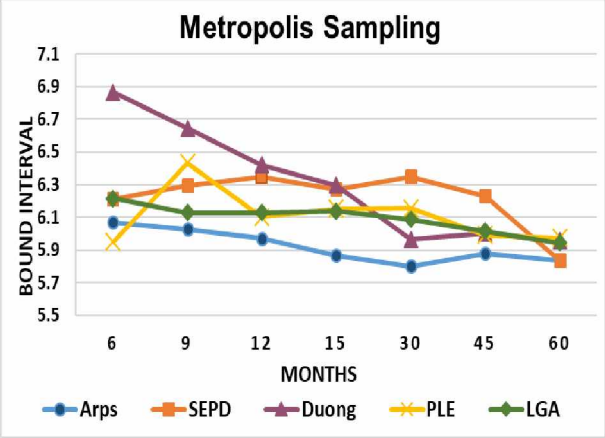

Fig. 3.18: Bound interval plot for varying production history using Metropolis sampling in Midland Basin (Gas wells)

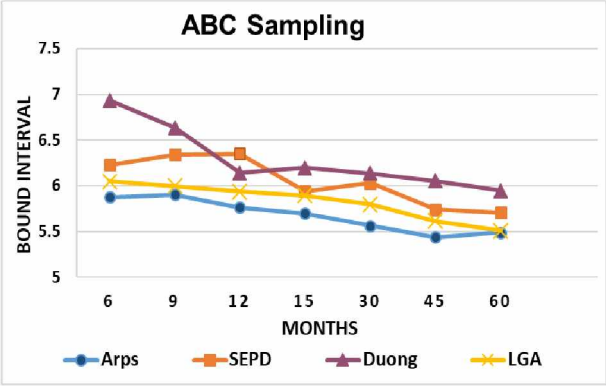

Fig. 3.19: Bound interval plot for varying production history using ABC sampling in Midland Basin (Gas wells)

For 12 months of available production history data, prediction error as low as 14.34% can be achieved using LGA-ABC hybrid model, CR as high as 89.47% can be achieved using LGA-Metropolis hybrid model and interval width as low as 5.76 can be achieved using Arps-ABC hybrid model.

For 45 months of available production history data, prediction error as low as 7.5% can be achieved using Duong-Metropolis hybrid model, CR as high as 94.74% can be achieved using SEPD-Metropolis hybrid model and interval width as low as 5.44 can be achieved using Arps-ABC hybrid model.

3.1.3 Midland Basin Oil wells

Figs. 3.20 to 3.28 represent the results for the prediction error comparison (**Figs. 3.20, 3.21 and 3.22**), CR comparison (**Figs. 3.23, 3.24 and 3.25**) and interval width comparison (**Figs. 3.26, 3.27 and 3.28**) for Gibbs, Metropolis and ABC sampling respectively.

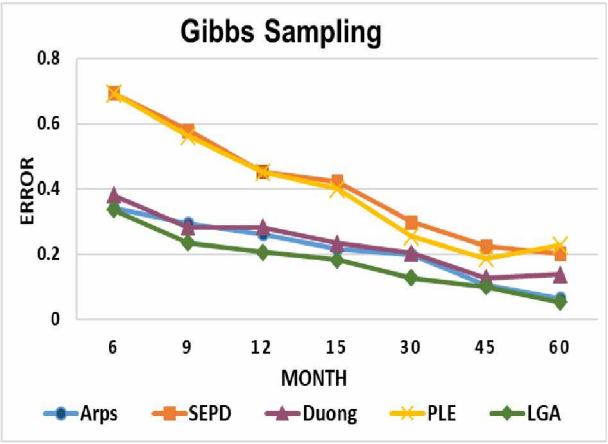

Fig. 3.20: Error plot for varying production history using Gibbs sampling in Midland Basin (Oil wells)

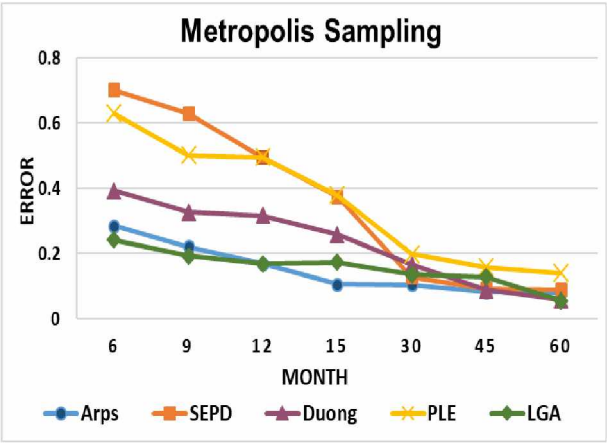

Fig. 3.21: Error plot for varying production history using Metropolis sampling in Midland Basin (Oil wells)

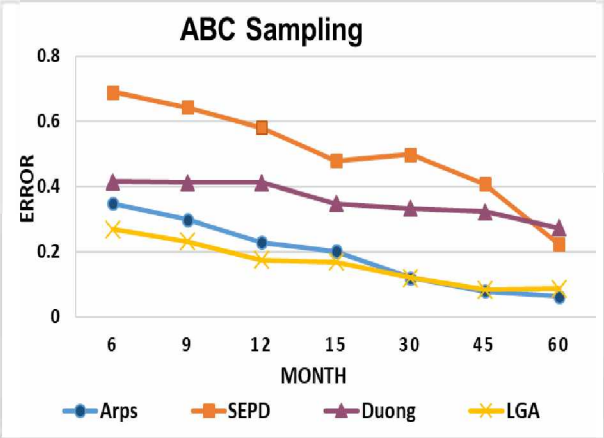

Fig. 3.22: Error plot for varying production history using ABC sampling in Midland Basin (Oil wells)

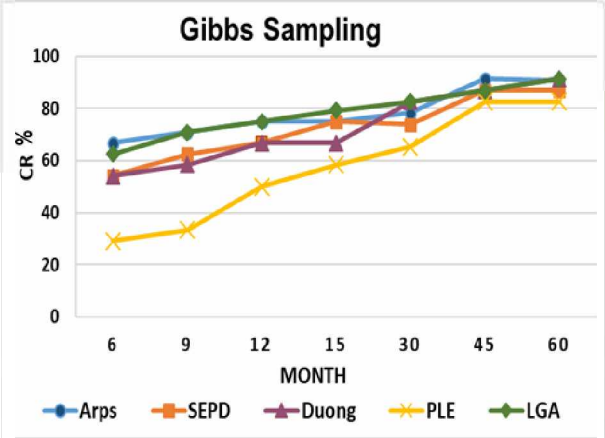

Fig. 3.23: CR plot for varying production history using Gibbs sampling in Midland Basin (Oil wells)

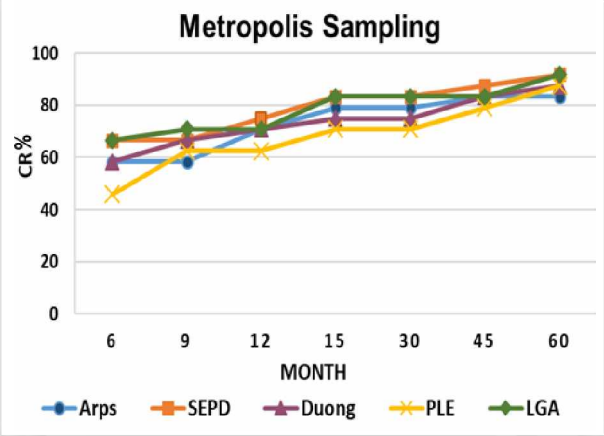

Fig. 3.24: CR plot for varying production history using Metropolis sampling in Midland Basin (Oil wells)

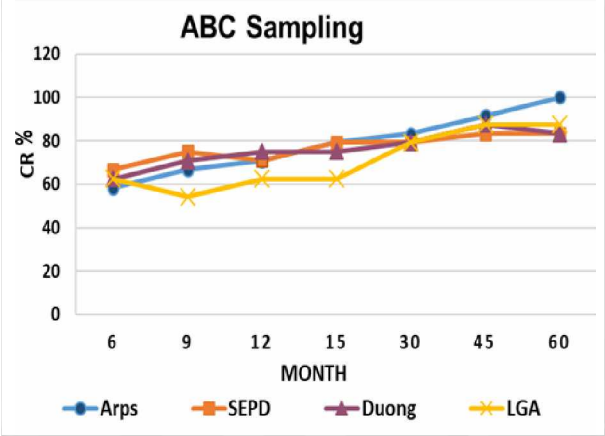

Fig. 3.25: CR plot for varying production history using ABC sampling in Midland Basin (Oil wells)

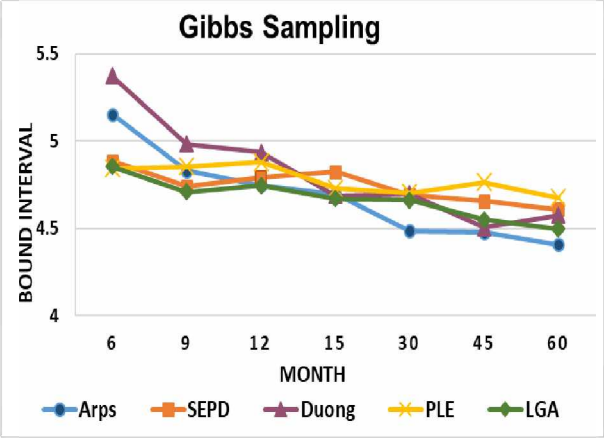

Fig. 3.26: Bound interval plot for varying production history using Gibbs sampling in Midland Basin (Oil wells)

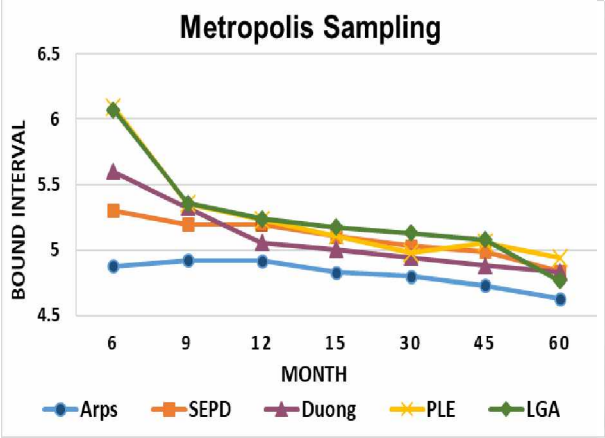

Fig. 3.27: Bound interval plot for varying production history using Metropolis sampling in Midland Basin (Oil wells)

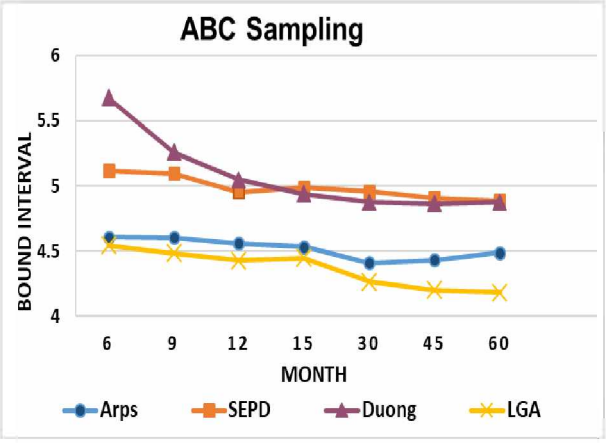

Fig. 3.28: Bound interval plot for varying production history using ABC sampling in Midland Basin (Oil wells)

For 12 months of available production history data, prediction error as low as 16.89% can be achieved using Arps-Metropolis hybrid model, CR as high as 75% can be achieved using SEPD-Metropolis, Arps-Gibbs, LGA-Gibbs, and Duong-ABC hybrid models and interval width as low as 4.42 can be achieved using LGA-ABC hybrid model.

For 45 months of available production history data, prediction error as low as 8% can be achieved using Arps-ABC hybrid model, CR as high as 91.70% can be achieved using Arps-ABC hybrid model and interval width as low as 4.20 can be achieved using LGA-ABC hybrid model.

3.1.4 Central Basin Platform Gas Wells

We applied Bayesian inferencing technique on using combined models 10 gas wells in the Central platform region. **Figs. 3.29 to 3.37** represent the results for the prediction error comparison (**Figs. 3.29, 3.30 and 3.31**), CR comparison (**Figs. 3.32, 3.33 and 3.34**) and interval width comparison (**Figs. 3.35, 3.36 and 3.37**) for Gibbs, Metropolis and ABC sampling respectively.

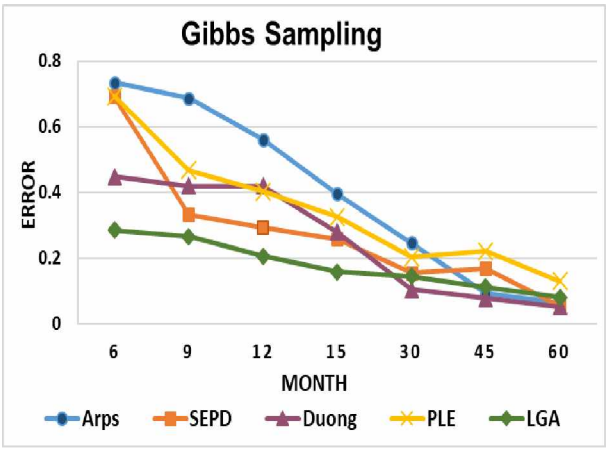

Fig. 3.29: Error plot for varying production history using Gibbs sampling in Central Basin Platform

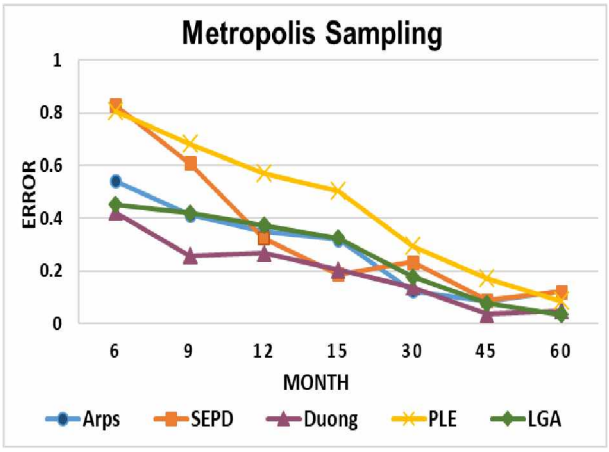

Fig.3.30: Error plot for varying production history using Metropolis sampling in Central Basin Platform

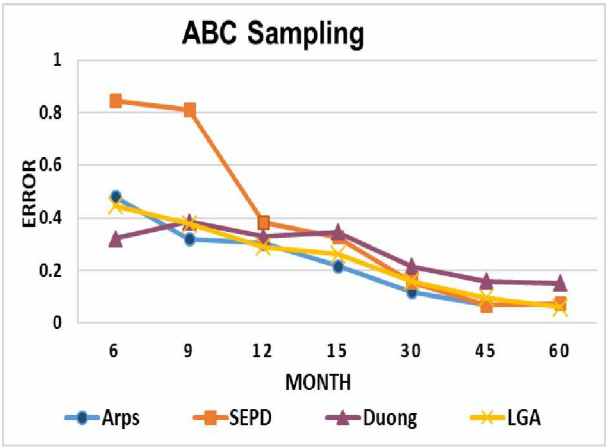

Fig. 3.31: Error plot for varying production history using ABC sampling in Central Basin Platform

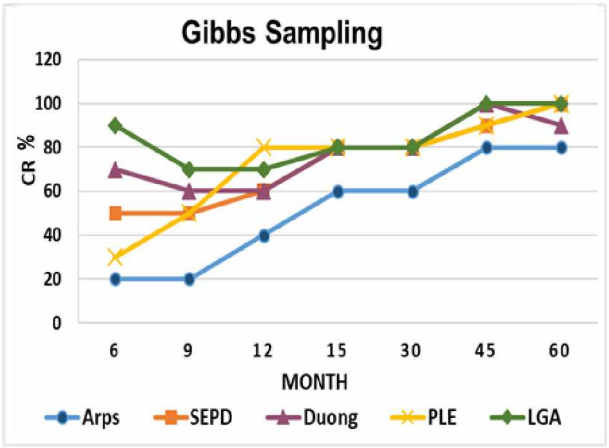

Fig. 3.32: CR plot for varying production history using Gibbs sampling in Central Basin Platform

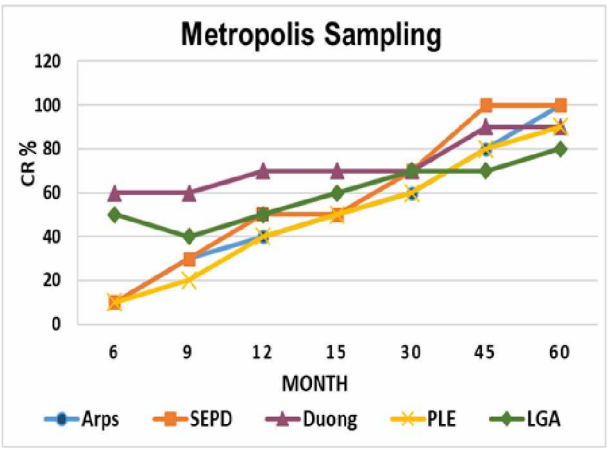

Fig. 3.33: CR plot for varying production history using Metropolis sampling in Central Basin Platform

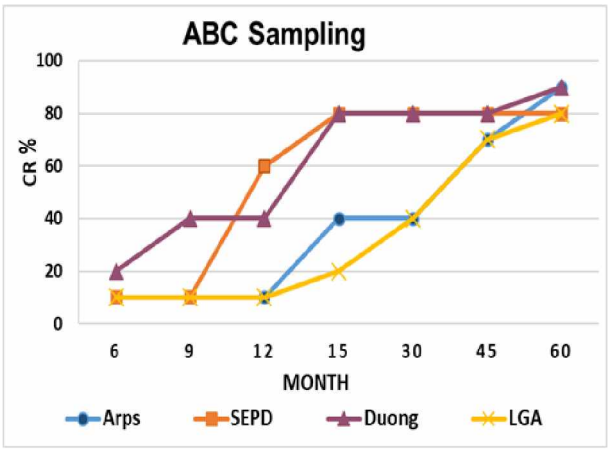

Fig. 3.34: CR plot for varying production history using ABC sampling in Central Basin Platform

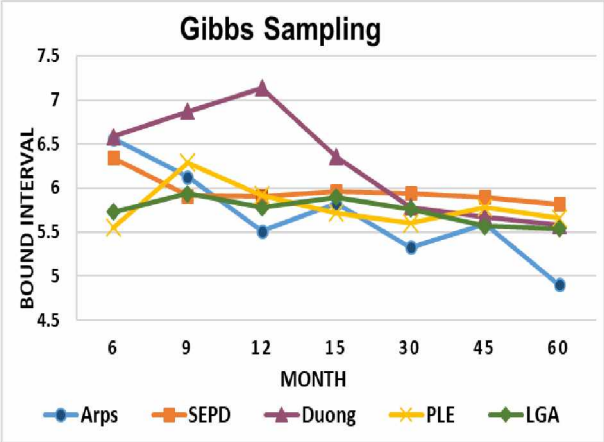

Fig. 3.35: Bound interval plot for varying production history using Gibbs sampling in Central Basin Platform

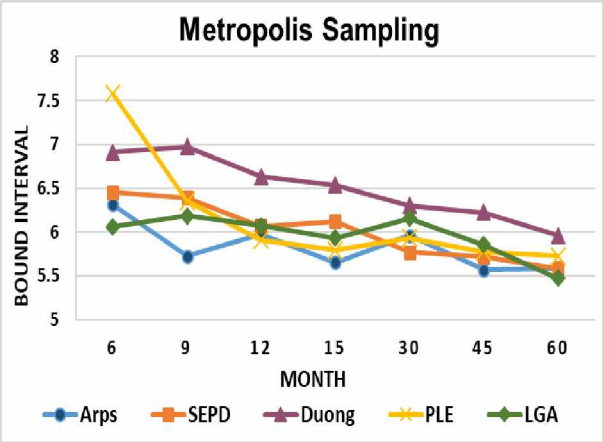

Fig.3.36: Bound interval plot for varying production history using Metropolis sampling in Central Basin Platform

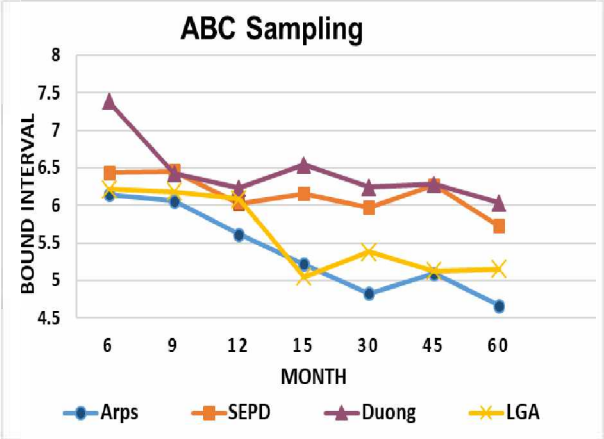

Fig. 3.37: Bound interval plot for varying production history using ABC sampling in Central Basin Platform

For 12 months of available production history data (hindcast), prediction error as low as 20.63% can be achieved using LGA-Gibbs hybrid model, CR as high as 80% can be achieved using PLE-Gibbs hybrid model and interval width as low as 5.51 can be achieved using Arps-Gibbs hybrid model.

For 45 months of available production history data (hindcast), prediction error as low as 3.6% can be achieved using Duong-Metropolis hybrid model, CR as high as 100% can be achieved using

Duong-Gibbs hybrid model and interval width as low as 5.09 can be achieved using Arps-ABC hybrid model.

3.1.5 Overall Permian Basin

Figs. 3.38 to 3.46 represent the results for the prediction error comparison (**Figs. 3.38, 3.39 and 3.40**), CR comparison (**Figs. 3.41, 3.42 and 3.43**) and interval width comparison (**Figs. 3.44, 3.45 and 3.46**) for Gibbs, Metropolis and ABC sampling respectively.

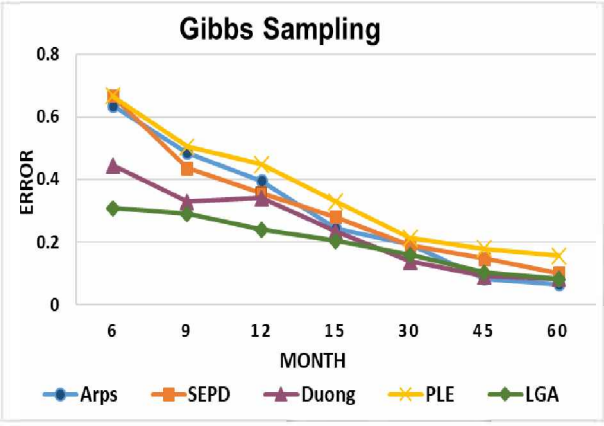

Fig. 3.38: Error plot for varying production history using Gibbs sampling in overall Permian Basin

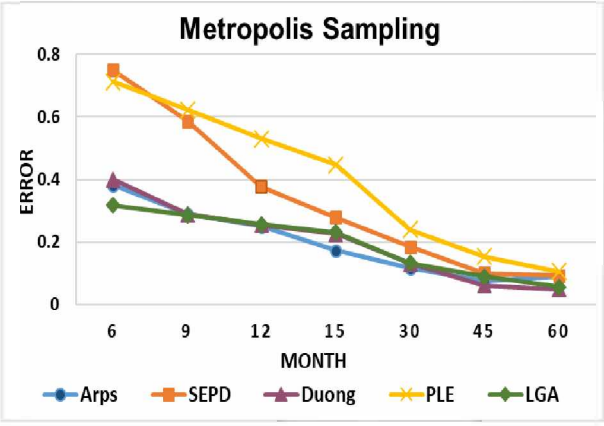

Fig. 3.39: Error plot for varying production history using Metropolis sampling in overall Permian Basin

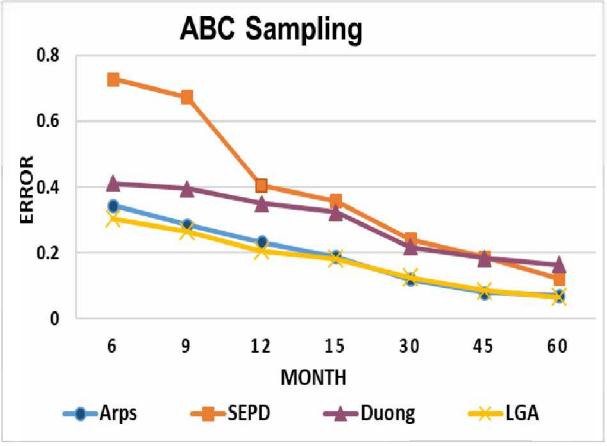

Fig. 3.40: Error plot for varying production history using ABC sampling in overall Permian Basin

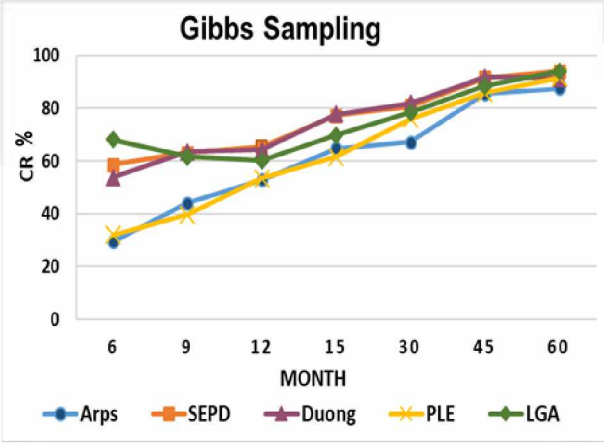

Fig. 3.41: CR plot for varying production history using Gibbs sampling in overall Permian Basin

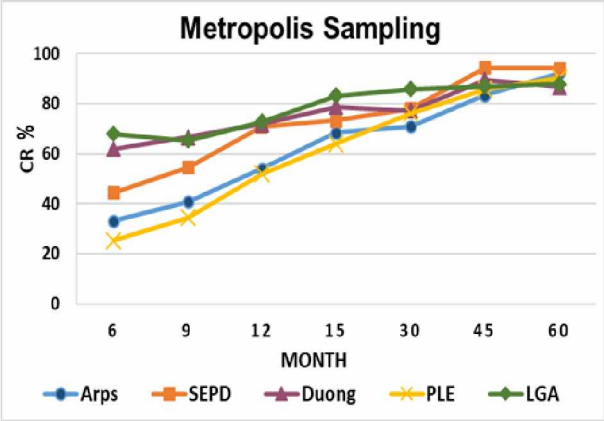

Fig. 3.42: CR plot for varying production history using Metropolis sampling in overall Permian Basin

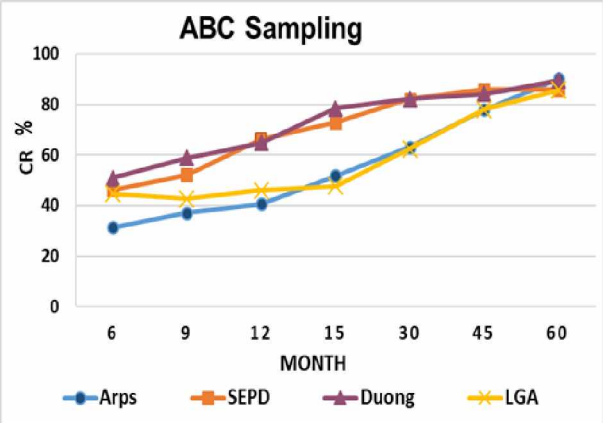

Fig. 3.43: CR plot for varying production history using ABC sampling in overall Permian Basin

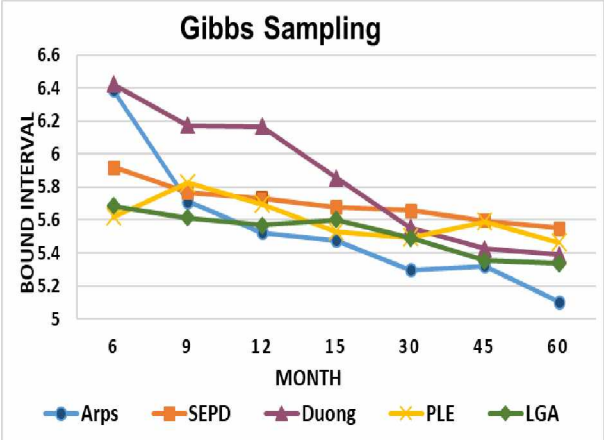

Fig. 3.44: Bound interval plot for varying production history using Gibbs sampling in overall Permian Basin

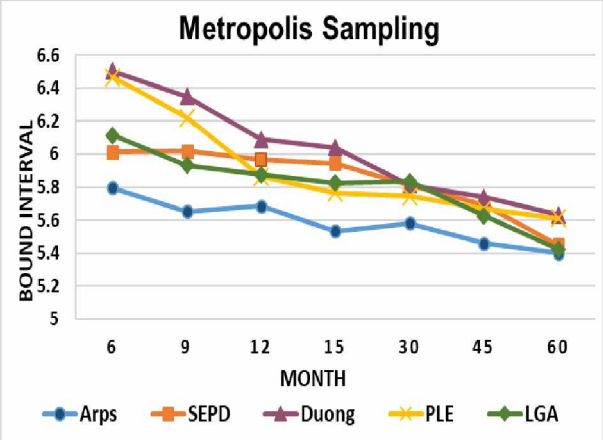

Fig. 3.45: Bound interval plot for varying production history using Metropolis sampling in overall Permian Basin

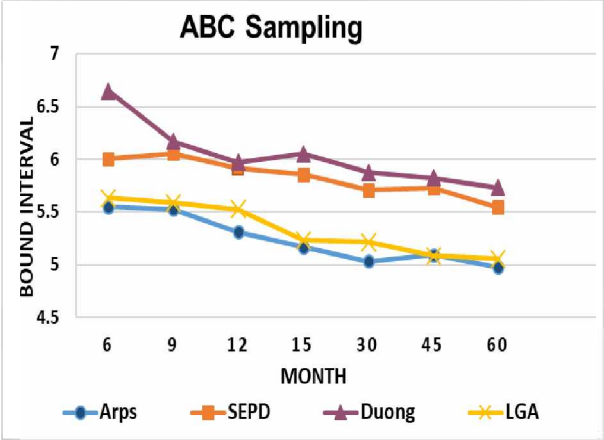

Fig. 3.46: Bound interval plot for varying production history using ABC sampling in overall Permian Basin

For 12 months of available production history data, prediction error as low as 20.58% can be achieved using LGA-ABC hybrid model, CR as high as 72.81% can be achieved using LGA-Metropolis hybrid model and interval width as low as 5.31 can be achieved using Arps-ABC hybrid model.

For 45 months of available production history data, prediction error as low as 7.6% can be achieved using Arps-Metropolis hybrid model, CR as high as 94.37% can be achieved using SEPD-Metropolis hybrid model and interval width as low as 5.08 can be achieved using Arps-ABC hybrid model.

One of the main reason behind the shortcoming of the PLE model, when used with ABC sampling, is the type of summary statistics chosen for comparing the simulated production history data to the actual production history data. As shown in the introduction section of this thesis, the PLE model has four key parameters in its governing equation; thus, it has a higher dimension than the other models used in the study. Due to the higher number of dimensions, PLE has a higher number of accepted sample sets of parameter values. This results in the acceptance of sample sets that are not representative of the actual production history data. To tackle the problem caused by the high dimensionality in PLE model, one plausible solution is to increase the number of summary statistics used. Another obvious solution is to decrease the set threshold percentage of the accepted sample sets. In an attempt to improve the performance of PLE model using ABC sampling, we applied various summary statistics like, mean, median absolute deviation, mode, standard deviation, and root mean square to the sampling technique. A threshold value as low as 0.5% percent was also considered for accepting more representative sample sets of parameter values. However, increasing the number of summary statistics and decreasing the set threshold increases the Bayesian inferencing time considerably and has a negligible effect on the performance of the model. Thus, the application of the ABC sampling technique in conjunction with PLE model is not recommended unless a better set of summary statistics can be used.

Apart from PLE model used with the ABC sampling technique, results from the hybrid models show that reserve estimation and uncertainty analysis can be carried out reliably using the described methodology.

Fig. 3.47 to **3.51** below show production forecast and cumulative production curves for each of the deterministic models using a sample well and available production history of 45 months.

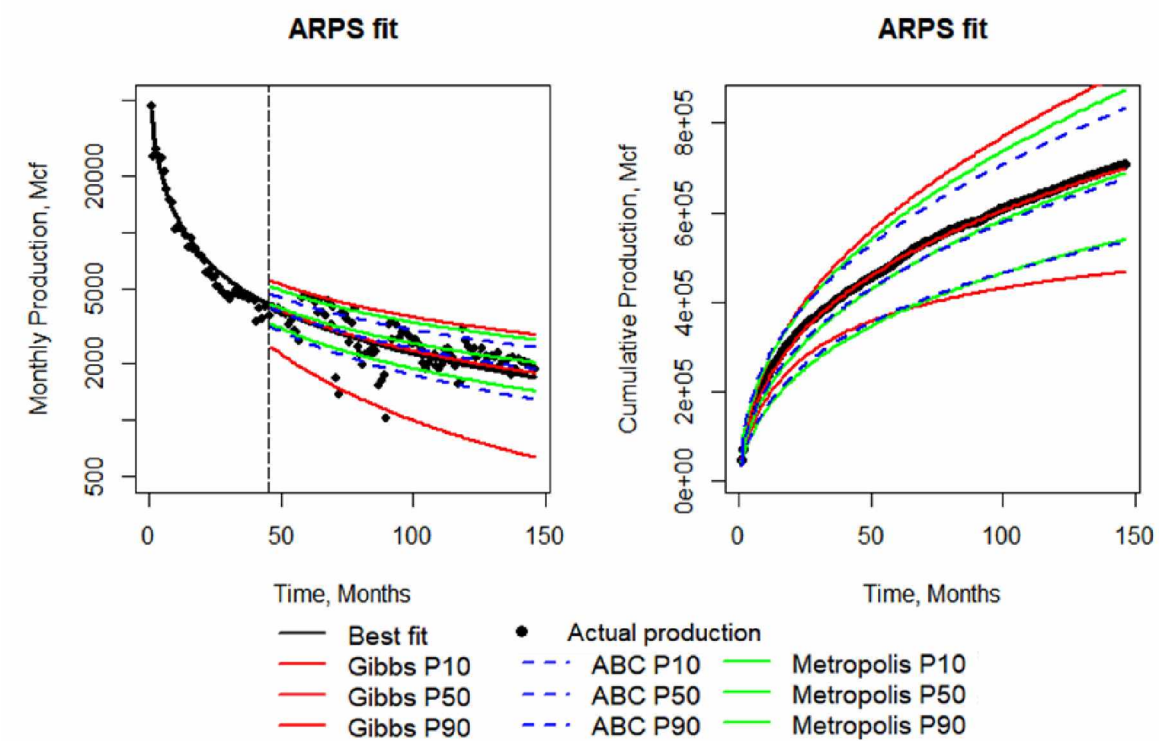

Fig. 3.47: Production forecast and cumulative production for Arps model with 45 months hindcast

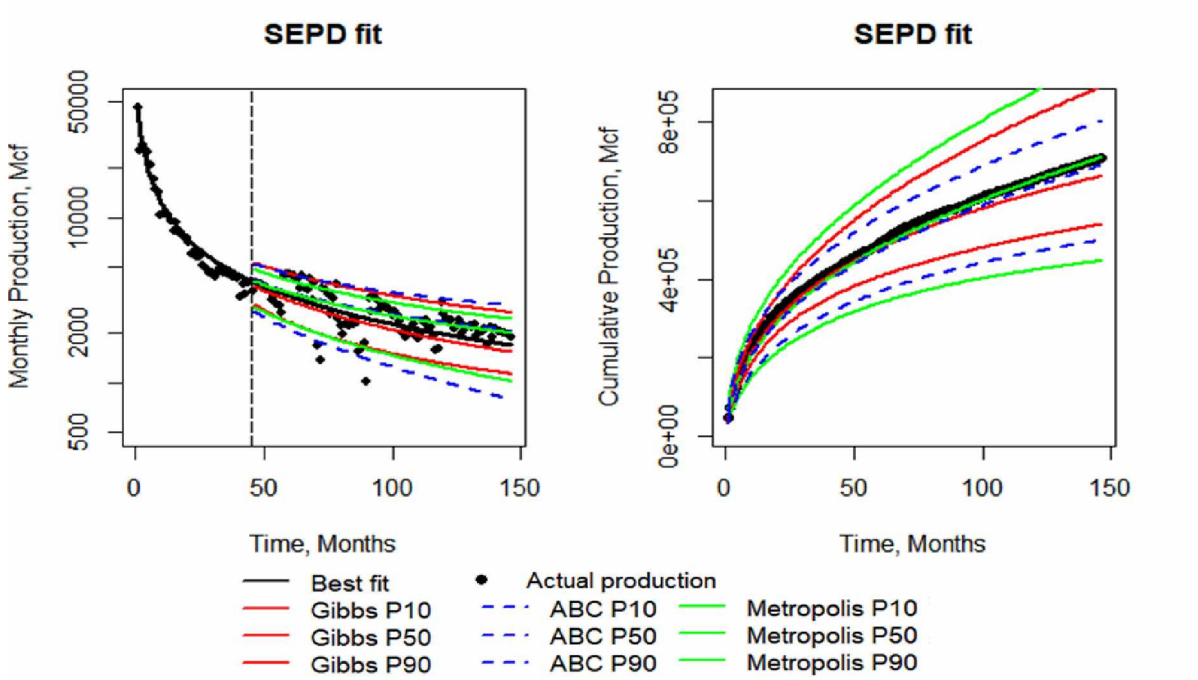

Fig. 3.48: Production forecast and cumulative production for SEPD model with 45 months hindcast

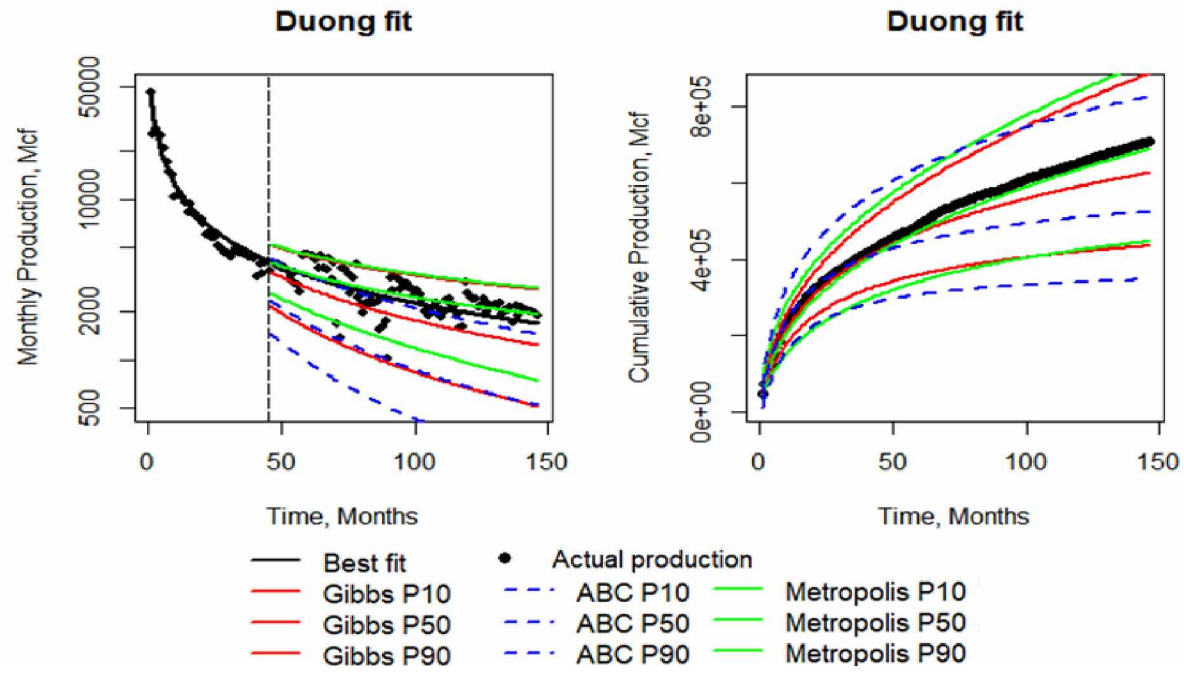

Fig. 3.49: Production forecast and cumulative production for Duong model with 45 months hindcast

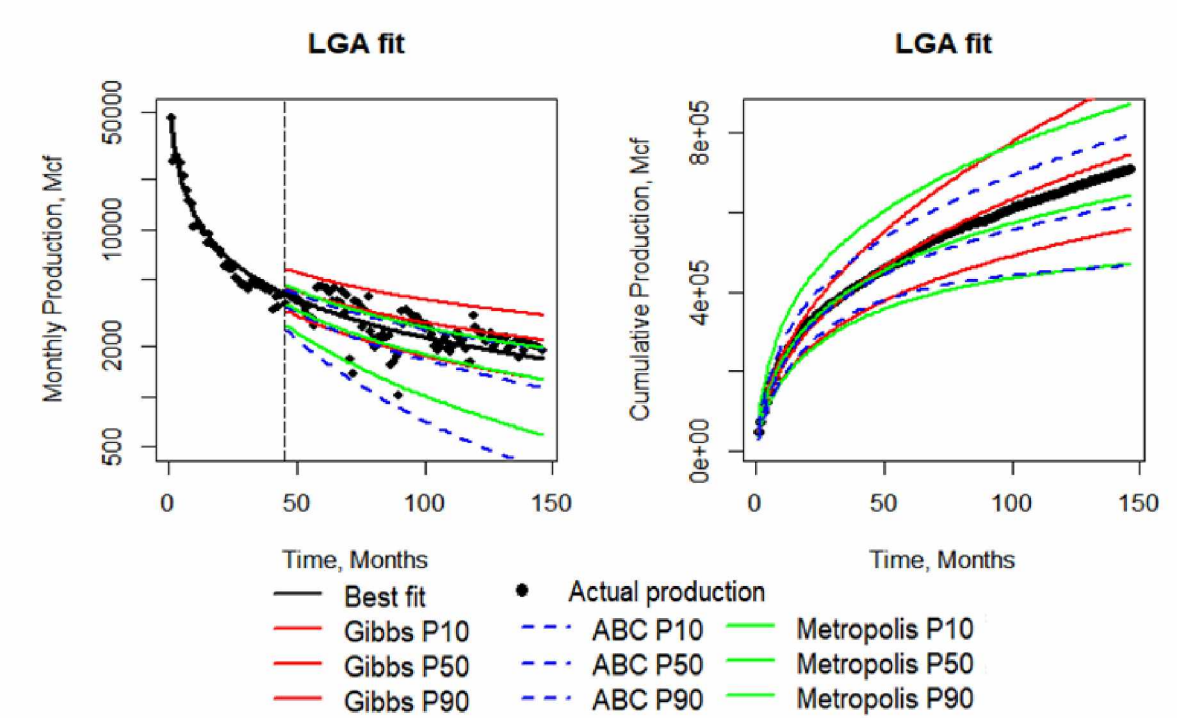

Fig. 3.50: Production forecast and cumulative production for LGA model with 45 months hindcast

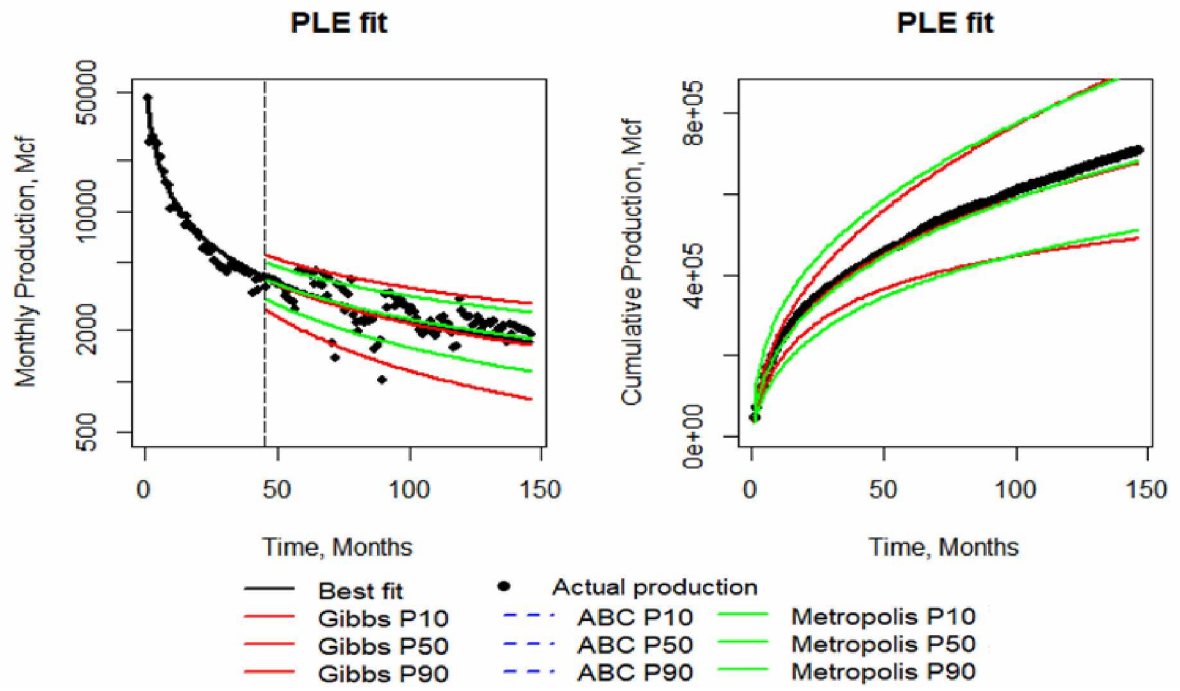

Fig. 3.51: Production forecast and cumulative production for PLE model with 45 months hindcast

Comparing the satisfactory (12 months) and excellent (45 months) results, the hybrid model producing the best fit model predictions varies for every production history data set. Likewise, the best fit hybrid model also varies when additional historical production data is available. Thus, it becomes absolutely necessary to apply and assess all hybrid models during reserve estimation and uncertainty quantification of a production history data set. This can help engineers to select better hybrid models for reserve estimation and uncertainty quantification depending on the observations made by setting a hindcast and comparing the model forecasts.

It is also important to realize that each of the hybrid model performs better (lowers prediction error, increases CR and lowers the interval width) as more and more production history data becomes available. Thus, it can be said that each of the hybrid model is necessary for production forecasting as it may take place of the best hybrid model as more and more production history data becomes available. Using all hybrid models can also provide assurance of their results when they are in agreement, thereby increasing the reliability of the process.

The computation time required for each of the hybrid models to generate the well prediction varies depending on the production history data under analysis. Average time required for each model is between 5 and 25 seconds.

Chapter 4

CONCLUSIONS

The research reviews the history of DCA and identifies MCMC sampling techniques that can be integrated with current deterministic models effectively. On the basis of Bayes theorem, the Bayesian and approximate Bayesian techniques discussed enabled the combined deterministic-stochastic models to forecast production and estimate reserves. In the analysis of 74 oil and gas wells from the Permian region with varying hindcasts, different hybrid models performed better to produce a sufficiently low prediction errors. Because of this variability, it becomes advisable to apply all hybrid models together. This helps to identify the best model for a given well production history data by setting hindcasts and comparing the predictions.

The conclusions drawn from the overall Permian Basin results in relation to the prediction error, CR and the interval width can be stated as follows:

1. The study can help to achieve low prediction errors. The prediction errors were between 5 and 18% prediction errors when 45 or more months of production history data was available.
2. The study also concludes that the hybrid models can produce high CR. For the overall Permian Basin, the CR was between 80% and 100% for all hybrid models when 45 or more months of production history data was available.
3. The hybrid models helped in assessing the uncertainty of the estimates by determining the model that can provide the narrowest P10-P90 interval width while having sufficiently high CR. This optimizes the uncertainty estimation and helps in identifying accurate models for uncertainty quantification of a given region.

Based on the varying production history data test, results produced in terms of production prediction errors and uncertainty bounds and CR improved when the available production history data was increased. The combined models proved to perform reasonably well when they were applied to low production history (12 months hindcast).

The reliability and confidence in the model forecast is increased as we achieve more evidence about the predicted production by applying all hybrid models together.

Each of the combined models discussed requires sufficiently low computation time with around 5 to 25 seconds per well depending on the data. In our case, the likelihood-free method (ABC sampling) required more computation time as compared to the likelihood-based methods (Gibbs and Metropolis sampling). Although likelihood-free methods eliminate the need for computing complex likelihood functions, they are required to compare summary statistics between the simulated and actual data. This process may require significant time depending on the amount of simulated data produced, set of summary statistics used and the threshold value.

Although there exists no simple and direct process to prove convergence of MCMC chains, a few convergence diagnostic methods can be used to provide evidence against non-convergence. Trace plots and Gelman and Rubin test were used to visualize and assess the convergence of the MCMC chains for each sampling technique. Depending on the analysis a burn-in of 2,000 iterations was set. Further, it was decided to sample a total 20,000 iterations to replicate posterior distribution.

Overall it can be said that the combined models can provide a better assessment of the upside potential and economic viability. The method can be applied to both conventional and unconventional oil and gas reservoirs and can provide a quick and easy way to constrain reserves based on limited production history data.

Chapter 5

LIMITATIONS AND RECOMMENDATIONS

Limitations

The chief limitation of this work is that the integrated hybrid models do not analyze the physics of the process. Physics-based models are complex, computationally expensive and require data which is not easily available. However, if physics-based models are available and are formed based on certain important parameters, they can be incorporated in the above methodology. PLE-ABC hybrid model doesn't perform well with the chosen summary statistic options. Choice of summary statistic to be used can differ as there is no set rule for it. However, plausible solutions to achieve better PLE-ABC model performance could be increasing the number of summary statistic used or to decrease the set threshold percentage for the accepted sample sets.

Recommendations

In terms of future recommendation, we would suggest development of a software tool for accessing the hybrid models described in this study to identify the best hybrid model depending on the production history data available. Using more informative priors could also help in increasing the accuracy of the models.

NOMENCLATURE

List of Abbreviations

Abbreviation	*Meaning*
DCA	Decline Curve Analysis
MMB/D	Million Barrel per Day
BCF/D	Billion Cubic Feet per Day
EIA	U.S. Energy Information Administration
PRMS	Petroleum Resource Management System
EUR	Estimated Ultimate Recovery
MMCF	Million Cubic Feet
BDF	Boundary Dominated Flow
SRV	Simulated Reservoir Volume
PLE	Power Law Exponential
SEPD	Stretched Exponential Production Decline
LGA	Logistic Growth Analysis
t	Time
q_t	Production at Time t
q_i	Initial Production

D_∞	Power Law Decline at Infinite Time in PLE
n	Dimensionless Time Exponent
m	Dimensionless Slope Parameter in Duong's model
k	Carrying Capacity (EUR)
PDCA	Probabilistic Decline Curve Analysis
PI/PIs	Prediction Interval/Prediction Intervals
MBM	Modified Bootstrap method
ABC	Approximate Bayesian Computation
TSA	Time Series Analysis
MCMC	Markov Chain Monte Carlo
ARMA	Auto-regressive Moving Average model
P(θ|Y)	Posterior distribution
P(Y|θ)	Likelihood Function
P(θ)	Prior Distribution
R	Ratio of Densities between Two Posterior Distributions
Y	Observed Data (Monthly production)
$\theta_{proposal}$	Parameters drawn from proposal distribution
PSRF	Potential Scale Reduction Factor
B/n	Variance between Chains
W	Mean Variance within Chains
MPSRF	Multivariate Potential Scale Reduction Factor

Actual	True Cumulative Production
CR	Coverage Rate

List of Symbols

Greek symbols	*Meaning*
$\widehat{D}$	Power Law Decline Constant in PLE
τ	Characteristic Time Parameter in SEPD
η	Dimensionless Exponent Parameter in SEPD
α	Intercept of Duong's model
ε	Difference between Simulated Results and Observed Data
σ	Variance
θ	Model Parameters

REFERENCES

Agarwal, A., Wei, Y., & Holditch, S. 2012. A Technical and Economic Study of Completion Techniques in Five Emerging US Gas Shales: A Woodford Shale Example. SPE Drilling & Completion. SPE-135396-PA. http://dx.doi.org/10.2118/135396-PA

Arps, J. J. 1945. Analysis of Decline Curves. Transactions of the AIME. 1 December. SPE-945228-G. https://doi.org/10.2118/945228-G

Cheng, Y., Wang, Y., McVay, D., & Lee, W. J. 2010. Practical Application of a Probabilistic Approach to Estimate Reserves Using Production Decline Data. SPE Economics & Management, 1 April. SPE-95974-PA. https://doi.org/10.2118/95974-PA

Clark, A. J., Lake, L. W., & Patzek, T. W. 2011. Production Forecasting with Logistic Growth Models. SPE Annual Technical Conference and Exhibition, 30 October-2 November, Denver, Colorado, USA. SPE-144790-MS. https://doi.org/10.2118/144790-MS

Csillery, K., Francois, O., Blum, M. G. 2012. abc: an R package for approximate Bayesian computation (ABC). Methods in Ecology and Evolution 3. doi:10.1111/j.2041-210X.2011.00179.x (accessed 17 July 2018)

Duong, A.N. 2011. Rate-Decline Analysis for Fracture-Dominated Shale Reservoirs. SPE Reservoir Evaluation & Engineering 14 (3): pp. 377-387. SPE-137748-PA. https://doi.org/10.2118/137748-PA

Drillinginfo. 1998. Drillinginfo https://app.drillinginfo.com/ (accessed 1 August 2017)

Fetkovich, M. J. 1980. Decline Curve Analysis Using Type Curves. Journal of Petroleum Technology. 1 June. SPE-4629-PA. https://doi.org/10.2118/4629-PA

Gelman, A., Rubin, D. B. 1992. Inference from Iterative Simulation Using Multiple Sequences. Statistical Science, Volume 7, number 4, 457--472. SS-1177011136. doi:10.1214/ss/1177011136. https://projecteuclid.org/euclid.ss/1177011136

Gong X., Gonzalez R., McVay D.A. et. al, 2011. Bayesian Probabilistic Decline-Curve Analysis Reliably Quantifies Uncertainty in Shale-Well-Production Forecasts. Presented at the Canadian Unconventional Resources Conference, Calgary, Alberta, Canada, 15-17 November. SPE-147588-MS. https://doi.org/10.2118/147588-MS

Gong, X., Gonzalez, R., McVay, D. A., & Hart, J. D. 2014. Bayesian Probabilistic Decline-Curve Analysis Reliably Quantifies Uncertainty in Shale-Well-Production Forecasts. SPE Journal. 19 (06): 1,047 - 1,057. SPE-147588-PA. http://dx.doi.org/10.2118/147588-PA

Ilk, D., Rushing, J. A., Perego, A. D., & Blasingame, T. A. 2008. Exponential vs. Hyperbolic Decline in Tight Gas Sands: Understanding the Origin and Implications for Reserve Estimates Using Arps Decline Curves. Presented at the SPE Annual Technical Conference and Exhibition, 21-24 September, Denver, Colorado, USA. SPE-116731-MS. http://dx.doi.org/10.2118/116731-MS

Jochen, V. A., & Spivey, J. P. 1996. Probabilistic Reserves Estimation Using Decline Curve Analysis with the Bootstrap Method. SPE Annual Technical Conference and Exhibition, 6-9 October, Denver, Colorado. SPE-36633-MS. https://doi.org/10.2118/36633-MS

Joshi, K. G., Awoleke, O. O., & Mohabbat, A. 2018. Uncertainty Quantification of Gas Production in the Barnett Shale Using Time Series Analysis. SPE Western Regional Meeting, 22-26 April, Garden Grove, California, USA. SPE-190124-MS. https://doi.org/10.2118/190124-MS

McCarthy, N. 2017. The American Shale Revolution. *Statistica,* 14 November 2017, https://www.statista.com/chart/11830/the-american-shale-revolution/ (accessed 22 February 2019)

McVay, D. A., & Dossary, M. N. 2014. The Value of Assessing Uncertainty. SPE Economics & Management, 1 April. SPE-160189-PA. https://doi.org/10.2118/160189-PA

Paryani, M. 2015. Approximate Bayesian Computation for Probabilistic Decline Curve Analysis in Unconventional Reservoirs. MS thesis, University of Alaska, Fairbanks (October 2015)

Paryani, M., Awoleke, O. O, Ahmadi, M., Hanks, C., & Barry, R. 2017. Approximate Bayesian Computation for Probabilistic Decline-Curve Analysis in Unconventional Reservoirs. Society of Petroleum Engineers. SPE-183650-PA. https://doi.org/10.2118/183650-PA

Plummer, M., Best, N., Vines, K. et al. 2006. CODA: Convergence Diagnosis and Output Analysis for MCMC, R News, vol 6, 7-11. https://www.r-project.org/doc/Rnews/Rnews_2006-1.pdf (accessed 17 July 2018)

Schoot, R., Kaplan, D., Denissen, J. et al. 2013. A Gentle Introduction to Bayesian Analysis: Applications to Developmental Research. *Child Development,* 85(3), 842-860, 1 May. https://doi.org/10.1111/cdev.12169

Shah, S. 2013. Development of new Decline Model for Shale oil reserves. MS thesis, University of Houston, Texas (August 2013)

Sinclair, T.D. 2007. The generation and continued existence of overpressure in the Delaware Basin, Texas. Doctoral thesis, Durham University (August 2007) http://etheses.dur.ac.uk/2289/

SPE, AAPG, WPC, SPEE & SEG. 2011. Guidelines for Application of the Petroleum Resources Management System. WP SPE General, November 2011. SPE-180937-WP. https://www.onepetro.org/general/SPE-180937-WP

Tarka Resources, Inc. Permian Basin Oil Exploration and Operations. https://tarka.com/permian-basin/ (accessed 1 March 2019)

U.S. Energy Information Administration. 2018a. EIA adds new play production data to shale gas and tight oil reports. 15 February 2019, https://www.eia.gov/todayinenergy/detail.php?id=38372 (accessed 22 February 2019)

U.S. Energy Information Administration. 2018b. Permian Basin Wolfcamp Shale Play Geology Review. October 2018, https://www.eia.gov/maps/pdf/PermianBasin_Wolfcamp_EIAReport_Oct2018.pdf (accessed 22 March 2019)

U.S. Energy Information Administration. 2019. EIA Permian Region Drilling Productivity report. January 2019, https://www.eia.gov/petroleum/drilling/pdf/permian.pdf (accessed 22 March 2019)

Valko, P. P. 2009. Assigning value to stimulation in the Barnett Shale: a simultaneous analysis of 7000 plus production histories and well completion records. SPE Hydraulic Fracturing Technology Conference, 19-21 January, the Woodlands, Texas. SPE- 119369-MS. https://doi.org/10.2118/119369-MS

Valko, P. P., & Lee, W. J. 2010. A Better Way to Forecast Production from Unconventional Gas Wells. Society of Petroleum Engineers. SPE Annual Technical Conference and Exhibition, 19-22 September, Florence, Italy. SPE- 134231-MS. https://doi.org/10.2118/134231-MS

Ward R.F., Kendall C.G., Harris P.M. 1986. Upper Permian (Guadalupian) Facies and Their Association with Hydrocarbons--Permian Basin, West Texas and New Mexico. AAPG Bulletin, Vol – 70, pp 239-262. http://archives.datapages.com/data/bulletns/1986-87/data/pg/0070/0003/0200/0239.htm?doi=10.1306%2F9488566F-1704-11D7-8645000102C1865D

APPENDIX

Supplementary trace plots using the Metropolis algorithm:

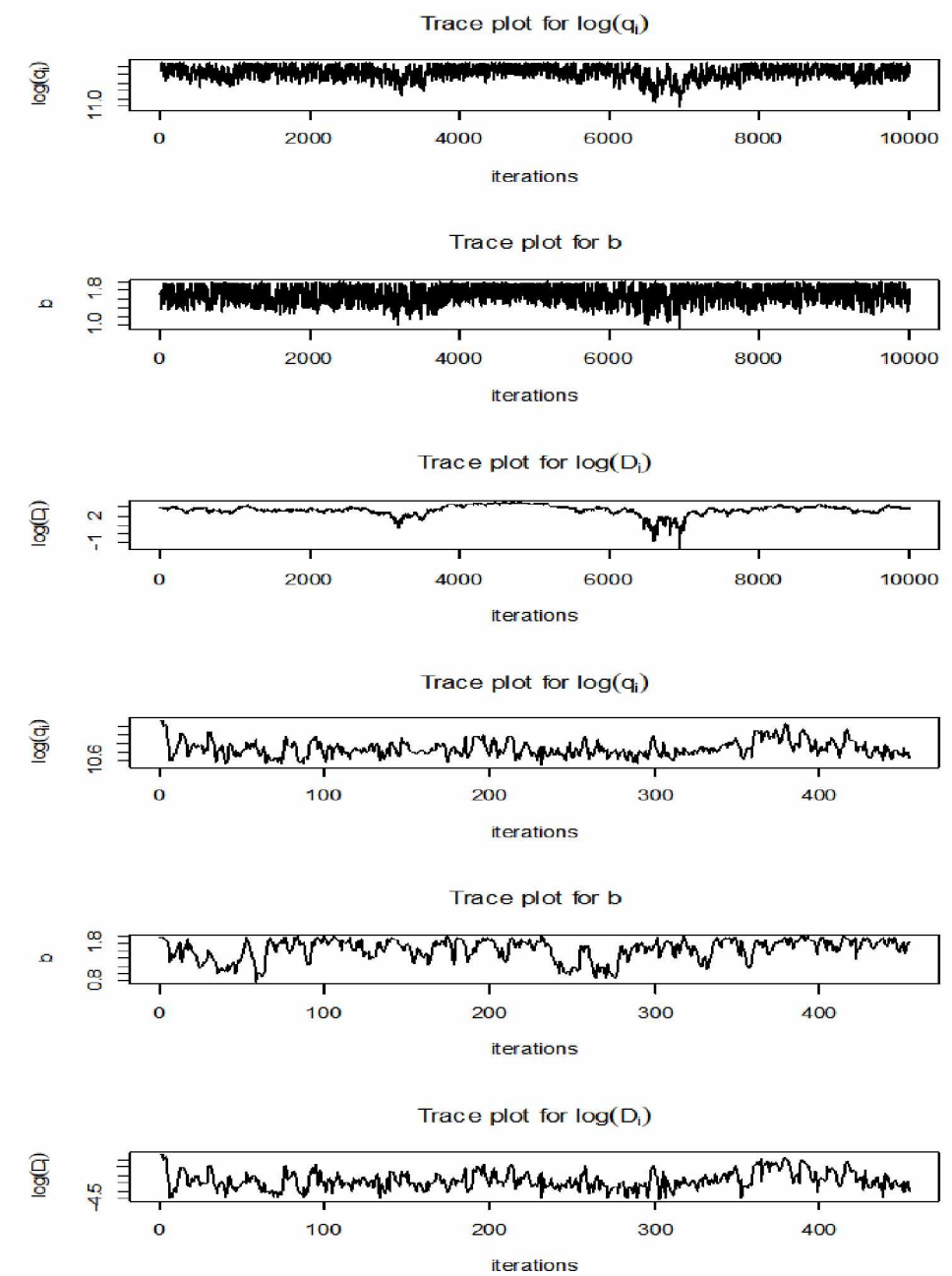

Fig. A.1: Sample trace plot for Metropolis algorithm (well 1 and well 2)

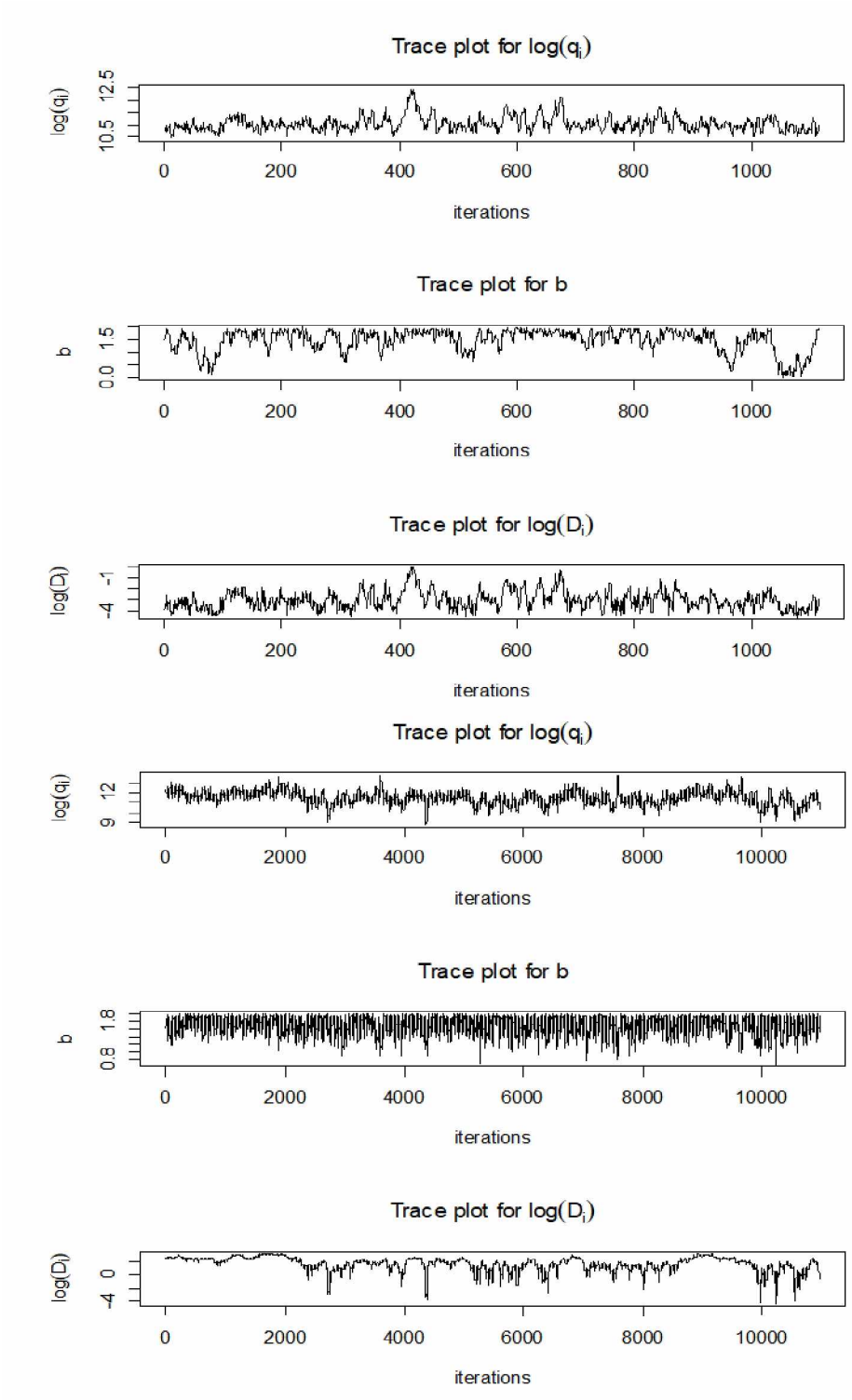

Fig. A.2: Sample trace plot for Metropolis algorithm (well 3 and well 4)

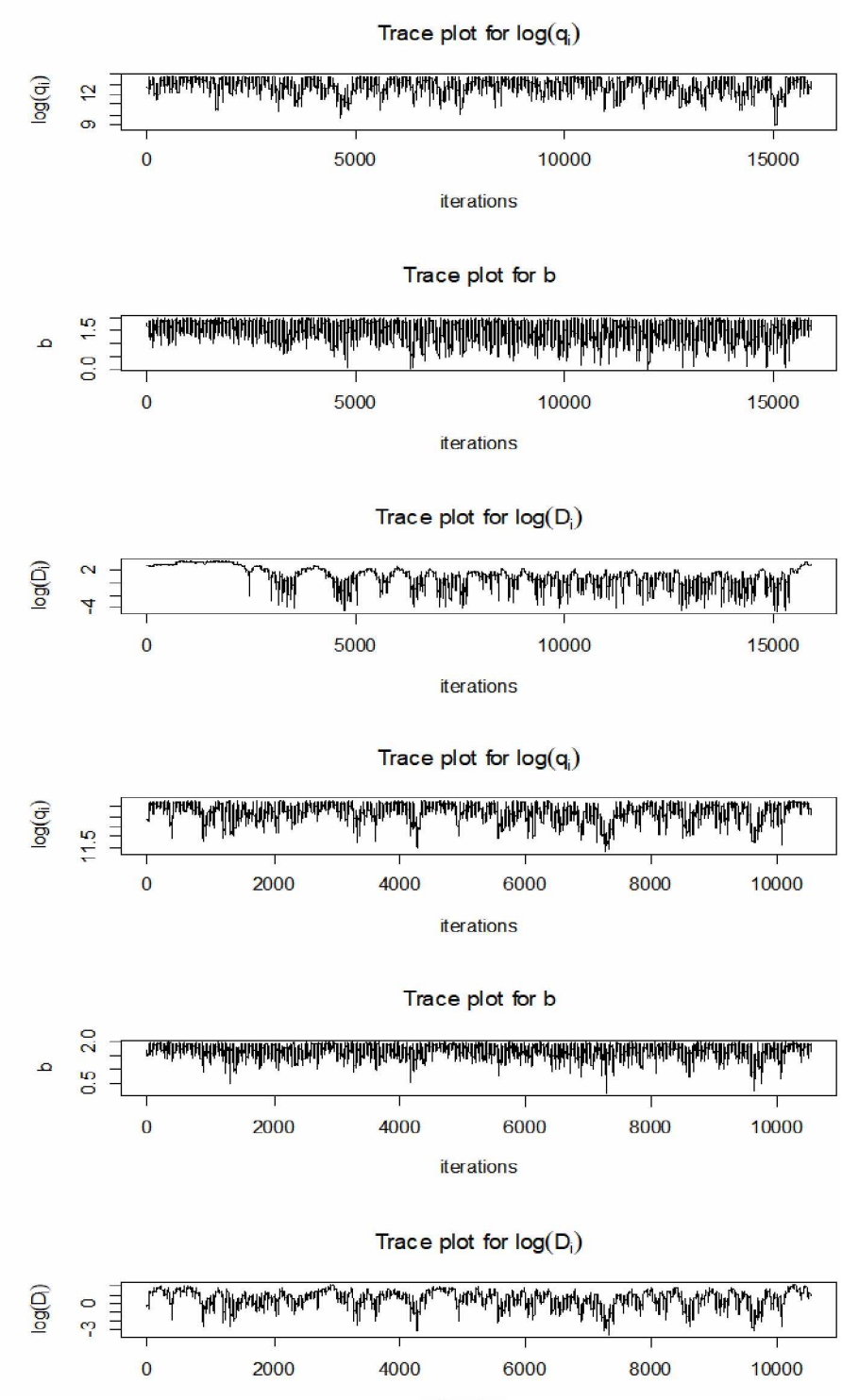

Fig. A.3: Sample trace plot for Metropolis algorithm (well 5 and well 6)

Supplementary trace plots for Gibbs sampler:

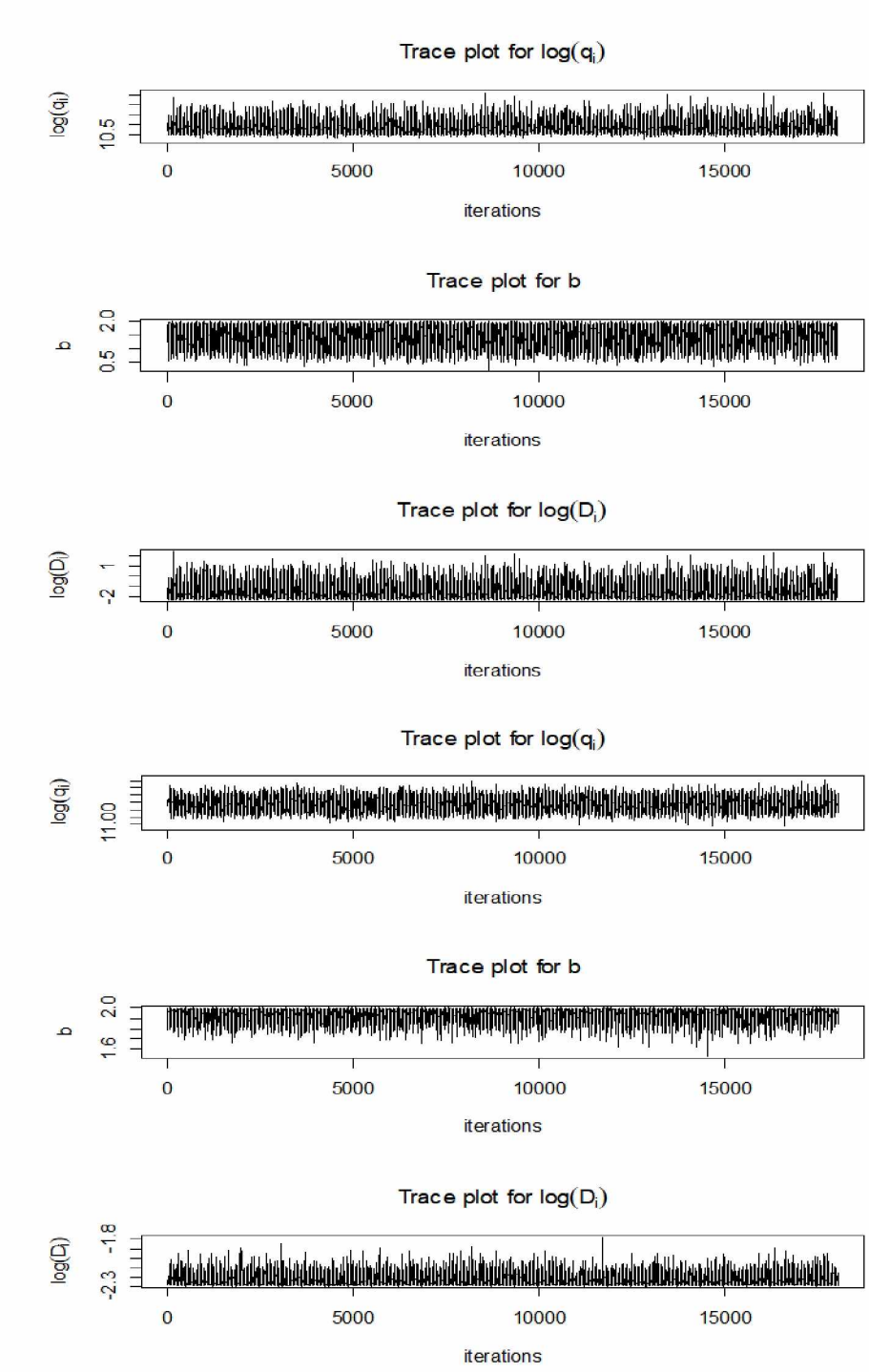

Fig. A.4: Sample trace plot for Gibbs sampler (well 1 and well 2)

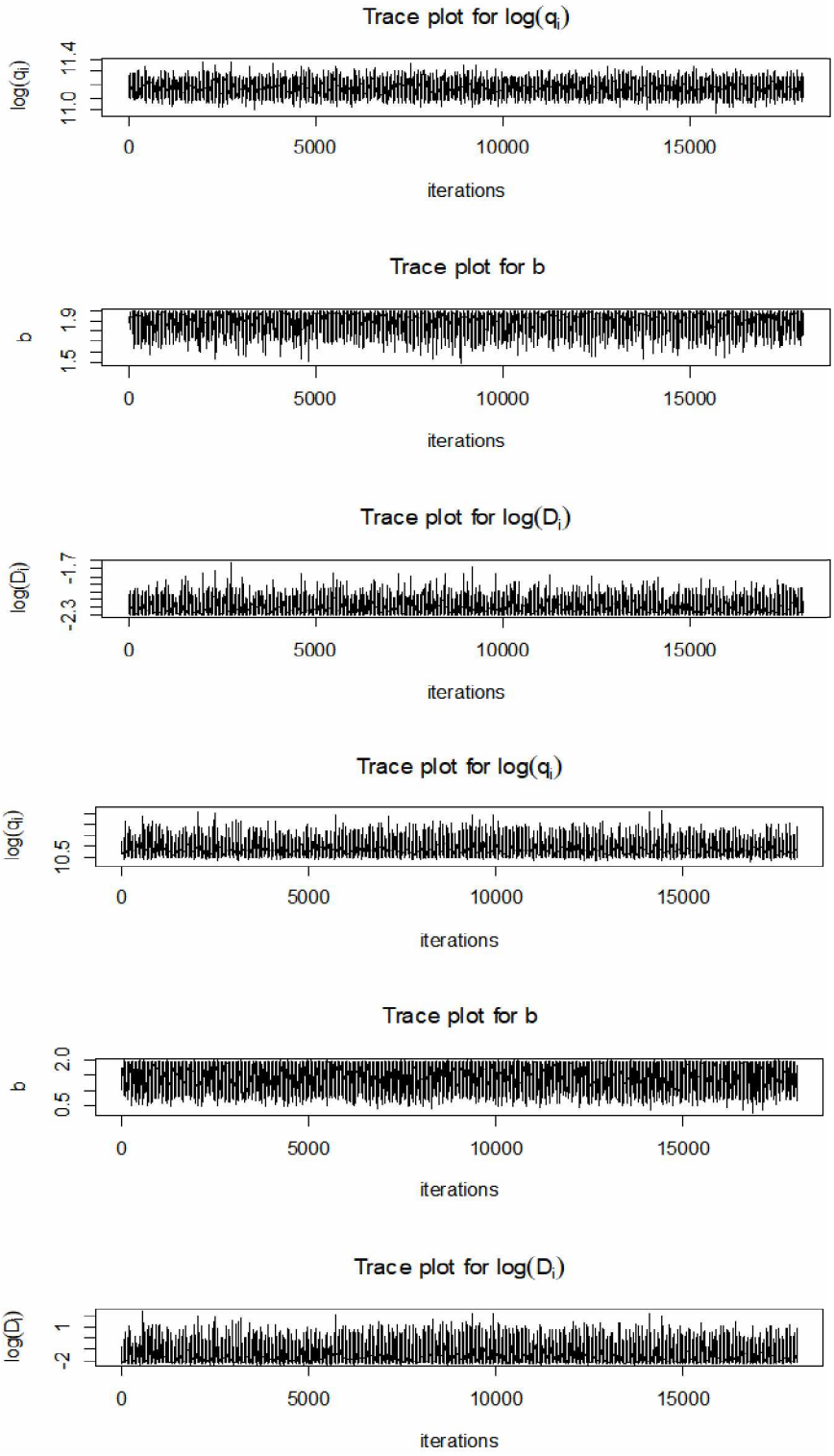

Fig. A.5: Sample trace plot for Gibbs sampler (well 3 and well 4)

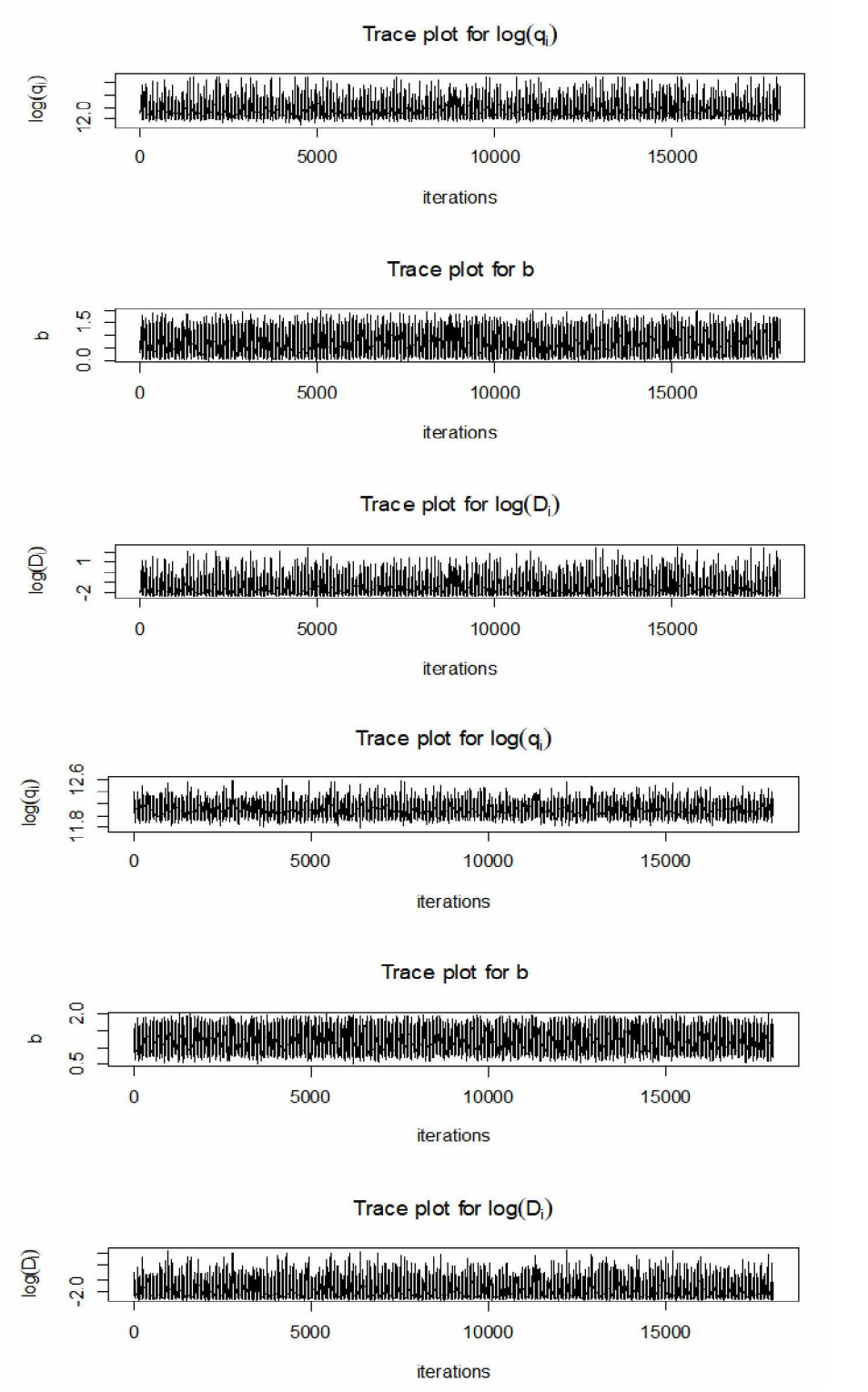

Fig. A.6: Sample trace plot for Gibbs sampler (well 5 and well 6)

Supplementary trace plots for ABC sampling:

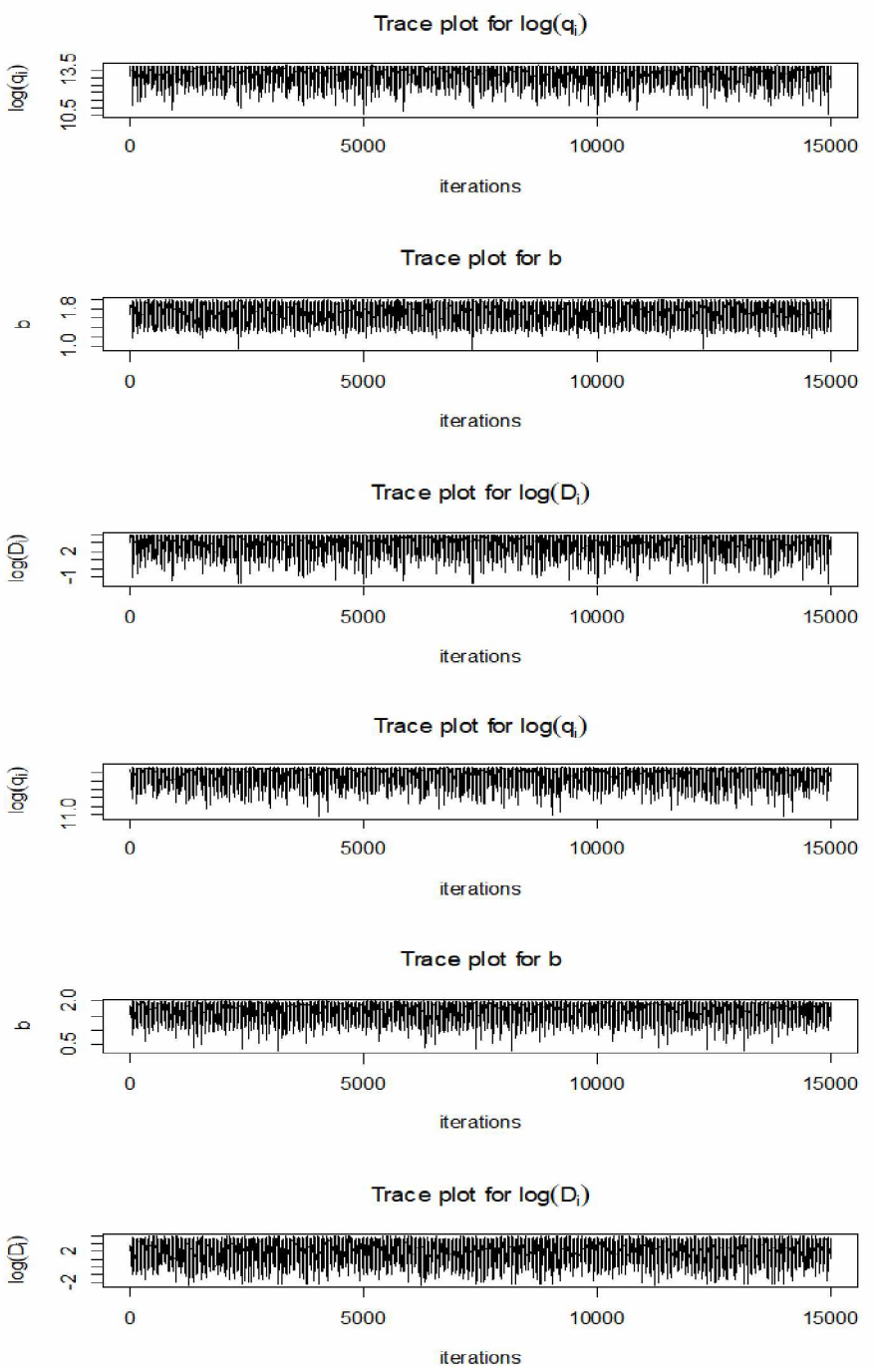

Fig. A.7: Sample trace plot for ABC sampling (well 1 and well 2)

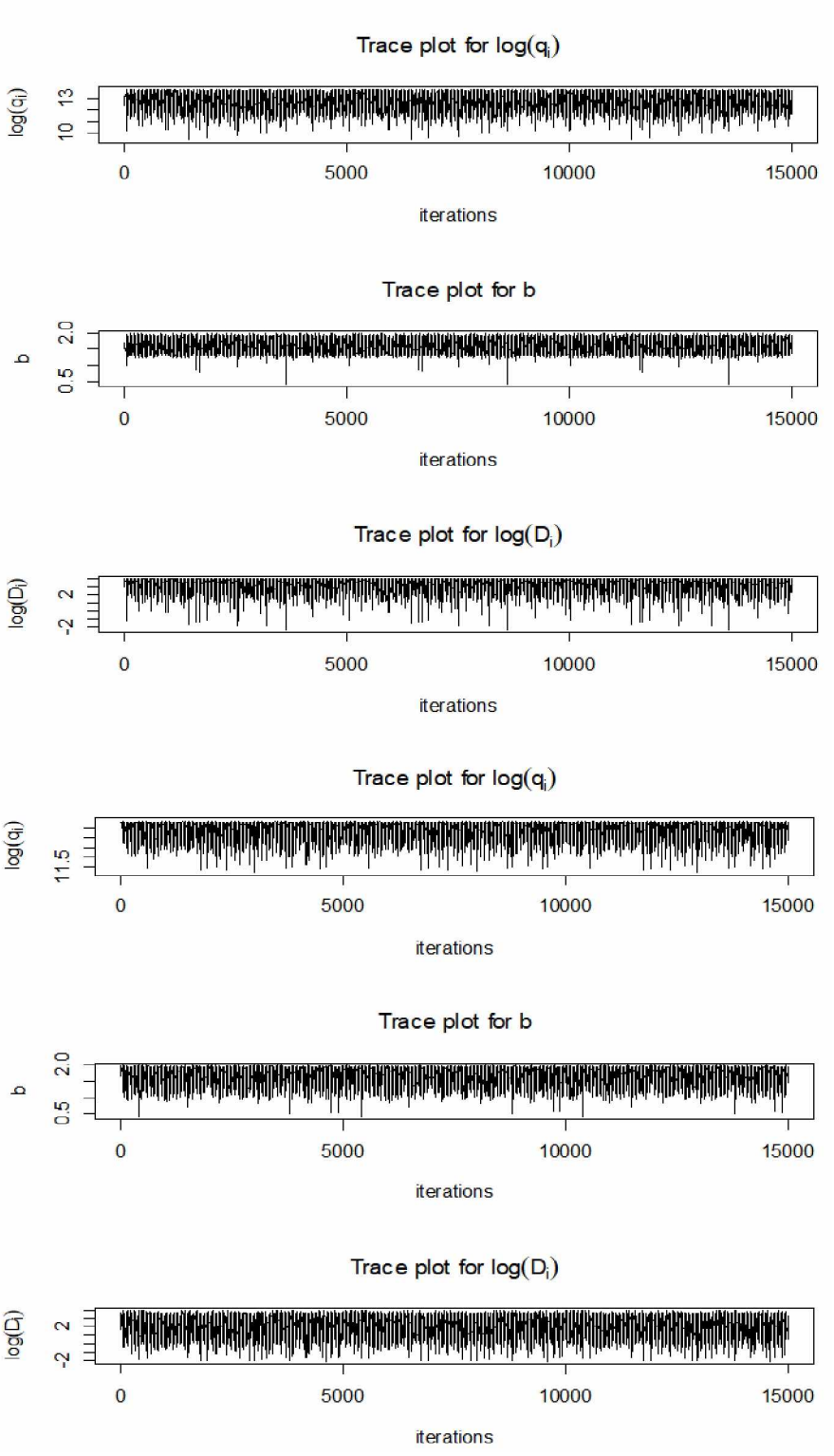

Fig. A.8: Sample trace plot for ABC sampling (well 3 and well 4)

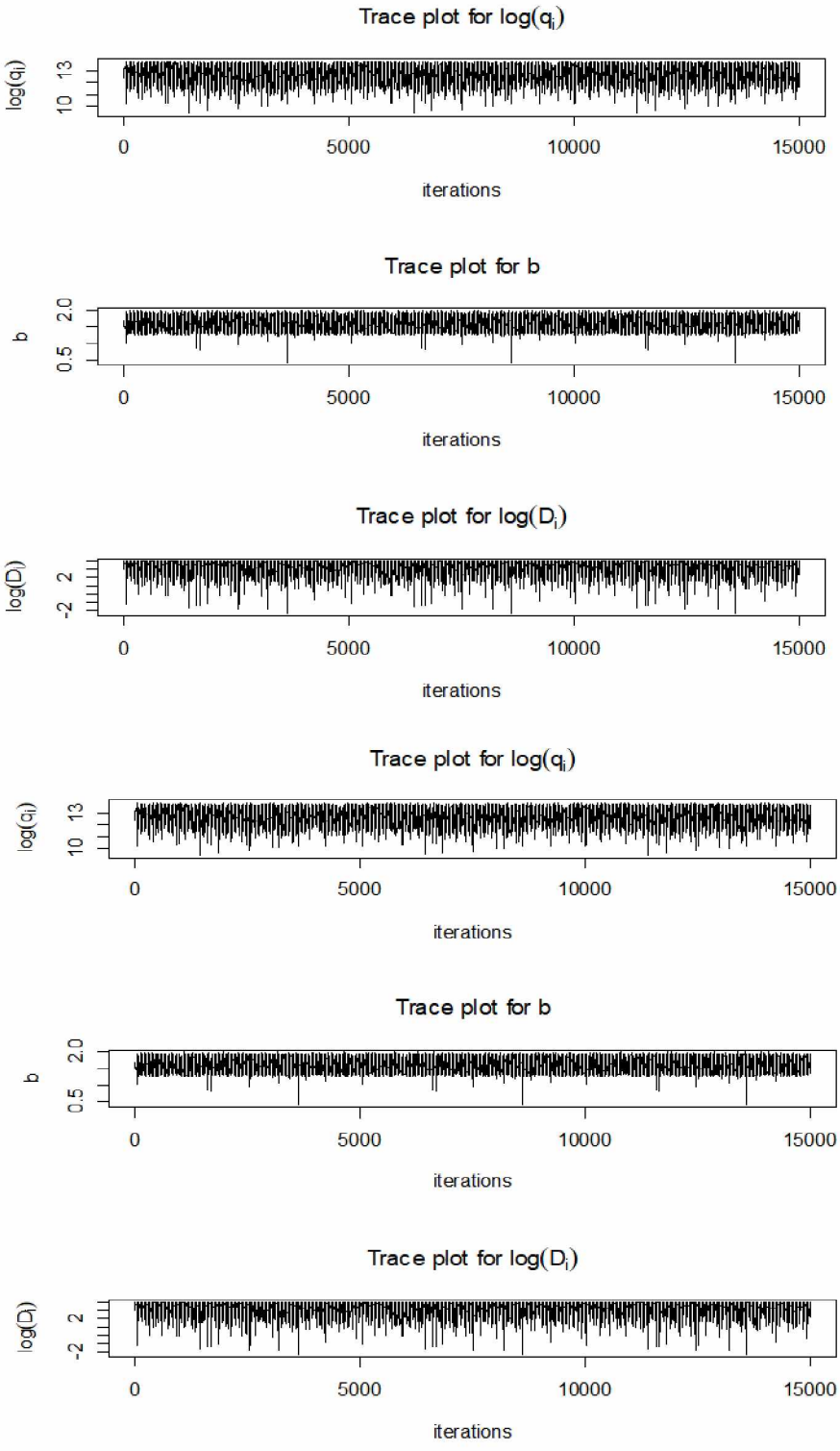

Fig. A.9: Sample trace plot for ABC sampling (well 5 and well 6)